SYNTHESIS AND EVALUATION
OF
RADIOACTIVE GOLD NANOPARTICLES FOR CANCER TREATMENT AND IMAGING

A Dissertation Presented to the Faculty of the Graduate School at the University of Missouri – Columbia

---

In Partial Fulfillment

Of the Requirements for the Degree

Doctor of Philosophy

By

AMAL YOUSIF AL-YASIRI

Dissertation Supervisors

Dr. Kattesh V. Katti and Dr. Sudarshan K. Loyalka

May 2015

The undersigned, appointed by the Dean of the Graduate School, have examined the dissertation entitled

SYNTHESIS AND EVALUATION OF RADIOACTIVE GOLD NANOPARTICLES FOR CANCER TREATMENT AND IMAGING

Presented by **Amal Yousif Al-Yasiri**
A candidate for the degree of Doctor of Philosophy
And hereby certify that, in their opinion, it is worthy of acceptance.

_____
Dr. Kattesh V. Katti

_____
Dr. Sudarshan K. Loyalka

_____
Dr. Tushar Ghosh

_____
Dr. Mark Prelas

_____
Dr. Cathy Cutler

_____
Dr. Robert Tompson

_____
Dr. Dabir Viswanath

Dedicated to my parents

ACKNOWLEDGEMENTS

I am indebted to many people who helped me through this journey of Ph.D. research. Without their help, this work would never see light.

First and foremost, I would like to thank my research advisors Dr. Kattesh Katti and Dr. Sudarshan K. Loyalka. I would like to express my sincere gratitude for their support, advice, help, and constant encouragement that has always kept me motivated in my research work and made my Ph.D. experience productive and stimulating. I also appreciate that they gave me the opportunity to work on the project that I like.

I would like to thank Drs. Tushar Ghosh, Mark Prelas, Cathy Cutler, Robert Tompson, and Dabir Viswanath for serving as my committee members. I am also thankful to them for teaching me in my academic course work.

I would like to thank Dr. Cathy Cutler for her help, advice and support throughout my work at the nuclear reactor. She always guided, encouraged and helped me with my research and in writing my dissertation, and I appreciate her collaboration for allowing me to work at her laboratories at MURR.

I am grateful to Dr. Tushar Ghosh for his encouragement and advices on my academic course work.

I would like to thank Dr. Menka Khoobchandani for her advices and help throughout my work at institute of Green Nano-Technology at MU. I appreciate her teaching me many things especially cell culture techniques.

I am very thankful to Dr. Charles Smith, Lisa Watkinson, and Terry Carmack (Harry S. Truman Memorial VA Hospital) for their valuable help with animal studies of radioactive MGF-^{198}AuNPs project. Really I appreciate their help.

I would like to thank Dr. Kvar Black (Washington University/ St. Louis) for his collaboration and sharing with me the results of animal study of radioactive citrate-^{199}AuNPs project.

I am very thankful to Nathan White for his help with the MCNP simulations. I appreciate his valuable time that he spent to help me with dose calculations.

I am very grateful to Kavita Katti, Maryna Kuchuk, Mary Embree, and Daniel O’ Connor for their assistance and advice with my experiments. They were very helpful at any time I needed help. Also, I must not forget to thank Latricia Vaughn, the NSEI secretary, for her help during my studies at MU.

I gratefully acknowledge the funding sources that made this research possible. This research has been supported by the Iraqi ministry of higher education and scientific research, the Nuclear Science and Engineering Institute, Institute of Green Nano-Technology, MURR, and Dr. Cathy Cutler.

At the personal level, I would like to thank my mother Faliha Al-Yasiri, my brother Muntadher, my sisters Khawlah, Tumadher, Kouwthar, Ghufran, and Yusra. I am grateful to them for their endless support, encouragement, and trust. Without my mother's prayers, I would have never succeeded. I am very grateful

to my father Yousif Al-Yasiri who was always proud of me and encouraged me to pursue Ph.D. degree before he passed away. He wished me to get Ph.D. one day, and I am happy to have fulfilled his wish.

I am also thankful to my friends for their help and support. I am thankful for everyone who was a part of my journey from the first day of my academic study till my graduation.

Amal Y. Al-Yasiri

TABLE OF CONTENTS

LIST OF FIGURES

LIST OF TABLES

LIST OF ABBREVIATIONS

Abbreviation	Definition
$NaAuCl_4$.	Sodium tetrachloroaurate
$HAuCl_4$	Gold(III) chloroauric acid
EGCG	Epigallocatechin-gallat
MGF	Mangiferin
SCID	Severe combined immunodeficiency
TEM	Transmission Electron Microscopy
THPAL	Trimeric alanine phosphine conjugate
AuNPs	Gold nanoparticles
MGF-AuNPs	Mangiferin-gold nanoparticles
GNPs	Gold nanoparticles
HSA	Human Serum Albumin
BSA	Bovine Serum Albumin
NaCl	Sodium chloride
SPR	Surface Plasmon Resonance
EPR	Enhanced Permeability and Retention effect
z	Zeta potential
γ	Gamma radiation
n	Neutron
B	Beta radiation
GA	Gum Arabic
DPBS	Dulbecco's Phosphate Buffered Saline
GA-AuNPs	Gum Arabic –gold nanoparticles
EGCG-AuNPs	Epigallocatechin gallat-gold nanoparticles

MCNP	Monte Carlo N-Particle code
HAEC	Human Aortic Endothelial Cells
PC-3	Prostate Cancer cells
TLC	Thin Layer Chromatography
MTT	3-(4,5-dimethylthiazol-2-yl)-2,5 diphenyltetrazolium bromide)
DAPI	40,6-diamidino-2-phenylindole dye
FBS	Fetal Bovine Serum
RPMI	Memorial institute medium
PFA	Paraformaldehyde
DMSO	Dimethyl sulfoxide anhydrous
MURR	University of Missouri Research Reactor
IUPAC	International Union of Pure and Applied Chemistry
BEAS-2B	Human bronchial epithelium from normal lung
MCF-7	Breast cancer cell line
Pt	Platinum
Au	Gold
MMP-9	Matrix metallopeptidase 9
Bq	Becquerel
R_f	Retention factor
A-150	Tissue equivalent plastic
SPECT	Single Photon Emission Computer Tomography

ABSTRACT

The main goal of this dissertation was to explore new protocols to synthesize biocompatible radioactive gold nanoparticles to treat and image cancer and calculate the dose distribution by using MCNP in tumor inside the human prostate as well as surrounding normal tissues.

This dissertation is classified into three parts or projects. The objective of the first project is production and evaluation of radioactive MGF-^{198}AuNPs and MGF-^{199}AuNPs towards prostate cancer treatment and imaging. Non-radioactive MGF-AuNPs were synthesized first and *in vitro* evaluated. Results of *In vitro* evaluation showed that this type of nanoparticles is stable, non toxic, and can be internalized into prostate cancer cells. Next, new modified protocols were devloped to produce radioactive MGF-^{198}AuNPs and MGF-^{199}AuNPs. UV-Vis spectroscopy and TLC measurements showed that these radioactive MGF-^{198}AuNPs and MGF-^{199}AuNPs are stable and more than 96% of radioactive gold was within nanoparticlate structure. Then, MGF-^{198}AuNPs were *in vivo* evaluated to investigate their *in vivo* stability, retention in tumor, and efficacy to cure prostate cancer. The results indicated that MGF-^{198}AuNPs are stable and have excellent ability to be retained within the tumor up to 24 hours with very minimum leakage to non-target organs. It was also found that radioactive MGF-^{198}AuNPs have significant therapeutic effect and that they were able to control the tumor size in comparison to control group.

The objective of the second project is production and evaluation of radioactive citrate-^{199}AuNPs as imaging probe for single photon emission computed tomography. In this study, a new protocol was developed to synthesize radioactive citrate-^{199}AuNPs, UV-Vis spectroscopy and TLC measurements showed that new protocol was successful to produce stable radioactive citrate-^{199}AuNPs. Also, *In vivo* evaluation results showed that citrate-^{199}AuNPs are stable *in vivo* and therfore, they can be used in imaging procedures.

The objective of the third project is estimation, by means of MCNP simulations, the dose distribution delivered by radioactive gold nanoparticles (^{198}AuNPs or^{199}AuNPs) to tumor inside the human prostate as well as to the normal tissues surrounding the tumor, using water and A-150 tissue equivalent plastic phantoms. A simple geometrical model of a human prostate was used, and the dose distribution that is deposited by radioactive gold nanoparticles (^{198}AuNPs or ^{199}AuNPs) was calculated using MCNP. The results showed that the deposited dose by ^{198}AuNPs or ^{199}AuNPs, which are distributed homogenously in the tumor, has maximum value at the tumor region and then decreases toward the normal tissue in the prostate as well as surrounding organs. However, the dose deposited by ^{198}Au is significantly higher than the dose deposited by ^{199}Au at the tumor region as well as normal tissues. Therefore ^{198}Au should be preferred to for therapeutic applications, while should be preferred for ^{199}Au in imaging applications.

CHAPTER 1

INTRODUCTION

Cancer is uncontrolled growth of cells and can metastasize to other parts of the human body. Despite considerable advances in the study of cancer, it remains one of the leading causes of mortality in the world with more than 10 million new cases every year [1]. Prostate cancer is more commonly diagnosed than any other non-skin cancer in the United States [2] and the second-leading cause of cancer death in men [3].

At present, there are many different modalities that are used clinically to treat prostate cancer such as chemotherapy [4], hormonal therapy, surgery, and radiation therapy [4, 5]. Oncologists determine the appropriate treatment modality that can be used to treat the tumor dependent on the stage of the prostate cancer and age of patient [4]. Several modalities are used for radiation treatment delivery which can be classified into two categories, external beam radiation therapy and internal radiation therapy. The first category external beam radiation therapy (EBRT) includes intensity-modulated radiation therapy (IMRT), proton beam therapy, and stereotactic body radiation therapy [6, 7]. Unfortunately, all these radiation therapy modalities have drawbacks (a) intensity-modulated radiation therapy (IMRT) suffers from imprecise dose delivery and complexity of treatment planning, (b) proton therapy exploits dose distributions of the Bragg peak effect has shown some superiority to IMRT, but is hampered by the very

high costs of building and maintaining the facilities,(c) stereotactic body radiotherapy (SBRT) for early-stage prostate cancer treatment exploits the alpha/ beta ratio typical of slow growing malignancies diminishes the volume of rectum and bladder irradiated during conformal therapy, but it shows only an average of 20% decrease in prostate tumor volume [7].

In all these modalities mentioned above, there is a dose that is delivered to normal tissue and it may damage healthy cells and tissues because ionizing radiation does not discriminate between cancerous and normal cells. Therefore, the administered dose is limited due to the toxicity to normal cells [8].

Second category is internal radiation therapy; only brachytherapy is used currently to treat prostate cancer inside. It uses a radioactive source such as iodine-125 or palladium-103 radioactive seeds which is put inside the body in or near the tumor. One of the major disadvantages of brachytherapy is unwanted dose delivered to the surrounding healthy tissues due to tumor shrinkage from therapy [7] and there is a rare chance of damaging normal tissue with an escaped radioactive seed [9]. Furthermore, the radiation dose is distributed heterogeneously; higher dose is delivered to an area of tumor close to the seed while lower dose is delivered to farther area. In addition, brachytherapy can cause side effects such as proctitis, cystitis, incontinence, and rectal bleeding—thus causing overall discomfort to patients [10]. Also, brachytherapy requires surgical intervention [11].

Therefore, a new cancer treatment modality is needed that can overcome all these drawbacks. Over the past two decades, there has been increasing

interest in radioactive nanotechnology for prostate cancer therapy and imaging. This interest stems from properties of radioactive nanoparticles that allow therapeutic nanoparticles to be designed and created to match the size of tumor vasculature, allowing oncologists to achieve optimal therapeutic payload with homogenous distribution and minimum leakage of radioactivity from the target site [7].

Radioactive gold nanoparticles are potentially useful for treatment and imaging of cancer, as they can deliver radiation dose directly into cancerous cells and cellular components with a higher concentration of radioactivity because each gold nanoparticle contains hundreds of atoms of gold, and some of these gold atoms are radioactive. Furthermore, radioactive gold nanoparticles can also be easily conjugated with targeting agents such as antibodies and peptides that are selective for receptors over-expressed by diseased tissue. These unique advantages present renewed opportunities in the design and development of tumor-specific nano-therapeutic agents for the diagnosis and treatment of cancer [12].

However, there are still some difficulties regarding the synthesis of radioactive gold nanoparticles that are used for medical applications. First, sodium borohydride ($NaBH_4$) used in the traditional method to reduce gold in gold salt ($AuCl_4$) to gold nanoparticles cannot be used for the production of radioactive gold nanoparticles because the radioactive gold, which is produced through neutron irradiation is available in dilute hydrochloric acid media. $NaBH_4$ reduction will not proceed in an acidic medium. Second, this production method

is unsuitable in the presence of target-specific peptides because sodium borohydride will reduce chemical functionalities present on peptide backbones, thus either reducing or eliminating the biogenecity and biospecificity of biomolecules [13]. Third, the process of nanoparticle production using $NaBH_4$ is time intensive. Therefore significant efforts have been devoted to find ways to produce radioactive gold nanoparticles to overcome the difficulties mentioned above.

This research explores an appropriate method to synthesize radioactive gold nanoparticles that may be more appropriate for cancer therapy and imaging, evaluate them in tumor models and use Monte Carlo simulations to calculate the dose distributions that is delivered by radioactive ^{198}Au and ^{199}Au nanoparticles.

This research comprises three related projects related to the production and evaluation of radioactive gold nanoparticles. The first project is an investigation of a new protocol to produce radioactive gold nanoparticles by using phytochemical reducing agent mangiferin and then perform detailed *in vitro* and *in vivo* evaluation in order to use them to treat and image prostate cancer. Second project is an investigation of a new protocol to produce radioactive ^{199}Au-nanoparticles by using sodium citrate as reductant and stabilizing agent in order to use them for imaging purposes. The third project is an estimation of dose distribution that is deposited by radioactive gold nanoparticles in human prostate tumor model using Monte Carlo N- Particle simulations (MCNP).

1.1- Nanotechnology

Nanotechnology is defined by the American Society for Testing and Materials (ASTM) as the design, characterization, production and application of structures, devices and systems by controlling shape and size at a nanometric scale [1, 14, 15]. It can offer new and improved materials that have physical and chemical properties different from those of the same material in the bulk form [1, 16] such as high surface to volume ratio, internalization into cells and their structures [17], and some types of nanoparticles can cross the blood-brain barrier [18] such as gold nanoparticles densely coated with nucleic acids, they have unique properties that allow them to pass through the blood-brain barrier and attack brain cancer [19].

Nanoparticles are defined as particles with lengths that range from 1 to 100 nm in two to three dimensions [1, 14, 15]. It is important to mention that nanoparticle size and size distribution are the most important characteristics of nanoparticles. They determine the *in vivo* distribution, biological fate, toxicity, and targeting ability of these delivery systems [18].

Cancer nanotechnology is the medical application of nanotechnology that will lead to useful research tools, advanced drug delivery systems, and new ways to diagnose and treat cancer or repair damaged tissues and cells [20]. The use of nanoparticles in medical applications has increased in recent years [10, 14]. Gold nanoparticles are one of these nanoparticles.

1.2- Gold nanoparticles

Gold compounds have been used as medicinal agents for long time [20]. Common oxidation states of gold metal include +1 (Au [I] or aurous compounds) and +3 (Au [III] or auric compounds). However, the gold within gold nanoparticles structure exists in a non-oxidized state (Au [0]) [15]. Synthesis of gold nanoparticles is not new; in the 19th century, Michael Faraday published the first scientific paper on gold nanoparticles synthesis, describing the production of colloidal gold by the reduction of aurochloric acid by phosphorous. In the late 20th century, techniques including transmission electron microscopy (TEM) and atomic force microscopy (AFM) enabled direct imaging of gold nanoparticles, and control of properties such as size and surface coating [15].

Gold nanoparticles have shown extraordinary promise for targeted imaging and therapy at the cellular and molecular level based on the following characteristics [1, 14, 20]. (a) Gold nanoparticles can selectively recognize receptors over expressed on cancer cells by conjugating vectors on their surface, (b) they have unique optical properties (i.e. surface plasmon resonance) and their optical properties are controlled by the geometry and size of AuNPs, (c) It is easy to synthesize AuNPs by several simple, economically cheap, safe, and reliable methods, and they can be easily synthesized with different shapes and sizes by using templates and changing reaction conditions, (d) gold compounds have long been used in medicine because they are biocompatible and non-toxic, (e) due to the presence of a negative charge on the surface of AuNPs, they are highly reactive. Due to the strong interaction between the gold surface

and thiol/amine containing molecules (such as organic molecules, DNA, protein, enzyme etc.), the surface of AuNPs can be easily modified [1, 14, 20]. Some characteristics which make gold nanoparticles the preferred choice for medical applications are explained below.

1.2.1- Surface plasmon resonance

Metals are characterized by the presence of free electrons [21]. For spherical metal nanoparticles much smaller than the wavelength of light (diameter d << ƛ), an electromagnetic field at a certain frequency induces a resonant coherent oscillation of the metal- free electrons across the nanoparticles. This oscillation is known as the surface plasmon resonance (SPR) [1, 21-23]. The resonance lies at visible frequencies for the noble metals Au, Ag, and Cu. The surface plasmon oscillation of the metal electrons results in a strong enhancement of absorption and scattering of electromagnetic radiation in resonance with the SPR frequency of the noble metal nanoparticles, giving them intense colors and interesting optical properties. The frequency and cross-section of SPR absorption and scattering is dependent on the metal composition, nanoparticle size and shape, dielectric properties of the surrounding medium/substrate, aggregation, and presence of inter-particle interactions [22, 24]. Au is the plasmonic metal of choice because of its much higher stability as compared to other metals [22].

1.2.2- AuNPs targeting for cancer

Among various approaches, two approaches are of profound importance for targeting nanoparticles to protein receptors that are overexpressed on various tumor cells. Those are passive and active targeting of functionalized nanoparticles [25]. Both passive and active targeting mechanisms are responsible for AuNPs entry to cancer cells [1]. Passive targeting uses the unique properties of the tumor microenvironment [26]. First, cancer tissues grow rapidly and form new blood vessels to fill their nutritional demand by a process known as angiogenesis. The angiogenic blood vessels formed in tumor tissues unlike normal blood vessels have large gaps (600-800 nm) between their vascular endothelium [27] results in leaky tumor vasculature, which is highly permeable to macromolecules relative to normal tissue. Second, a dysfunctional lymphatic drainage system, which results in enhanced fluid retention in the tumor interstitial space. As a result of these characteristics, the concentration of NPs found in tumor tissues can be up to 100X higher than those in normal tissue [1, 26]. The tumor- specific deposition, which is called Enhanced Permeability and Retention effect [28] occurs as NPs extravasate out of tumor microvasculature, leading to an accumulation of drugs in the tumor interstitium [26]. The leaky structure of cancer vessels enhances the permeability and retention effect of nanoparticles whose diameters are less than 200 nm in cancer tissues. In addition, the physico-chemical properties of nanoparticles, such as size, charge, and surface hydrophobicity, can affect the passive targeting efficiency [27].

Figure 1 shows the schematic representation of the enhanced permeability and retention effect.

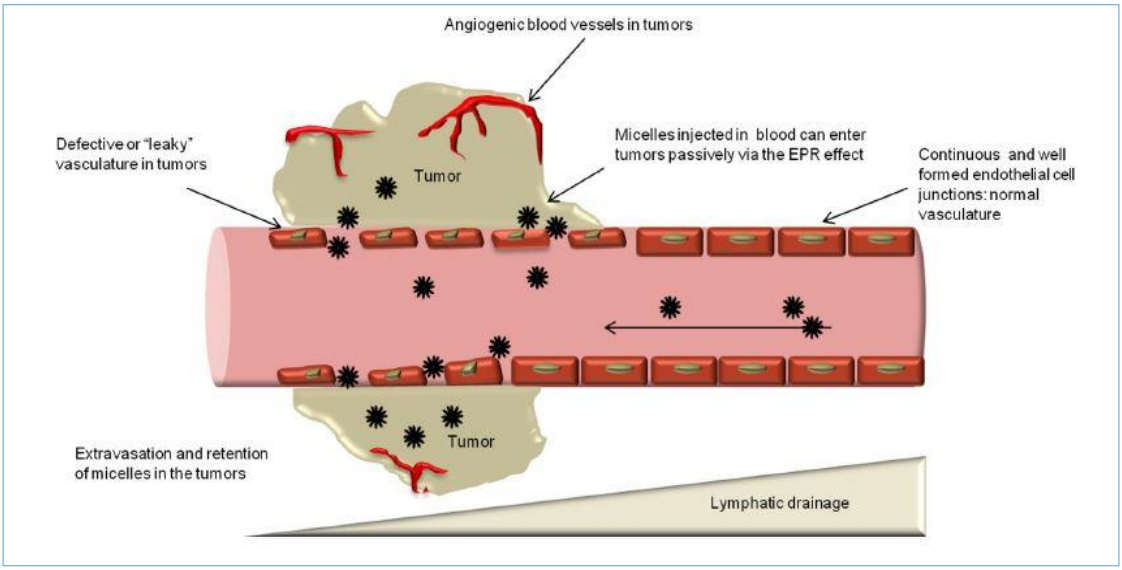

Figure 1: Schematic representation of the enhanced permeability and retention effects in tumor vasculature. Reprinted with permission from the authors of [29].

For any drug to achieve desirable therapeutic effects, it is necessary to reach the required concentration in the target tissue to exert its pharmacological effects. However, particulate drugs are rapidly removed from circulation by the reticulo endothelial system (RES). NPs are rapidly coated with serum proteins in a process known as opsonization and are ingested by phagocytes [30]. Hydrophobic particles are more rapidly opsonized than hydrophilic particles as serum proteins show enhanced absorbability to the former type of particles [30]. This effect can be improved by coating NPs with compounds such as poly

ethylene glycol (PEG). PEG can inhibit both aggregation and the adsorption of blood serum proteins on its surface, reduce uptake by the liver and consequently extend circulation time; therefore, more NPs have a chance to accumulate in the cancer through passive targeting [1].

Active targeting is an advanced approach for targeted delivery of drugs to their designated sites [27]. It takes advantage of the fact that cancer cells over-express certain receptors on their cell surface. If a nanoparticle is coated with vectors that bind specifically to these receptors, the concentration of NPs in the cancer region could be enhanced. Because of the high surface area of NPs, it is possible to attach a large number of vectors, such as peptides, antibodies, and other molecules [1].

The targeted receptors may be categorized as internalization (endocytosis) receptors or endothelium receptors. The targeting internalization receptors upon binding to the nanoparticles internalize their payload into cancer cells. While targeting endothelium receptors can destroy the cancer cells by inhibiting their growth or nutrient supply. Targeting receptors on cancer cells is a promising strategy to kill the cancerous cell without affecting normal cells [27].

1.2.3- Zeta potential

Zeta potential is a determination of the charge between two particles that keeps them separated from one another [31, 32]. To explain zeta potential in more detail, nanoparticles have a surface charge that attracts a thin layer of ions

of opposite charge to the nanoparticle surface, and this double layer of ions travels with the nanoparticle as it diffuses throughout the solution. The electric potential at the boundary of the double layer is known as the zeta potential of the particles and has values that typically range from +100 mV to -100 mV [33] . See Figure 2.

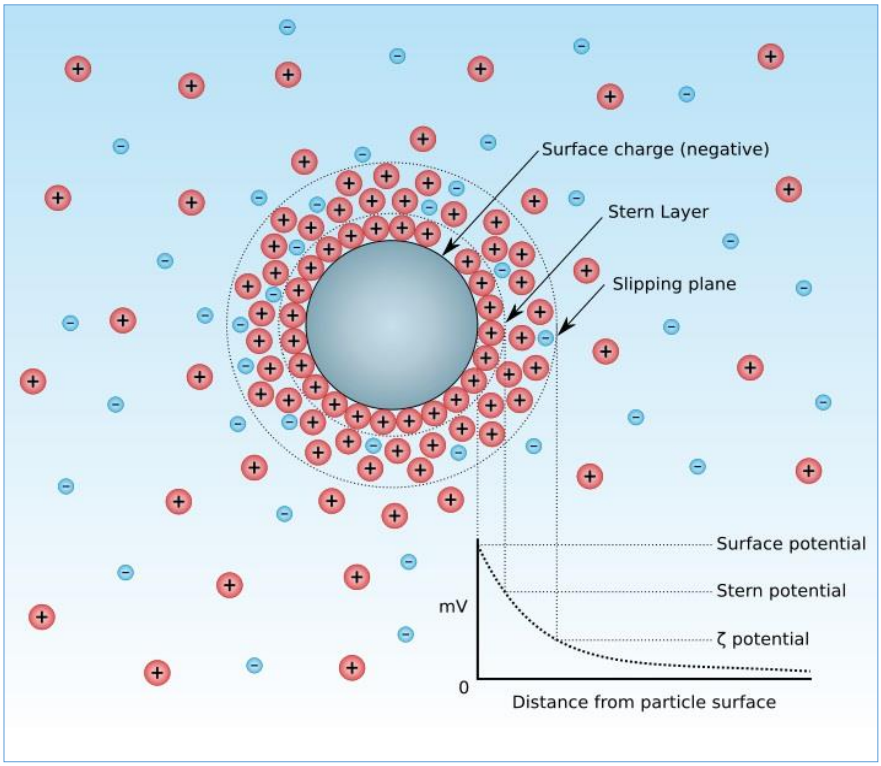

Figure 2: Schematic diagram showing the mechanism of zeta potential in nanoparticles. Reprinted under license of free use from [34].

It is important to note that zeta potential is the potential at the slip plane, not the charge on the surface of the particle as is often assumed [32]. The slip plane is a hypothetical location about 2 nm from the surface of a particle [35]. The magnitude of the zeta potential gives an indication of the potential stability of

the colloidal system. As the zeta potential increases, repulsion between particles will be greater, leading to more stable colloidal dispersion. If all particles in the suspension have a large negative or positive zeta potential then they will tend to repel each other, and there will be no tendency for the particles to come together [31, 36]. For example, nanoparticles with zeta potential values greater than +25 mV or less than -25 mV typically have high degrees of stability whereas dispersions with a low zeta potential value will eventually aggregate due to van der Waal inter-particle attractions [33].

1.3- Synthesis of gold nanoparticles

There are two basic approaches for the synthesis of nanostructured materials [37], the top-down approach which involves breaking down the bulk material into particles with nanometer sized grains, and the bottom-up approach in which individual atoms or molecules are put together to form nanoparticles [21, 37]. The first technique is performed by using a spark generator whereas the second is by using a chemical reaction [37].

1.3.1- Synthesis of GNPs by spark generator

The GFG-1000 spark aerosol generation system (Palas) consists of two electrodes, made of material of interest for generation of nanoparticles, separated by a 1.8 mm gap. One of the electrodes is connected to a high voltage (3,000 V) supply in parallel with a capacitor (20 nF) as shown in Figure 3. A

charge stored in the capacitor is discharged at a set frequency which produces sparks across the electrode gap. Each electric spark locally evaporates the electrode material in the vicinity of the spark. The evaporated material (atoms/ions) nucleates to very fine primary particles in a controlled gaseous flow, and grows further via agglomeration and condensation. The particle production rate and size are dependent on the spark frequency, the size and shape distributions are also affected by the gaseous environment and flow rate [38, 39]. The spark generation is simple, easily deliverable, and environmentally friendly [38]. However, the spark generation technique produces a very small amount of gold nanoparticles as powder every time [40]; therefore it is considered time consuming to use this method for synthesis of large amounts of nanoparticles for medical applications. Moreover, gold nanoparticles that are produced by this technique are non suspendable in comparison to those produced by wet chemistry technique which is essential for *in vivo* applications.

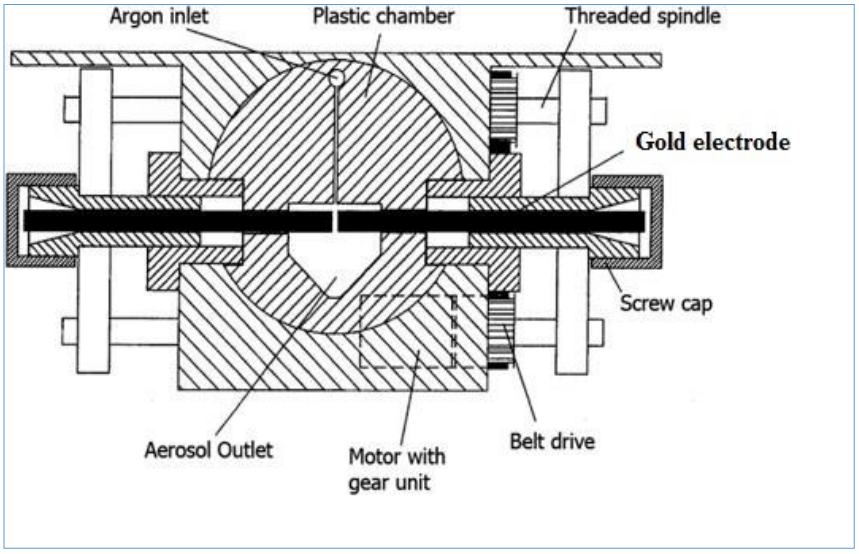

Figure 3: Schematic diagram of the electrode arrangement in the spark generator GFG-1000. Reprinted with permission from the authors of [41].

1.3.2- Synthesis of GNP by chemical reaction

Gold nanoparticles(GNP) can be synthesized by chemical reduction and there are several methods that are used to synthesize GNP based on chemical reduction such as the Turkevich method [42], Brust method [43], and Zhong method [21]. The basic principle of synthesis of GNP by chemical reduction is use of a reductant to reduce gold, which exists in oxidation state of +3, within chloroauric acid ($HAuCl_4$ to gold nanoparticles that have gold exists in a non-oxidized state (0) [15, 21]. In order to prevent the nanoparticles from aggregating, a stabilizing agent is added to the solution [21].

The bottom-up or the chemical approach is the preferred choice for nanoparticles production for medical applications. This is because the synthesis technique allows: (a) a tight control of the surface composition, such as coating, functionalization and stability, (b) production of large quantities of nanoparticles, and (c) the reaction processes are based on the reduction salts of the metal of interest (the precursor) in the presence of reducing and stabilizing agents in aqueous or organic media. By changing some key variables such as the reactants, their relative molar concentrations, the temperature, or stirring velocity, it is possible to control the nucleation and growth processes, achieving nanoparticles with the desired properties [21].

Therefore, in this study, gold nanoparticles were synthesized by the chemical reduction approach.

1.4- Green nanotechnology

Green nanotechnology involves deliberate efforts aimed at developing meaningful and reasonable protocols for generating products and their associated production processes in an environmentally benign fashion to minimize the use of toxic chemicals [44]. Green nanotechnology, directly or indirectly, is intended to save living organism thus causing minimal/no damage to our environment. Green synthesis of gold nanoparticles means using phytochemicals as reducing agents as well as stabilizing agents instead of chemical compounds that have some toxicity which may adsorb on the surface and cause adverse effects in medical applications [45]. Several studies have shown that production of nanoparticles using phytochemicals derived from plant species minimizes or eliminates the use of harsh chemicals, thereby resulting in true green and eco-friendly industrial processes for the manufacture of nanoparticle- based smart materials [46]. Furthermore, the size and rate of formation of nanoparticles can be manipulated by controlling parameters such as pH, temperature, substrate concentration and exposure time to substrate [47].

Various herbs and plant sources contain powerful antioxidants in their seeds, stems, fruits and leaves. These naturally occurring antioxidants have existed in the human food chain for thousands of years and are known to be non-toxic to living organisms and to the environment [46]. Several studies reported the application of phytochemicals that are available in soy [48], tea [13], and cinnamon [46] as dual reductant and stabilizing agents for the synthesis of gold

nanoparticles. In this study, mangiferin has been used as the reductant and stabilizing agent for the green synthesis of radioactive gold nanoparticles.

1.4.1- Mangiferin

Mangiferin is a naturally occurring glucosylxanthone, and the IUPAC ID is (1, 3, 6, 7-tetrahydroxyxanthone-C (2)-β-D-glucoside). Mangiferin exists in several folk medicines and food such as the mango, which is one of the most popular, nutritionally rich tropical fruits [49, 50].

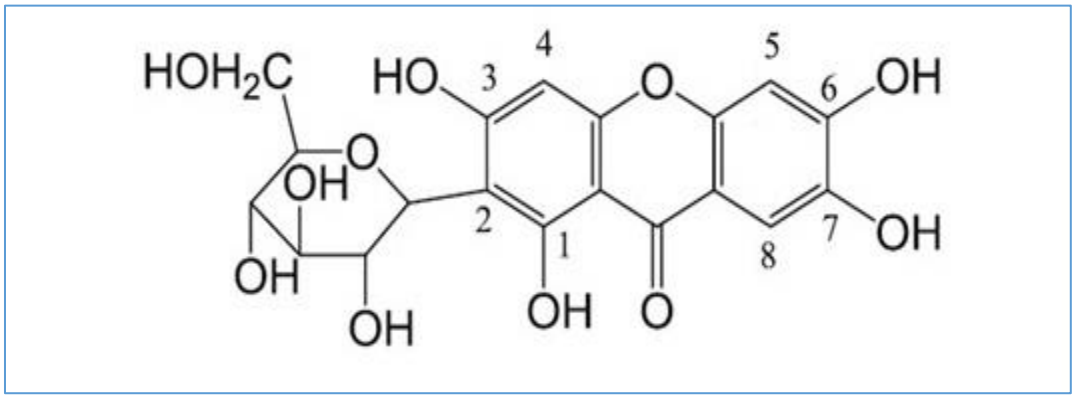

Figure 4: Chemical structure of mangiferin. Reprinted with permission from the authors of [51].

Mangiferin has been shown to exert many beneficial biological activities including anti-oxidant, anti-tumor growth, anti-inflammatory, metabolic regulations, immune regulations, and neuroprotective [49, 50]. The two most important biological activities that we are concerned about in this research are anti-oxidant and anti-tumor growth.

The anti-oxidative activity of mangiferin has been demonstrated as the free radical scavenger in medicinal plants. Mangiferin bears a catechol moiety, a pharmacophore with well-established antioxidant properties. Also, mangiferin has several free hydroxyl groups. The anti- oxidative mechanisms of mangiferin come from its free hydroxyl groups and catechol [49, 50].

Mangiferin is being evaluated as a drug candidate for cancers because it could inhibit tumor cellular proliferation and activate the lymphocytes in cancer-bearing mice[49, 50]. The possible antitumor mechanisms of mangiferin included the anti-genotoxic action on cadmium chloride($CdCl_2$)-induced toxicity in mice, the inhibition of the telomerase and the gene and the enhancement of the cellular apoptosis [50]. On the other hand, Hongzhong Li et al indicated in their study on breast cancer that mangiferin exhibits significant effects on inhibition of cell proliferation and metastatic ability in breast cancer cells through modulating matrix metalloproteinases(MMPs), epithelial-mesenchymal transition (EMT) and β-catenin pathway [49].

The anti-oxidative and anti-cancer activities make mangiferin an excellent candidate to use as part of nanoparticles synthesis process.

1.5- Sodium citrate

Sodium citrate refers to the sodium salts of citric acid [52]. The IUPAC ID is (trisodium; 2-hydroxypropane-1, 2, 3-tricarboxylate), and the molecular formula is $C_6H_7NaO_7$ [53] as shown in figure 5. Sodium citrate is a white, odorless,

crystalline compound found in granular form. A small amount of this substance is found naturally in the body [52].

There are many uses for sodium citrate such as medicinal and nutritional uses. Sodium citrate is used to make the urine less acidic to help the kidneys get rid of uric acid to prevent gout and certain types of kidney stones (urate). Sodium citrate can also prevent and treat certain metabolic problems (acidosis) caused by kidney disease [54, 55]. For nutritional uses, sodium citrate is mainly used as a food additive, usually for flavor or as a preservative. It reduces the acidity of foods. sodium citrate is also used as an antioxidant in food [56]. The antioxidant characteristic makes sodium citrate good candidate to produce radioactive gold nanoparticles.

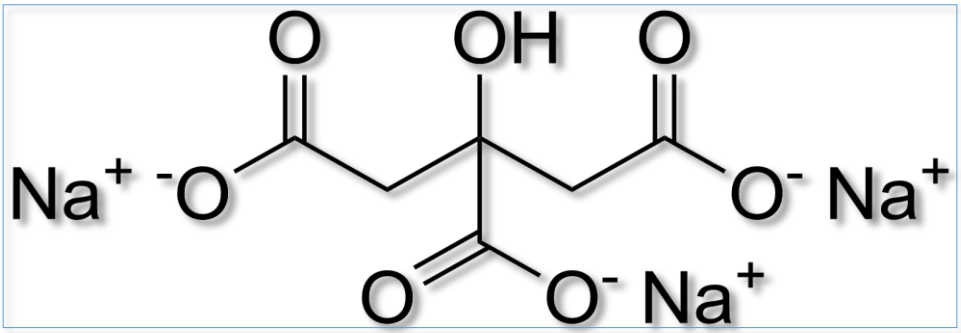

Figure 5: Chemical structure of sodium citrate. Reprinted under the license of free use from [57].

1.6- Radioactive gold nanoparticles

The synthesis of radioactive gold nanoparticles is somewhat similar to that of non-radioactive gold nanoparticles with some differences. First, radioactive

gold salt, which containing the radioactive gold isotope (^{198}Au/^{199}Au), is used as the precursor in radioactive gold nanoparticle synthesis instead of non-radioactive gold salt [58]. Second, the solution is more acidic and changes maybe required to accommodate the higher acidity and low pH.

In this research, ^{198}Au and ^{199}Au were used to produce radioactive gold nanoparticles. Gold-198 is an artificial radioactive isotope with atomic mass of 198 and atomic number of 79. Gold-198 is prepared by irradiation of gold foil (^{197}Au) by neutrons [59].

$$^{197}\mathbf{Au} + \mathbf{n} \longrightarrow {}^{198}\mathbf{Au} + \beta \longrightarrow {}^{198}\mathbf{Hg}^{*} + \gamma \longrightarrow {}^{198}\mathbf{Hg}$$

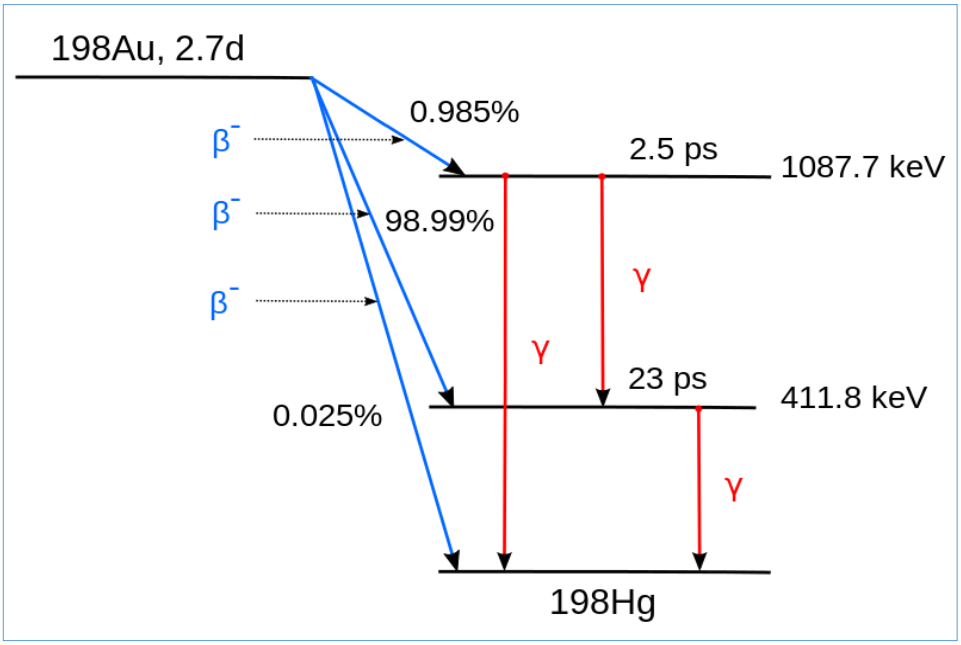

Figure 6: Gold-198 decay scheme. Reprinted under the license of free use from [60].

gold-198 has a half-life of 2.7 days and disintegrates with the emission of a 0.96 MeV beta with a branching ratio of 98.9% to unstable mercury which emits a 0.41 MeV photon with a branching ratio of 95.6% to reach the stable state of mercury as the end-product of the disintegration [59] as shown in Figure 6.

Gold-199 is also an artificial radioactive isotope with an atomic mass of 199 and atomic number of 79. Gold-199 can be obtained as a β-decay product of neutron activated natural or enriched platinum (^{198}Pt), and separated by liquid–liquid extraction. gold-199 produced in this manner is carrier free and thus high specific activity [61, 62].

$$^{198}Pt + n \longrightarrow {}^{199}Pt + \beta \longrightarrow {}^{199}Au + \beta \longrightarrow {}^{199}Hg^{*} + \gamma \longrightarrow {}^{199}Hg$$

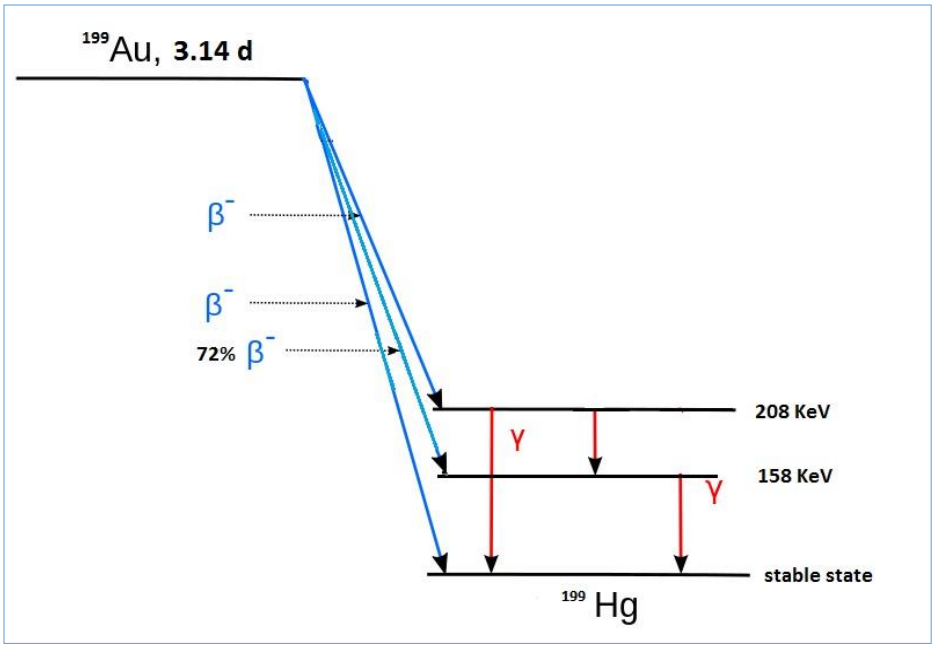

Figure 7: Gold-199 decay scheme. Gold-199 decay scheme. It was plotted according to the information from [62].

Gold-199 has a half-life of 3.13 days; it decays to unstable mercury (^{199}Hg*) by the emission of a 0.294 MeV beta with a branching ratio of 72.0%, then unstable mercury emits 0.1584 MeV photon with a branching ratio of 40% to reach the stable state [62] as shown in Figure 7. The radioactive properties of ^{198}Au and ^{199}Au make them ideal candidates for use in radio -therapeutic applications. In addition, they both have imageable gamma emissions for dosimetry and pharmacokinetic studies [12].

The range of the β-particle is sufficiently long enough to deliver a high dose to kill tumor cells within the prostate gland and is short enough to minimize significant radiation dose to critical tissues near the periphery of the tumor. The 2.7 and 3.1 day half-life of ^{198}Au and ^{199}Au allows enough time for radioactive gold nanoparticles to reach the tumor and deposits their radiation dose in the tumor [58]**.** Therefore, it is not necessary to remove the source of radiation as is the case with other sources, because after approximately 10 days of radioactive gold nanoparticles administration, there is very low percentage of the activity, and this is an important matter regarding radiation safety to the patient as well as the public.

Gold-198 is being evaluated as a potential therapeutic agent for the treatment of prostate cancer. It has been used in brachytherapy applications as permanent seed implants. However, there is a limitation of using ^{198}Au seeds because of a heterogeneous dose distribution with a higher dose near the seeds and lower doses between them. Therefore use of ^{198}Au-nanoparticles can overcome this limitation. Gold-198 nanoparticles can deliver dose with

homogeneous distribution to tumor tissues while minimizing the dose to normal tissues [63].

Gold-198 nanoparticles and gold-199 nanoparticles deliver dose through the emission of beta and gamma. The dose distributions delivered to tumor as well as to normal tissues surrounding the tumor can be estimated by using Monte Carlo method.

1.7- Monte Carlo method

The Monte Carlo method is based on random simulations of events with the knowledge of the probabilities associated therein. As with most Monte Carlo simulations, the results are governed by Poisson statistics, thus the error decreases as the square root of the number of simulations is performed [64].

Monte Carlo can be used to duplicate theoretically a statistical process (such as the interaction of nuclear particles with materials) and is particularly useful for complex problems that defy deterministic methods. The individual probabilistic events that comprise a process are simulated sequentially. The probability distributions governing these events are statistically sampled to describe the total phenomenon. In general, the simulation is performed on a digital computer because the number of trials necessary to describe the phenomenon is usually quite large. The statistical sampling process is based on the selection of random numbers—analogous to throwing dice in a gambling casino. In particle transport, the Monte Carlo technique is a theoretical

experiment. It consists of actually following each of many particles from a source throughout its life to its death in some terminal categories (absorption, escape, etc.). Probability distributions are sampled to determine the outcome at each step of the “rahdom walk” [65]. This “particle tracking” nature of Monte Carlo allows the user to study complex areas of radiation transport [66].

Among the methods available for complex cases, Monte Carlo is considered the most accurate method of dose calculation because it models the actual processes that culminate in dose deposition [66]. MCNP is a general-purpose Monte Carlo N–Particle code, which is developed and maintained by the Los Alamos National Laboratory. MCNP can be used for neutron, photon, electron, or coupled neutron/photon/electron transport, including the capability to calculate Eigen-values for critical systems. The code treats an arbitrary three-dimensional configuration of materials in geometric cells bounded by first- and second-degree surfaces and fourth-degree elliptical tori [65, 67].

Important standard features that make MCNP very versatile and easy to use include a powerful general source, criticality source, and surface source, geometry and output tally plotters, a rich collection of variance reduction techniques, a flexible tally structure, and an extensive collection of cross-section data [65, 68].

1.8- Prostate gland physiology

The prostate is a walnut-sized gland located in front of the rectum and below the urinary bladder. The urethra runs through the center of the prostate, from the bladder to the penis, letting urine flow out of the body [69, 70].

A healthy human prostate is slightly larger than a walnut. The mean weight of the "normal" prostate in adult males is about 11 grams [71] and it measures 4 x 2 x 3 centimeters. The size of the prostate varies with age, the size increases as a man gets older [28].

The human prostate is the site of origin for the two most prevalent diseases of elderly men: benign prostatic hyperplasia and prostate cancer. These two prostate diseases account for a significant proportion of the health care dollars spent on morbidity and mortality in the aging male population [70].

The predominant treatment of benign prostatic hyperplasia over the last 60 years has been based on an ablative surgical approach. In recent years, different new treatment modalities for symptomatic benign prostatic hyperplasia ranging from watchful waiting to surgery. Determination of the appropriate treatment method depends on the disease stage and the patient age nevertheless, this disease is rarely lethal [72].

Prostate cancer can be aggressive and it can be lethal if not treated at the early stages. As mentioned previously, there are many different modalities that are used clinically to treat prostate cancer such as chemotherapy[4], hormonal therapy, surgery, and radiation therapy [4, 5]. Oncologists determine the

appropriate treatment modality that can be used to treat the tumor depending on the stage of the prostate cancer and patient's age[4].

Use of radioactive gold nanoparticles is a promising treatment modality to treat prostate cancer. At present, it is still in the experimental phase in animals. The results from these trials are promising and further investigations could bring this modality to clinical use in future.

1.9- Literature review

In recent years, there is spawning of interest toward the application of functionalized gold nanoparticles for drug delivery, cancer therapy, and as contrast agents in imaging [15, 73].

The present research is in the field of radiotherapy is about production and use of radioactive gold nanoparticles to treat and image the cancer and to calculate dose distribution by MCNP simulations. Therefore, in this review of the literature, we limit the review of publications to those that contain one of the aspects that are mentioned below.

- Production and use of radioactive gold- nanoparticles to treat cancer.
- Synthesis of gold nanoparticles by using mangiferin.
- Synthesis of gold nanoparticles by using sodium citrate
- Calculation of the dose distribution which is deposited by radioactive nanoparticles via using MCNP.

1.9.1- Production and use of radioactive gold nanoparticles to treat cancer.

The pioneering experimental work of production of radioactive gold nanoparticles by using non-toxic compounds was done by Katti and coworkers. In 2006, Katti and his team [12] reported an efficient methodology to generate radioactive gold nanoparticles by using a nontoxic reductant and a stabilizing agent. They used trimeric alanine phosphine conjugate (THPAL), which is referred to it now as Katti peptides [74, 75], as the reductant agent which is a nontoxic compound, and gum arabic which is edible and nontoxic as stabilizing agent. After the radioactive gold was prepared and mixed with gold salt, next was added the gum arabic and Katti peptides (THPAL) which resulted in an immediate color change from yellow to burgundy and that is a good indication of formation of ^{198}Au-nanoparticles. Notice that, surrogate non-radioactive THPAL gold nanoparticles are synthesized by the same procedure that was used to synthesize ^{198}Au-nanoparticles, except the gold salt precursor was non-radioactive while in ^{198}Au-nanoparticles production, a radioactive gold precursor was used.

After they produced the new radioactive gold nanoparticles, they studied *in vitro* as well as *in vivo* stability. *In vitro* stability studies carried out with AuNPs stabilized by gum arabic demonstrated that the GA-radioactive gold nanoparticles are stable. Also, addition of 10 % of NaCl or pH 7.0 phosphate buffer solutions to the GA- nanoparticles did not cause any aggregation or decomposition of nanoparticles. The bio-distribution study or *in vivo* stability of

nanoparticles was carried out by the injection of normal mice with GA-^{198}AuNPs. *In vivo* stability of nanoparticles in animal models is measured by their accumulation in blood after administration. Unstable nanoparticles interact with serum proteins and would be expected to show higher uptake in blood and/or aggregate in blood to form macro nanoparticles, while stable nanoparticles show minimal accumulation in blood. Therefore, the degree of aggregation *in vivo* can be measured by analyzing the concentration of nanoparticles in blood. The results clearly showed these nanoparticles are stable *in vivo* because they showed minimal accumulation in blood [12].

Kannan et al (2011) studied the GA-^{198}AuNPs that were discovered by Katti et al. Kannan et al investigated and evaluated the intra prostate tumoral delivery and retention of GA-^{198}AuNPs, and calculated the approximate dose that can be delivered to a tumor by radioactive gold nanoparticles. They performed a detailed *in vivo* investigation involving intratumoral administration of GA-^{198}AuNPs (3.5 μCi/tumor) in SCID mice (n = 5) bearing human prostate cancer xenografts. This study involved the analysis of ^{198}Au in various organs post-euthanasia of animals at 30 min, 1, 2, 4, and 24 h. An analysis of ^{198}Au radioactivity revealed that over 75% of the injected dose (ID) of GA-^{198}AuNPs was retained in prostate tumors at 24 h, and was nearly constant from 30 min to 24 h. This study confirmed the excellent retention and homogeneous distribution of therapeutic payloads of GA-^{198}AuNPs nanoparticles within prostate tumors with only minor leakage to non-target organs [58].

In 2010, Chanda et al [10] synthesized gum arabic radioactive gold nanoparticles (GA-^{198}AuNPs) by using the same procedure that was reported by Katti et al, and they studied the *in vivo* therapeutic efficacy of this type of nanoparticle. They used SCID mice bearing a flank model of human prostate cancer derived from a subcutaneous implant of 5×10^{6} PC-3 cells. Unilateral solid tumors were allowed to grow for 3 weeks, and animals were randomized at day 0 into control and treatment groups (n = 7) with no significant differences in tumor volume. On eighth day, 30 µL of GA-^{198}AuNPs (408 µCi) was injected directly into the tumor to deliver an estimated dose of 70 Gy. Control SCID mice received 30 µL DPBS. Tumors were then measured twice each week. This therapeutic study was maintained throughout the 30-day period post treatment. Tumor growth in the treated animals compared to the controls was slower with the controls being fully fivefold larger than those in the radiotherapy group after three weeks. The control group exhibited weight loss, deteriorating overall health status, and were euthanized before the end of study period .By contrast, none of the seven animals in the treatment group reached early-termination criteria.

The results of Chanda et al (2010) study showed that GA-^{198}AuNPs are able to reduce the tumor volume by 82% in prostate tumor–bearing SCID mice, and this is an important clinical development showing the potential for clinical translation of this agent in reducing the size of tumors before surgical resection and possibly even reducing or eliminating the need for surgical resection in certain circumstances.

A new protocol of synthesis of radioactive gold nanoparticles by using phytochemicals has been developed. EGCG-^{198}AuNPs were produced by using EGCG as reductant and stabilizing agent to convert the radioactive gold precursor to radioactive gold nanoparticles. EGCG is a phytochemical and has been used for a long time as a food supplement because of its strong antioxidant properties [7]. The study performed by Shukla et al (2012) showed the excellent retention of therapeutic payloads of EGCG-^{198}AuNPs within prostate tumors in mice, this study has confirmed that over 70% of the injected dose of EGCG-^{198}AuNPs was retained within prostate tumors up to 24 h. This excellent retention was attributed to EPR effect as well as to the high affinity of the EGCG-gold nanoparticles toward Laminin receptors which are over-expressed on prostate cancer cells. Also, therapeutic efficacy study results showed that the reduction of tumor volume after administration of EGCG-^{198}AuNPs was comparable to results of volume reduction by using GA-^{198}AuNPs although less activity (136 µCi) of EGCG- ^{198}AuNPs was used [7].

This present study, a new protocol was established to produce radioactive ^{198}Au-nanoparticles; mangiferin was used in the current study as a reductant and stabilizing agent.

Regarding ^{199}Au, to date, there is only one research paper about GA-^{199}AuNPs that was conducted by Cutler and coworkers (2012). The authors evaluated GA-^{199}AuNPs in normal dogs. And they found that these nanoparticles remain trapped in the prostate gland for at least 8 days and exhibit minimal leakage into other organs. They showed that the nanoparticles distributed

uniformly resulted in a homogeneous radiation dose to prostate cancer cells located within the gland [76].

To date, there has been no other publication reporting the use of mangiferin or citrate as reductant and stabilizing agent to produce radioactive ^{198}Au- nanoparticles or ^{199}Au-nanoparticles.

1.9.2- Synthesis of gold nanoparticles by using mangiferin

Indeed there are many authors who reported synthesis of gold nanoparticles by using phytochemicals such as cinnamon [46], soybeans [48], tea [13], EGCG [7], and others, but no researcher has reported to date the use of mangiferin as the reductant and stabilizing agent to produce gold nanoparticles. For example, Philip (2010) reported the synthesis of gold nanoparticles using the extract of Mangifera indica leaves, which is the source of mangiferin. He mentioned that Mangifera indica as whole can cause the reduction of gold to gold nanoparticles. However he did not mention any specific compound in Mangifera indica that is responsible for the reduction reaction [45]. Also, Lal and Nayak (2012) wrote about using Mango leaves to synthesize gold nanoparticles, they mentioned that the main active components are mangiferin and chinoin. However they did not mention that mangiferin is acting as reductant and stabilizing agent and was responsible for synthesis of gold nanoparticles. And they used a different procedure to produce gold nanoparticles [77].

1.9.3- Synthesis of gold nanoparticles by using sodium citrate

In 1951, Turkevich et al [78] discovered the citrate reduction method to produce citrate gold nanoparticles. They used sodium citrate as reductant to reduce the chlorauric acid solution ($HAuCl_4$) to gold nanoparticles. They described the procedure of preparation in which $HAuCl_4$ was stirred and heated to the boiling point. At the boiling point, sodium citrate solution was added to the boiling solution with continuous stirring. After about a minute a very faint greyish-pink or greyish-blue tone appeared gradually darkening over a period of about 5 min. The final color was deep wine red which indicates the formation of citrate gold nanoparticles that have a size of approximately 20 nm. This method is called the Turkevich method relative to John Turkevich who discovered it.

After the discovery of the Turkevich method, there were many researchers who have used it with or without modifications to produce and characterize citrate-gold nanoparticles with different sizes [79-89]. These previous studies have shown the characteristics of citrate-gold nanoparticles. The characteristics of citrate-gold nanoparticles are mentioned below.

The surface Plasmon resonance wave length (λ_{max}): According to previous studies, λ_{max} of citrate- AuNPs is approximately 520 nm [80, 81, 83].

Morphology and size distribution: Grabar et al (1995) indicated that the size of citrate gold nanoparticles falls in the range of 13 ± 1.7 nm. The TEM

image in that article showed that citrate gold nanoparticles have spherical shape and dispersed uniformly [80].

The hydrodynamic size and zeta potential measurements: In 2014, Verma et al [83] synthesized and characterized citrate gold nanoparticles by the citrate reduction method (Turkevich method). They measured the hydrodynamic size and zeta potential. According to their study, the hydrodynamic size was (18 nm) and zeta potential was highly negative, its value was approximately (-40 mV).

In vitro stability study: In 2014, Vijayakumar [85] investigated the *in vitro* stability of citrate gold nanoparticles. The stability of gold nanoparticles was analyzed by the addition of different concentrations of electrolyte (NaCl), change of pH of the gold solution and time of storage at room temperature. The stabilities were monitored by using UV-Visible spectroscopy and measuring zeta potential of the gold nanoparticle solution. He found that these nanoparticles are stable out to 10 days.

Uptake and cytotoxicity of citrate- gold nanoparticles: Several studies have shown that citrate gold nanoparticles are taken up by different human cell lines [86-88]. There were many studies undertaken to study the cytotoxicity of citrate-gold nanoparticles on different human cell lines in order to determine whether or not citrate-gold nanoparticles are biocompatible and can be used in medical applications [86-89]. In 2005, Connor et al [86] studied the viability of human leukemia cells after these cells were incubated with different concentrations of citrate- gold nanoparticles for three days. Cell viability was

determined using the MTT assay. They found that the 18-nm citrate-gold nanoparticle did not appear to be toxic at concentrations up to 250 μM (gold atoms).

Another study was carried out by Vijayakumar and Ganesan (2012) to investigate *In vitro* cytotoxicity of three types of gold nanoparticles citrate-AuNPs, starch-AuNPs, and gum arabic-AuNPs using MTT assay. PC-3 and MCF-7 cells were incubated with (20, 50, 80, 110, and 140 μg/mL) concentration of AuNPs for 24h, after that, they were subjected to the MTT assay for cell viability determination. The results showed that PC-3 and MCF-7 cells have excellent viability even up to the concentration of 140 μg of citrate-, starch-, and gum arabic-capped gold nanoparticles. However, the citrate stabilized gold nanoparticles show less viability compared to starch and gum arabic. The gum arabic is highly more viable than starch and citrate [89].

Freese et al (2012) examined the effects of citrate- gold nanoparticles on the viability of human microvascular endothelial cells. They also investigated the relationship between cytotoxicity and the amount of internalized citrate- AuNPs. In that study, cells were exposed to different concentrations (50-100-500-1000 μM) of 10 nm- and 25 nm-sized citrate-gold nanoparticles for 48 h, and cell viability was measured using the CellTiter 96W AQueous Non-Radioactive Cell Proliferation Assay (MTS). The results showed there is a decrease in the cell viability of hCMEC endothelial cells when citrate- AuNPs concentrations were above 500 μM [87].

In 2013, Vetten et al [88] investigated the cytotoxicity and uptake of 14 nm and 20 nm citrate-AuNPs in three cell lines which are the bronchial epithelial cell line BEAS-2B, the Chinese hamster ovary cell line CHO, and the human embryonic kidney cell line HEK 293. The cytotoxicity of the 14 nm AuNPs was determined by the CytoTox-ONE™ assay. From this assay data, the citrate-AuNPs are considered non-toxic.

In the present study, the protocol by Graber et al [80] was chosen to produce radioactive citrate-gold nanoparticles that are less than 15 nm. Unfortunately, that protocol was not successful and radioactive gold nanoparticles were not formed. The reason behind the failure was the pH of the solution being too low after adding ^{199}Au which prevented the formation of nanoparticles. Therefore, a series of experiments were performed to develop a new protocol.

1.9.4- Calculation of the dose distribution which is deposited by radioactive nanoparticles via using MCNP

Only a few papers have reported using MCNP to calculate the dose distribution deposited by radioactive nanoparticles [90, 91]. Bouchat et al (2007) studied the doses deposited inside and around a spherical solid tumor by radioactive ^{90}Y-nanoparticles of 5 nm diameter. They developed new three-dimensional vascular models representing the tumor, and then they calculated the deposited dose distribution for each model by using MCNPX. Nuttens et al

(2008) built a simple geometrical model for the simulation. They assumed the solid tumor is a sphere of radius R, and then they studied the distribution of the dose inside the tumor and in the surrounding healthy tissues as a function of the tumor radius.

In this research study, MCNP is used to simulate a simple geometrical model of a human prostate, and then calculate the dose distribution that is deposited by radioactive gold nanoparticles (^{198}AuNPs / ^{199}AuNPs).

1.10- Objectives of this study

The main goal of this research was to explore new protocols to synthesize biocompatible radioactive gold nanoparticles to treat and image cancer and calculate the dose distribution by using MCNP in human prostate.

This project is classfied into three parts. The objective of the first part is production and evaluation of radioactive MGF-^{198}AuNPs and MGF-^{199}AuNPs in order to use them for prostate cancer treatment and imaging. In this study, radioactive MGF-^{198}AuNPs and MGF-^{199}AuNPs were produced and evaluated.

The objective of the second part is production and evaluation of radioactive citrate-^{199}AuNPs as imaging probe for single photon emission computed tomography. In this study, radioactive citrate-^{199}AuNPs were produced and characterized.

The objective of the third part is an estimation, by means of MCNP simulations, the dose distribution delivered by radioactive gold nanoparticles

(^{198}AuNPs or^{199}AuNPs) to tumor inside the human prostate as well as to the normal tissues surrounding the tumor using water and A-150 tissue equivalent plastic phantoms.

CHAPTER 2

MATERIALS AND METHODS

2.1- Materials

Chemicals: All chemicals were research grade unless otherwise stated. Sodium tetrachloroaurate (Na_2AuCl_4) (99.999%) and mangiferin were purchased from Sigma Aldrich Company (St. Louis, MO). Sodium citrate was obtained from Fisher Scientific Company (Pittsburgh, PA). Gold foil used to produce ^{198}Au was purchased from Alfa Aesar Company (Ward Hill, MA). Enriched 95.83% platinum-198 metal powder used to produce ^{199}Au was obtained from Trace Sciences (Ontario, Canada).

Other Chemicals used in the study such as Human serum albumin (HSA) and bovine serum albumin (BSA) were purchased from Sigma Company. Cysteine and histidine were bought from Acros organics. Sodium chloride (NaCl) and buffer solution (pH=7 and pH=9) were procured from Fisher Scientific. Ethyl acetate and sodium hydroxide (NaOH) were obtained from Fisher Scientific Company (Pittsburgh, PA). Dulbecco's Phosphate Buffered Saline x1(DPBS) was obtained from Sigma Aldrich Company (St. Louis, MO).

Milli-Q water produced in-house (18.2 MΩ·cm at 25 °C) was used in the synthesis of radioactive mangiferin gold nanoparticlrs and radioactive citrate gold nanoparticles.

Measurements: The absorption measurements were performed using a Varian Cary 50 UV–Vis spectrophotometer at the institute of Green Technology and Ocean optics USB 2000 at MURR. The TEM images were obtained on a JEOL 1400 TEM (JEOL, LTE, Tokyo, Japan) at the University of Missouri's Electron Microscopy Core Facility. The hydrodynamic diameter and zeta potential were obtained using Zetasizer Nano S90 (Malvern Instruments Ltd., USA). Internalization study of MGF-AuNPs was performed using dark field cyto-viva microscopic techniques. The concentration of gold metal was estimated by Neutron Activation Analysis at MURR. The radio-nuclidic purity of non-carrier added ^{199}Au was measured using a High Purity Germanium detector with Genie-2000 Procount software. Dose Calibrator (Capintec) was used to measure the activity of radionuclides. The yield of radioactive gold nanoparticles was evaluated through using Radio-Thin Layer Chromatography (TLC) technique at MURR. Radio-TLC was conducted on a Bio-scanner AR-2000 radio-TLC scanner equipped with 10% methane: argon gas supply and a PC interface running Winscan V.3 analysis software.

Cell culture: All chemicals used in cell culture were procured from standard vendors. Roswell Park Memorial Institute Medium (RPMI), Medium 200, Trypan blue, dimethyl sulfoxide anhydrous (DMSO), MTT (3-(4,5-dimethylthiazol-2-yl)-2,5 diphenyltetrazolium bromide)), and DAPI dyes(40,6-diamidino-2-phenylindole Dye) were obtained from Sigma (St. Louis, MO). Fetal bovine serum and (FBS) and TryplE were purchased from Gibco BRL (Grand Island, NY). Paraformaldehyde (PFA) was bought from Electron Microscopy Sciences

and Gentamicin antipitic from APP Pharmaceuticals LLC. Dulbecco's Phosphate Buffered Saline x1(DPBS) was obtained from Sigma Aldrich Company (St. Louis, MO).

Prostate cancer cells (PC-3) and human aortic endothelial cells (HAEC) lines were obtained from the American Type Culture Collection (ATCC; Manassas, VA), Analytical standards were purchased from Fluka-Sigma-Aldrich. Double distilled water was used throughout the experiments.

Animal studies: All experiments of radioactive MGF-^{198}AuNPs involving animals were approved by the Institutional Animal Care and Use Committees (IACUC) of the Harry S. Truman Memorial Veterans Hospital and the University of Missouri, and were performed according to the Guide for the Care and Use of Laboratory Animals. Normal, female CF-1 mice were used in the bio-distribution study of the MGF-^{198}AuNPs while imprinting control regions- Severe combined immunodeficiency (ICR - SCID) female mice (from Taconic Farms, Hudson, New York) were used in the intra-tumoral and therapeutic study. The mice weighed 23-28 grams. The PC-3 human prostate cancer cell line, that was implanted in the mouse's flank, was obtained from the American Type Culture Collection (ATCC; Manassas, VA), and cultured by the University of Missouri Cell and Immunobiology Core facility using procedures recommended by ATCC.

Statistical Analysis: All values are expressed as average ± SD in the experiments addressing cytotoxicity, biodistribution, intratumoral, and therapeutic studies.

2.2- Method of production and evaluation of radioactive MGF-^{198}AuNPs and MGF-^{199}AuNPs.

In this section, methods of synthesis, characterization, and *in vitro* evaluation of non-radioactive mangiferin gold nanoparticles are described first. After that, methods of synthesis, characterization, and *in vivo* evaluation of radioactive MGF-^{198}Au NPs are described. Finally, the methods of synthesis and characterization of radioactive MGF-^{199}AuNPs is mentioned.

2.2.1- Synthesis and characterization of MGF-AuNPs

MGF- AuNPs were synthesized by adding 1.4 mg of MGF to a glass vial (20 ml scintillation vial), followed by the addition of 2 mL of double distilled water. The reaction mixture was stirred vigorously and continuously and brought to a rolling boil (99-100°C). Next 33.5 µL of 0.1M Na_2AuCl_4 solution was added to the reaction solution resulting in an immediate color change from pale yellow to red-purple. The heat was turned off, and stirring continued for an additional hour. The red- purple color of the mixture was a good indication of the formation of MGF-gold nanoparticles.

The surface plasmon resonance wave length (λ_{max}) was measured by UV-Vis spectroscopy. Two hundred microliters of nanoparticles solution was added to 800 µl of H_2O in a transparent cuvette. Then, the λ_{max} was measured.

Nanoparticles images were obtained using Transmission Electron Microscope (TEM) technique. TEM samples were prepared by placing 5 µL of gold nanoparticles solution on the 300 mesh carbon coated copper grid and allowed to sit for five minutes; excess solution was removed carefully and the grid was allowed to dry for an additional ten minutes. The core size distribution of gold nanoparticles was performed by the analysis of TEM images through the Image J program software.

Hydrodynamic size of MGF coated gold nanoparticles and zeta potential were measured using the dynamic light scattering method (DLS). Nanoparticles sample was added in a transparent cuvette, and this cuvette was placed inside DLS machine, next the hydrodynamic size and zeta potential were measured.

2.2.2- Dilution study

Some medical applications require different concentrations of gold nanoparticles. Therefore, to ascertain that dilution of nanoparticles into different concentrations does not affect their stability and does not alter their physical and chemical properties *in vivo*, a dilution study was performed by diluting NPs to different concentrations.

Nanoparticles solution was diluted to different concentrations (82.15, 55, 41.25, 20.62, 10.31, 5.15 µg/ml), and UV-Vis spectroscopy was used to record absorbance spectrum for each concentration.

2.2.3- *In vitro* stability study

In Vitro stability study was performed by mixing gold nanoparticles solution with NaCl, histidine, cysteine, BSA, HSA, pH7, or pH 9.

Typically, 1 mL of gold nanoparticle solution was added to glass vials containing 0.5 mL of each NaCl (1%), histidine (0.2 M), cysteine (0.5%), BSA, (0.5%), HSA (0.5%), pH7, pH 9, or H_2O and incubated at different time periods. The stability of gold nanoparticles was evaluated by monitoring the UV absorbance spectrum at the following time points: 1 h, 4 h, 24 h, 48 h,1 week, and 2 weeks. If the nanoparticles are stable, they should have approximately the same wavelength (λ_{max}) which is equal to wavelength of control sample.

2.2.4- Cellular internalization study

In order to ensure that MGF-gold nanoparticles have the ability to internalize into the cancer cells, cellular internalization study was performed by using three techniques which are cyto-viva, TEM, and Neutron Activation Analysis.

Cyto-viva procedure: The *in vitro* cellular internalization study of MGF-AuNPs was performed using dark field cyto-viva microscopic techniques. Ultraclean and sterile cover slips were kept in 6-wells plate (n=3). The PC-3 ($6x10^5$ cells) were plated into 6-wells plate in RPMI medium and incubated for 24 h in CO_2 incubator at 37 ^oC. After 24 h, the cells were exposed to MGF-AuNPs (25 and 50 µg/mL) and incubated for 4 h at 37 ^oC. The cells were washed 10

times with 1xDPBS, and fixed with 4% PFA and left for 15 minutes inside the bio-hood. Then, cells were further washed 3 times with 1x DPBS. Next, Coverslips were taken out from the 6 wells plate and were put on the upper surface of microscope glass slides. Before putting the coverslips on the slides, DAPI nuclear dye was put on the upper surface of the slide at dark place and then upper surface of coverslips was put on the dye. Any bubble of air between the slide and the coverslip should be removed before observing the slide under the microscope. Then the slides were observed using cyto-viva dark field microscope coupled with dual mode fluorescence. Images were captured via Dage Imaging Software.

TEM procedure: The PC-3 cells ($5x10^5$ cells) were plated into 6-well plate (n=1) in RPMI medium and allowed to grow for 24 h in CO_2 incubator at 37 ^oC. After 24 h incubation time, the cells were exposed to MGF- AuNPs (25 and 50 µg/mL) and incubated for 12 h at 37 ^oC. Then, the cells were washed three times with PBS, centrifuged into small pellets, and fixed with 2% glutaraldehyde and 2% paraformaldehyde (PFA) in sodium cacodylate buffer (0.1 M). The cells were further fixed with 1% buffered osmium tetraoxide in 2-Mercaptoethanol buffer and dehydrated in graded acetone series and embedded in Epon-Spurr epoxy resin. Sections were cut at 85 nm using a diamond knife (Diatome, Hatfield PA). The sections were stained with Sato's triple lead stain and 5% aqueous uranyl acetate for organelle visualization [92, 93]. Then, the prepared samples were observed under TEM microscope (JEOL 1400, Peabody, MA) operated at 80 kV at the University of Missouri's Electron Microscopy Core Facility.

Neutron Activation Analysis: The PC-3 ($5x10^5$ cells) were implanted in a Petri dish (10 mm) in RPMI medium, and incubated in CO_2 incubator at 37 ^oC until they reached 70 % confluency. Then, the cells were exposed to MGF-AuNPs (25 µg/mL) and incubated for 4 h in CO_2 incubator at 37 ^oC. The cells were washed 10 times with 1xDPBS. Then the cells were dislodged and centrifuged to get the cell pellet. Cell pellets were submitted to NAA facility at MURR to determine the amount of gold.

At NAA facility, samples were prepared by placing the cell pellet (dry weight) into pre-cleaned, high-density polyethylene irradiation vials. The weight of each sample was recorded and the vial was capped. Blanks, duplicates, and spiked samples were included in the NAA sample sets. Samples were loaded in polyethylene transfer "rabbits" in sets of nine and were irradiated for 90 seconds in a thermal flux density of approximately $5x10^{13}$ $n/cm^2/s$. The samples were then allowed to decay for 24–48 h and counted in real time for 1,200 second at a sample-to-detector distance of approximately 5 mm. The spectrometer consisted of a 21% high-purity germanium detector, with a full-width-at-half-maximum resolution of 1.8 keV at 1331 keV, and a Canberra 9660 digital signal processor. Dead times ranged from 1 to 11%. The mass of gold was quantified by measuring the 411.8 keV gamma ray from ^{198}Au ($t_{1/2}$ = 2.7 days). The area of this peak was determined automatically with the Genie ESP spectroscopy package from Canberra. Nine geometrically equivalent comparator standards were prepared by pipetting approximately 0.1 mg of gold from a (10.0± 0.5) µg/mL

certified standard solution (High-Purity Standards) on paper pulp in the polyethylene irradiation vials [7].

2.2.5- Cytotoxicity studies (MTT assay)

The in vitro cytotoxicity evaluation of MGF-AuNPs and MGF compound was performed as described by the supplier (Promega, USA). 100µl of 2 $x10^5$ cell/mL PC-3 or HAEC cells were seeded in each well of a flat-bottomed 96-well polystyrene-coated plate (n=3) separately and were incubated at 37°C for 24 h in CO_2 incubator at 5% CO_2 environment. After that, cells were exposed to either mangiferin compound at the concentrations of (12.5, 25, 50, 100, 200 µg/mL) or to MGF-gold nanoparticles with the concentrations of (31.25, 62.2,125, 250, 500 µg/mL) that contain mangiferin with the concentrations of (12.5, 25, 50, 100, 200 µg/mL) respectively. After 24 h incubation, 10 µL of MTT (stock solution 5mg/ mL PBS) was added to each well, and then cells were incubated for 4 h, only cells that are viable after incubation time are capable to metabolize a MTT dye efficiently and produce purple colored crystals which are called Formazan crystals. Formazan crystals so formed were dissolved in 100 µL detergent (DMSO) and incubated for 10 min. The intensity of color was measured by micro plate reader (BioTek, USA) operating at 570 nm wavelength. Wells with complete medium, nanoparticles and MTT but without cells were used as blanks. Untreated cells were used as controls.

2.2.6- Synthesis and characterization of radioactive MGF-^{198}AuNPs

Production of radioactive gold (^{198}Au): ^{198}Au was produced by direct irradiation of natural gold foil or metal according to the following nuclear equation **Au-197(n,γ) Au-198**. Gold foil was irradiated at a neutron flux of 8×10^{13} n/cm^2/s. Irradiation time varies according to how much activity is needed and how much mass of gold foil is irradiated; it ranges from 6 to 40 h. After irradiation, the radioactive foil was dissolved in 400 µL of aqua regia and heated to bring it to near dryness. Then, 400 µL of 0.05 M HCl was added twice and heated to azeotrope off the nitric acid. Next, the product was dissolved in a desired volume of water to make final solution of ^{198}Au which is used for the production of MGF-^{198}AuNPs.

After the radioactive gold solution (^{198}Au) was prepared, it was mixed with Na_2AuCl_4 to form radioactive gold precursor (Premix). A radioactive gold precursor (Premix) is prepared by mixing specific mass of ^{198}Au with specific mass of gold salt results in a radioactive gold precursor that has total mass of radioactive^{198}Au and non-radioactive Au of 0.66 mg and a particular activity. The mass of ^{198}Au that is mixed with Na_2AuCl_4 is determined according to the required activity of final solution of nanoparticles. For instance, for therapeutic study, the mass of ^{198}Au was 0.082 mg (this mass was chosen because it has the required activity which is 13 mCi). Then 0.082 mg of ^{198}Au was mixed with gold salt that has mass of gold equal to 0.578 mg in order to make the total mass of gold in the solution equal to 0.66 mg always for 2 ml gold nanoparticles

preparation. If less activity is needed, then the mass of ^{198}Au would be decreased and mass of gold within gold salt would be increased, so that the total mass of gold would be 0.66 mg. And so on.

Production of radioactive MGF-^{198}AuNPs: The protocol that has been used to produce non-radioactive MGF-AuNPs was not successful to produce radioactive MGF-^{198}AuNPs. Therefore, that protocol has been modified by changing the mass of MGF from 1.4 mg for non-radioactive MGF-AuNPs preparation to 1.55-1.6 mg for radioactive MGF-^{198}AuNPs preparation. Using of 1.55-1.6 mg MGF results in successful preparation of radioactive MGF-^{198}AuNPs. Also, in preparation of radioactive MGF-^{198}AuNPs, radioactive gold precursor solution (^{198}Au+Na_2AuCl_4) that has the desired activity (390µCi- 13mCi) was used instead of Na_2AuCl_4 that was used in preparation of nonradioactive MGF-^{198}AuNPs. The method of this protocol starts with adding 1.55-1.6 mg of MGF to 2 ml of milli-Q water. Then the mixture was stirred at room temperature for 10 minutes, stirred and heated until 99^{o}C. At this temperature, radioactive gold precursor solution (^{198}Au+Na_2AuCl_4) that has desired activity (390µCi- 13mCi) was added to the MGF solution resulted in immediate color change from pale yellow to red purple color. After that, the solution stirred for 1 h at room temperature.

UV-Vis spectroscopy measurements: The resulting solution of radioactive gold nanoparticles was characterized by measuring the surface plasmon resonance wave length (λ_{max}) using UV-Vis spectroscopy.

Thin-layer chromatography (TLC) measurements: Radio-TLC was performed to estimate the yield of radioactive gold nanoparticles. The procedure was done by adding 1µL of nanoparticles solution to the origin of cellulose TLC plate. After 5 min, TLC plate was developed in 4 mL of methanol containing two drops of concentrated HCl. Then the yield of radioactive gold was measured using a Bio-scan, free ^{198}Au moves to the solvent front whereas ^{198}Au-nanoparticles remain at the origin.

2.2.7- Stability study of radioactive gold nanoparticles

Before the administration of the nanoparticles in animals, the nanoparticles solution should be brought to pH 7 and made isotonic by using NaOH and Delbecco's phophate buffered saline (DPBS). Addition of NaOH and DPBS may have an effect on the stability of the nanoparticles; they may or may not aggregate. Therefore stability study was conducted to see whether the nanoparticles remain stable after adding NaOH and DPBS.

The stability study procedure of radioactive MGF-^{198}AuNPs was performed first by raising the pH 7 by addition of NaOH and DPBS. Quality control included measuring the pH, λ_{max}, and Radio-TLC every day for seven days.

2.2.8- *In vivo* stability study (bio-distribution) of MGF-^{198}AuNPs

25 Normal female CF-1 mice were intravenously injected with 8.0 μCi/100μL MGF-^{198}AuNPs via the tail vein. Mice were euthanized (n=5) at 30 minutes, 1, 2, 4, and 24 h post-injection. Next, organs of interest (heart, liver, spleen, lungs, muscle, bladder, brain, bone, kidney, gut, blood and stomach) were excised weighed and counted along with standards in a NaI well counter. Radioactivity obtained from different organs was calculated as the percentage of injected dose (%ID) and the percentage of injected dose per gram (% ID/g) of each organ. The %ID in whole blood was estimated assuming a whole-blood volume of 6.5% the total body weight.

Stable nanoparticles are expected to show minimal uptake in blood and lung.

2.2.9- *In vivo* tumor retention (intra-tumoral) study of MGF-^{198}AuNPs

Severe combined immunodeficiency (SCID) mice received unilateral subcutaneous hind flank inoculations of $10x10^6$ PC-3 cells suspended in 0.1 mL of sterile DPBS and Matrigel® (2:1, v:v) under inhalational anesthesia (isoflurane/ oxygen). Solid tumors were allowed to develop for four weeks. After 4 weeks, the mice received a single dose of MGF-^{198}AuNPs (4 μCi / 30μL for each tumor). The dose of MGF-^{198}AuNPs was injected directly into the prostate tumor.

Then, mice were euthanized (n=5) at intervals of 30 min, 1, 2, 4, and 24 h post-injection. Next, organs of interest and tumors were excised weighed and counted along with standards in a NaI well counter. Radioactivity obtained from different organs was calculated as the percentage of injected dose (%ID) and the percentage of injected dose per gram (% ID/g) of each organ.

2.2.10- Therapeutic efficacy study of MGF-^{198}AuNPs

The right hind flank of severe combined immunodeficiency (SCID) female mice (n=28) were subcutaneously inoculated with 10x10^6 PC-3 cells suspended in 0.1 mL of sterile DPBS and Matrigel® (2:1, v:v) under inhalation anesthesia (isoflurane/ oxygen). After inoculation, tumors were allowed to grow for 4 weeks, at which time the tumors were measured by digital caliper measurements, in which the tumor volume was calculated as length x width x height. Then, the mice were randomly divided into four groups with no significant difference in tumors volume for three groups while the fourth group had larger tumors than the other groups (day of randomization was considered day 0 of therapy study). After 2 days of mice randomization into four groups, mice were treated as following, first group (n=6) and fourth group (n=3) of mice were directly injected into the prostate tumor with a single dose of MGF-^{198}AuNPs (160 µCi / 30 uL per tumor), whereas 30 µL of non-radioactive MGF-AuNPs and 30 µL of DPBS was directly injected into the prostate tumor of the second (n=6) and third (n=6) group of mice respectively. The fifth group (n=7), which is normal and do not bear tumor, was left without any treatment and served as control for complete blood count (CBC)

values. Post injection of mice, body weight and tumor volume measurements were taken 2 times per week for all groups, for approximately 5 weeks. Animals were sacrificed at the end of study period or when tumors reached endpoint. At the time of sacrifice, blood was collected from each animal and transported to IDEXX analyzer for CBC analysis and organs of interest of the first and fourth group were harvested to measure the radioactivity level using NaI well counter.

2.2.11- Synthesis and characterization of radioactive MGF-^{199}AuNPs

The production of carrier-free ^{199}Au**:** enriched ^{198}Pt metal powder targets encapsulated in quartz ampoules were irradiated with neutrons to produce ^{199}Pt according to the nuclear equation **Pt-198(n, γ) Pt-199** which rapidly decays by beta- emission to ^{199}Au. Enriched Pt metal powder (1.76 mg) was irradiated at flux of $2.4x10^{14}n/cm^2/s$ for 152.11 h at MURR. Initial activity of ^{199}Pt/^{199}Au was 115.6 mCi. The material was dissolved in 400 µL of aqua regia and brought to near dryness. Next, 400 µL of 0.05M HCl was added twice and heated to azeotrope off the nitric acid. The final was dissolved with 400 µL of 3M HCl with a final activity of 104.3 mCi that was measured by a dose calibrator. To this was added 400 µL of ethyl acetate and resultant solution vortexed for 1 minute. After sitting for 5 min at room temperature, the layers were separated. The top layer contained 76 mCi of carrier-free ^{199}Au in ethyl acetate. Radionuclidic purity was

evaluated by adding a small aliquot of the separated ^{199}Au to 10 ml of 0.05M HCl and analyzed by HPGe spectrometer.

The ^{199}Au in ethyl acetate was dried to remove the ethyl acetate. Next, 400 µL of 0.05 M HCl was added and brought to near dryness this was repeated twice. The material was brought to a final volume of 60 µL with H_2O and a total activity of 32 mCi.

Production of radioactive MGF-^{199}AuNPs: The method that was used to produce MGF-^{198}AuNPs was initially tried for MGF-^{199}AuNPs but was not successful. Mass of MGF was increased from 1.55 mg to 1.7 mg and due to the fact that ^{199}Au has negligible mass, a new procedure was developed to synthesize MGF-^{199}AuNPs. To 2 mL of Milli-Q water was added 1.7 mg of MGF. The mixture was initially stirred at room temperature for 10 minutes and then heated to 99^{o}C. At this temperature a mixture of ^{199}Au and Na_2AuCl_4 (2.5 µl, 1.2 mCi of ^{199}Au that has negligible mass+33.5 ul of Na_2AuCl_4, 1.21 mg) was added to the MGF solution resulting in an immediate color change from pale yellow to red purple. The solution was left to stir for 1 hour at room temperature.

It is important to mention that repeating the same procedure except increasing the volume of ^{199}Au from 2.5µl to 4µl resulted in failure of the experiment. The reason behind this might be the lower pH when the volume of ^{199}Au is increased

UV-Visible Spectroscopy and Thin-layer chromatography (TLC) measurements of MGF-^{199}AuNPs were performed in a similar manner previously described in section (2.2.6).

2.3- Method of production of radioactive citrate-^{199}AuNPs

Previous studies of the non-radioactive citrate gold nanoparticles showed that these nanoparticles are stable [85], non-toxic [86-89], and are internalized inside the cells [86-88] . Therefore, this section only describes the method of synthesis and characterization of radioactive citrate-^{199}AuNPs.

The production of carrier-free ^{199}Au**:** It was performed as previously described in section (2.2.11).

Synthesis of radioactive citrate-^{199}AuNPs**:** Graber et al (1995) used a protocol based on the Turkevich method to produce citrate-gold nanoparticles with sizes formed of approximately 15 nm. In this present study the protocol by Graber et al (1995) was used to produce radioactive citrate-^{199}AuNPs. Unfortunately, that protocol was not successful, and radioactive gold nanoparticles were not formed. The reason for the failure being the low pH of the solution after the addition of ^{199}Au. Therefore, a series of experiments were performed to develop a new method.

Successful radioactive citrate gold nanoparticles were produced using the following method. 2 mL of 0.5 mM $NaAuCl_4$ was added to a V-bottom vial, followed by the addition of 15 µL of ^{199}Au (8.5 mCi). The mass of ^{199}Au is

negligible and the volume of ^{199}Au that is mixed with Na_2AuCl_4 is based on the required activity of the final solution of nanoparticles. Next, the vial containing the solution of Na_2AuCl_4 and ^{199}Au was stirred vigorously and continuously and brought to a boil (99-100°C). When the solution's temperature reached the boiling point, 206 µL of 38.8 mM sodium citrate was added to the solution. This resulted in a gradual color change from pale yellow to greyish-blue to the expected wine red color. The boiling and stirring was continued for 10 minutes. The solution was then removed from heat and stirring was continued at room temperature for an additional 15 minutes.

UV-Visible spectroscopy and thin-layer chromatography (TLC) measurements of MGF-^{199}AuNPs were performed as previously described in section (2.2.6).

2.4- Method of MCNP simulations

This section describes using MCNP code to estimate the dose distribution that is deposited by radioactive gold nanoparticles (^{198}AuNPs or ^{199}AuNPs) in tumor inside human prostate and surrounding healthy tissues.

2.4.1- Physical model

In order to simplify the calculations, simple geometrical model of the tumor, prostate, and the organs at risk (bladder and rectum) was used. The prostate gland and solid tumor were assumed to be spherical. The radius of the

prostate was taken as 2 cm with a tumor of radius 0.4 cm inside. Since the urethra passes through the center of prostate, the tumor was assumed to be (left) off-center within the prostate (Figure 8).

Radioactive gold nanoparticles were assumed to be accumulated homogeneously inside the tumor tissue. For prostate cancer beta therapy the organs at risk for excess dose are the prostate (healthy tissue), the bladder, and the rectum. The organs at risk were assumed to be spherical with radii of 3.5 cm, and 1.5 cm respectively. Water and A-150 tissue equivalent plastic phantoms have been used to simulate the soft tissues as well as tumor tissues.

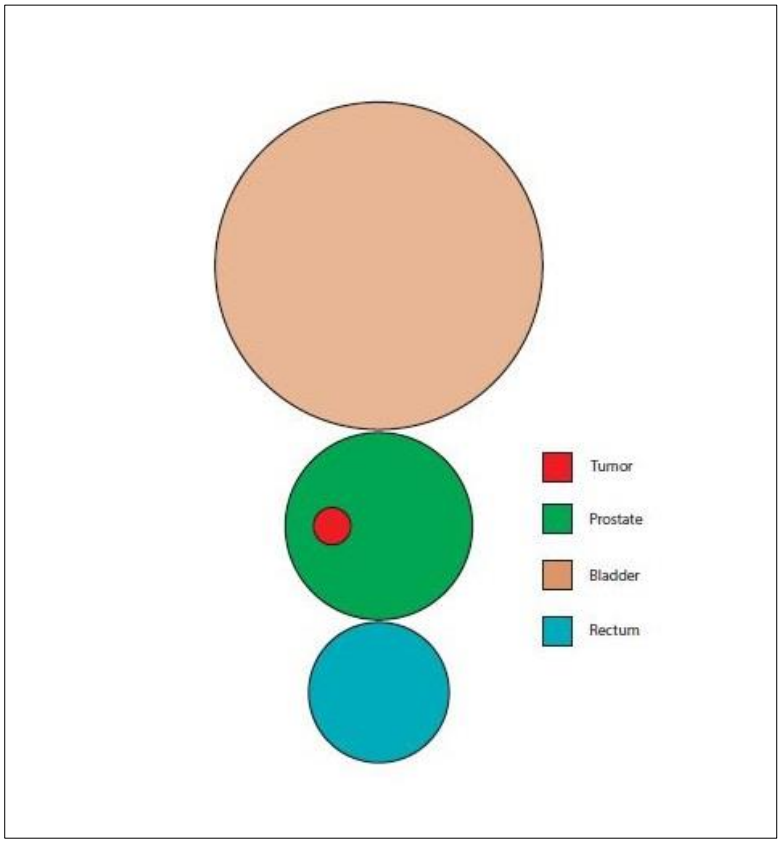

Figure 8: Schematic representation of the simple geometrical model of tumor, human prostate, and organs at risk. The geometry shown in this figure is not drawn to scale.

2.4.2- MCNP model

Dosimetry calculations for radioactive gold nanoparticles were performed using the MCNP code (version 6.1.1). Specifically, this code was used to estimate the dose distribution of ^{198}Au and ^{199}Au nanoparticles independently inside the tumor and in the surrounding healthy tissues of the human. This approach allowed the computation of dose as a function of distance.

Both ^{198}Au and ^{199}Au isotopes emit gamma and beta radiation which deposit dose to tissue (the characteristics of these two isotopes have been mentioned in section 1.6). The photons and betas emitted per decay of ^{198}Au and ^{199}Au and their intensities were used for MCNP simulations model (See Figures 6&7 in chapter 1). Only photons and electrons with energies higher than 150 eV are counted for the simulations. The reason for this cutoff is that at the present MCNP does not support general beta interactions at low energies; i.e. molecular energy deposition mechanisms are dependent on material. Further developments in MCNP may model these mechanisms for common materials such as water; in the future including these mechanisms could be an interesting way to extend this work. Additionally, below 150 eV, elastic collisions become an increasingly prevalent mode of particle interaction. Without the aforementioned low energy stopping mechanisms (and elastic interaction cross sections of billions of barns), collision densities increase to the point where calculation is intractable.

The source was assumed to be spherical with a radius similar to that of the tumor because radioactive nanoparticles are assumed to spread

homogenously throughout the tumor tissues. F6 tally and spherical mesh tally (SMESH) were used to estimate the dose distribution of both betas and gammas that are emitted by radioactive gold nanoparticles and deposited within tumor and neighboring healthy tissues of bladder and rectum.

CHAPTER 3

RESULTS AND DISCUSSION

3.1- Production and evaluation of radioactive MGF-^{198}AuNPs and MGF-^{199}AuNPs

The objective of this project is production and evaluation of radioactive MGF-^{198}AuNPs and MGF-^{199}AuNPs in order to use them for prostate cancer treatment and imaging.

3.1.1- Synthesis and characterization of MGF-AuNPs

MGF- gold nanoparticles were synthesized through direct interaction of sodium tetrachloaurate with mangiferin in double distilled water. The red purple color of resulting solution was a good indication of the formation of MGF-gold nanoparticles. mangiferin plays dual role as reductant and stabilizing agent in this synthesis.

In order to determine whether the MGF-AuNPs are stable, the resulting solution of nanoparticles was characterized by measuring the surface plasmon resonance wave length (λ_{max}), morphology, size distribution, and charge. These physicochemical properties were determined by three techniques: UV-Vis. spectroscopy, transmission electron microscopy (TEM), and dynamic light scattering (DLS).

UV-Visible spectroscopy was used to measure the surface plasmon resonance wave length. It is known that the spectrum surface plasmon resonance of nanoparticles is influenced by the size, shape, inter-particle interactions, free electron density and surrounding medium, which indicates that UV-Visible spectroscopy is an efficient tool for monitoring the stability or aggregation of nanoparticles.

The surface plasmon resonance wave length (λ_{max}) of MGF-AuNPs is in the range of 530-535 nm, indicating the formation of MGF-AuNPs. Figure 9 shows the UV-vis spectrum of MGF-AuNPs.

TEM images showed that the MGF-AuNPs were dispersed uniformly and have nearly spherical shape as shown in Figure 10. The measurement of core size was performed by the analysis of TEM images through the Image J software. The resultant size distribution histogram for several TEM images showed that the core size of MGF-AuNPs is around 35 nm (Figure 10).

The dynamic light scattering method (DLS) was used to measure the hydrodynamic size of MGF coated gold nanoparticles as well as the zeta potential. From DLS measurements, the hydrodynamic diameter of MGF-AuNPs was determined to be 60 nm.

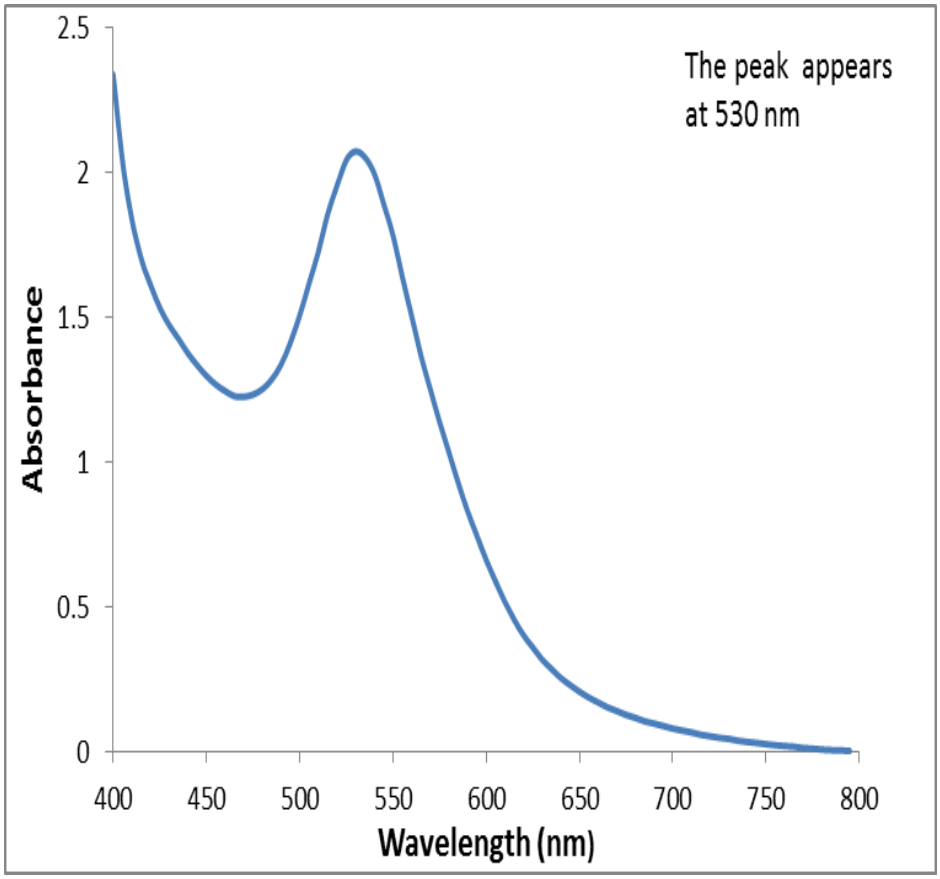

Figure 9: UV-Visible spectrum of MGF-AuNPs, The peak appears at 530 nm.

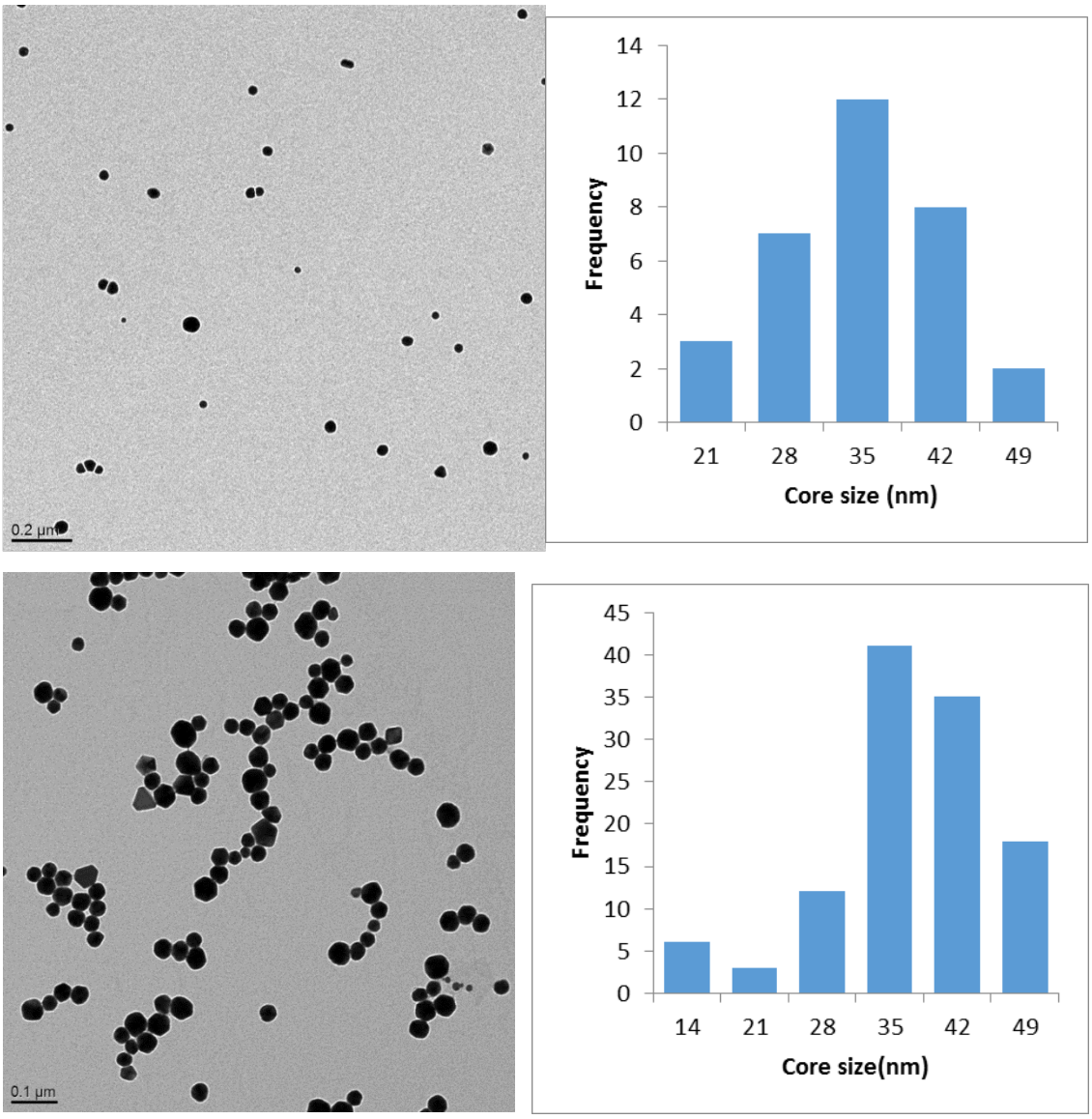

Figure 10: TEM image and core size distribution histogram of MGF-AuNPs.

The measurement of the zeta potential (z), provides crucial information on the stability of the nanoparticles dispersion. The magnitude of z is an indication of the repulsive forces present and can be used to predict the long-term stability of the nanoparticle dispersion. The stability of the nanoparticle dispersion depends on the balance of the repulsive and attractive forces between the nanoparticles as they approach one another. If all the particles have a mutual repulsion, then the dispersion will remain stable. However, little or no repulsion between particles leads to aggregation.

From the DLS measurement, the zeta potential was (-50.5 mv), the high negative z value of (-50.5 mv) for MGF-AuNPs indicates the particles repel each other, and that there is no tendency for the particles to aggregate. Therefore, MGF-AuNPs are stable (Table 1).

Sample	**Size nm**		**Zeta mv**	**λ_{max} nm**
MGF-AuNPs	Core size	Hydrodynamic size	-50.5	530 - 535
	35	60		

Table 1: Size, zeta potential, and λ_{max} measurements of MGF-AuNPs.

It is worth mentioning that, after four months of synthesis and storage of some samples of MGF-AuNPs, no change was observed in the λ_{max} or the absorbance indicating these nanoparticles are very stable.

3.1.2- Dilution study evaluation

Some medical applications require different concentrations of gold nanoparticles. Therefore, to ascertain that dilution of nanoparticles into different concentrations does not affect their stability and does not alter their physical and chemical properties *in vivo*, a dilution study was done by diluting NPs to different concentrations (82.15, 55, 41.25, 20.62, 10.31, and 5.15 µg/mL), and UV-Vis spectroscopy was recorded for each concentration. From the UV-Vis spectra (Figure 11), it can be seen that the surface plasmon resonance wave length has the same value for all the solutions, indicating that the dilution of nanoparticles has no effect on the stability of MGF-gold nanoparticles, and the nanoparticles remained stable.

Furthermore, the absorption intensity was found to be linearly dependent on the concentration of AuNPs (Figrue 12). The linearity relationship between the absorbance and concentration of AuNPs also confirms that these nanoparticles are stable and that they do not precipitate upon dilution.

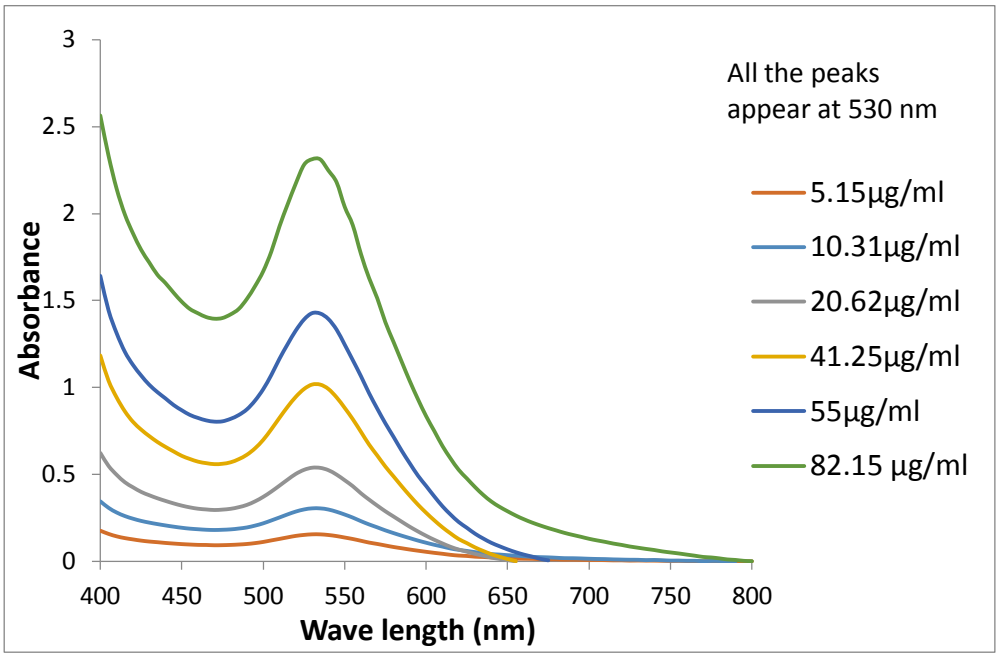

Figure 11: Surface plasmon resonance wavelength (λ_{max}) of different concentrations of MGF-AuNPs. It can be seen that all the diluted solutions have the same value of λ_{max} (530 nm).

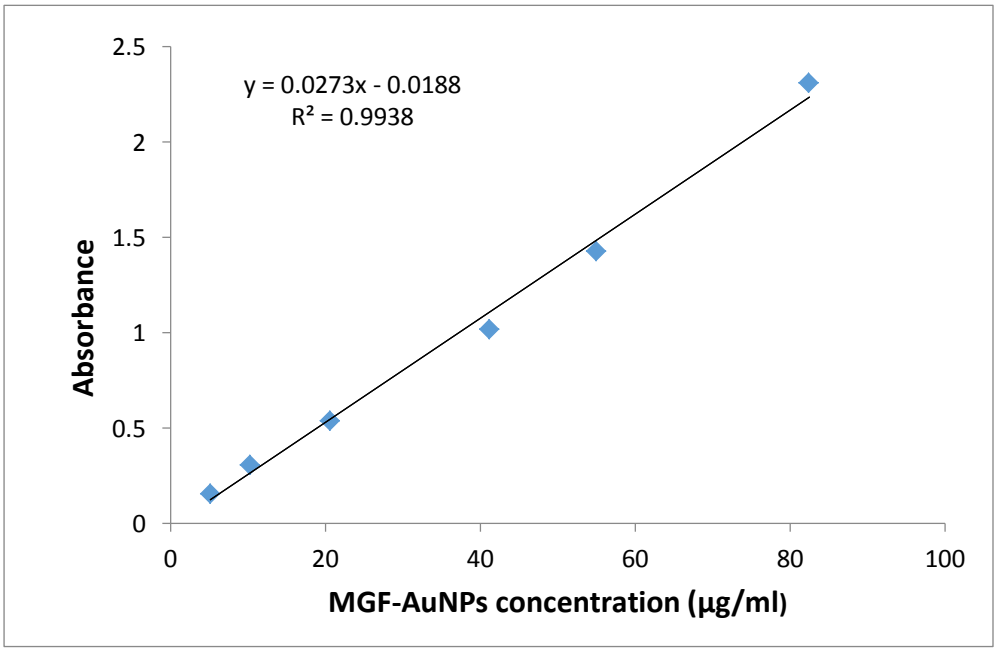

Figure 12: Plot of absorbance vs. concentration showing the absorbance intensity is proportional linearly with MGF-nanoparticles concentration. R^2=0.99.

3.1.3- *In vitro* stability study

Nanoparticles that are produced to be used in medical applications must remain stable and not aggregate or decompose in biological solutions over a reasonable period of time. The *in vitro* stability of MGF-AuNPs was evaluated by monitoring the surface plasmon resonance wave length(λ_{max}) in NaCl (1%), histidine (0.2 M), cysteine (0.5%), bovine serum albumin (BSA, 0.5%), or human serum albumin (HSA, 0.5%) at different time points (1, 4, 24, and 48 h,1, and 2 weeks). The stability of MGF-AuNPs was also evaluated in phosphate-buffer solutions at pH 7 and 9. Although pH 9 solution is higher than the pH of human body fluids, it was chosen to give us extra information whether nanoparticles are still stable at this high PH.

The results showed that the plasmon wave length (λ_{max}) remained the same in all the above formulations except in bovine serum albumin (BSA, 0.5%) and in human serum albumin (HSA, 0.5%), in which it shifted by approximately 5 nm which is a very low shift. This indicates that the MGF-AuNPs remain intact and do not aggregate, and therefore demonstrate high *in vitro* stability in biological fluids at physiological PH (Table 2, Figure 13 & 14).

Biological fluid	**NaCl (1%)**	**Histidine (0.2 M)**	**Cysteine (0.5%)**	**BSA (0.5%)**	**HSA (0.5%)**	**PBS PH7**	**PBS PH9**
λ_{max}	530	530	530	535	535	530	530

Table 2: λ_{max} of MGF-AuNPs in different biological solutions.

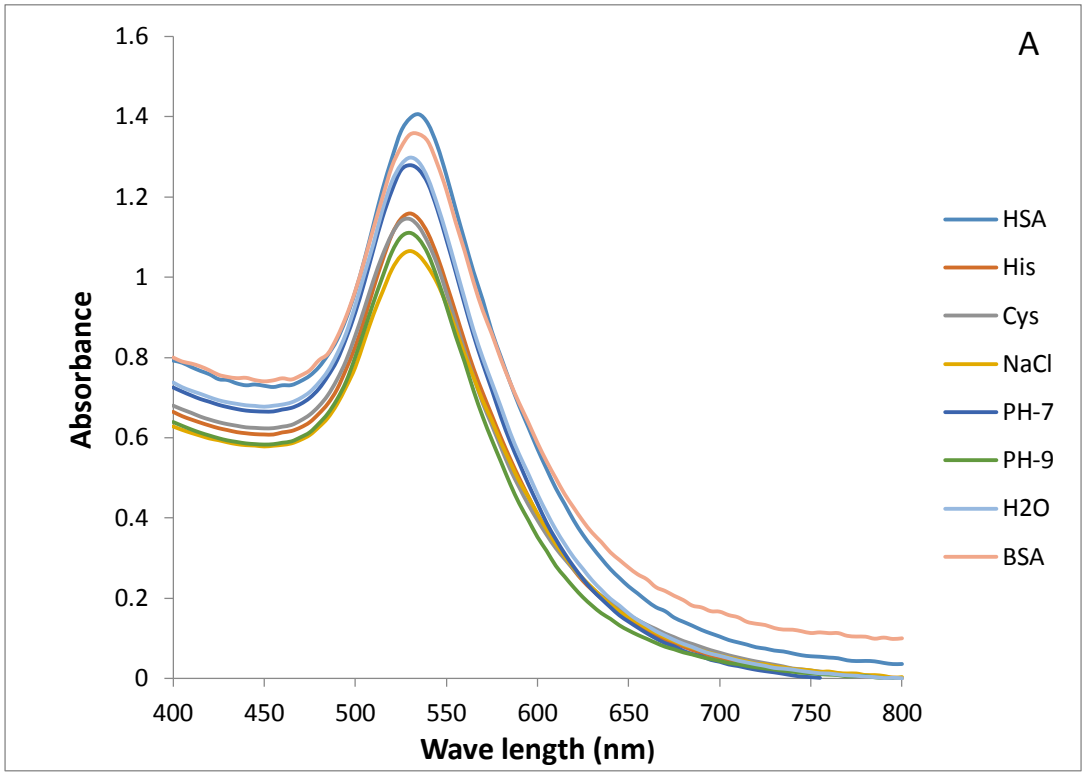

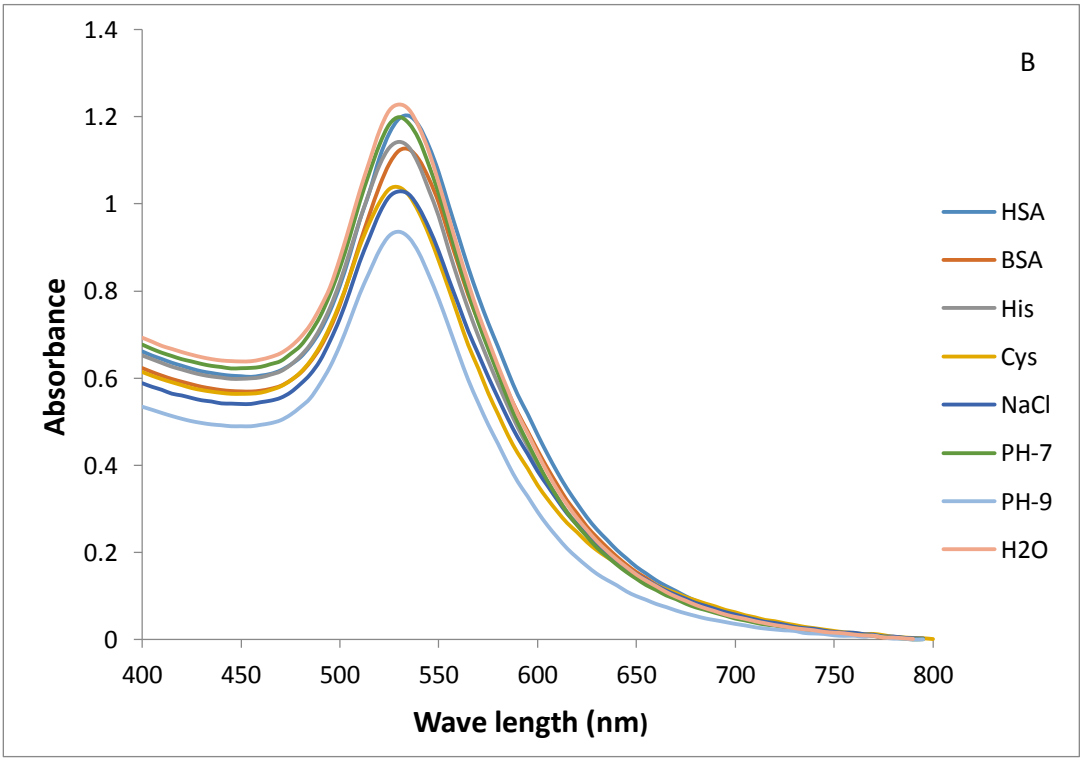

Figure 13: UV-Vis spectra showing the *in vitro* stability of MGF-AuNPs in biological solutions after 1 h (A) and 24 h (B) incubation.

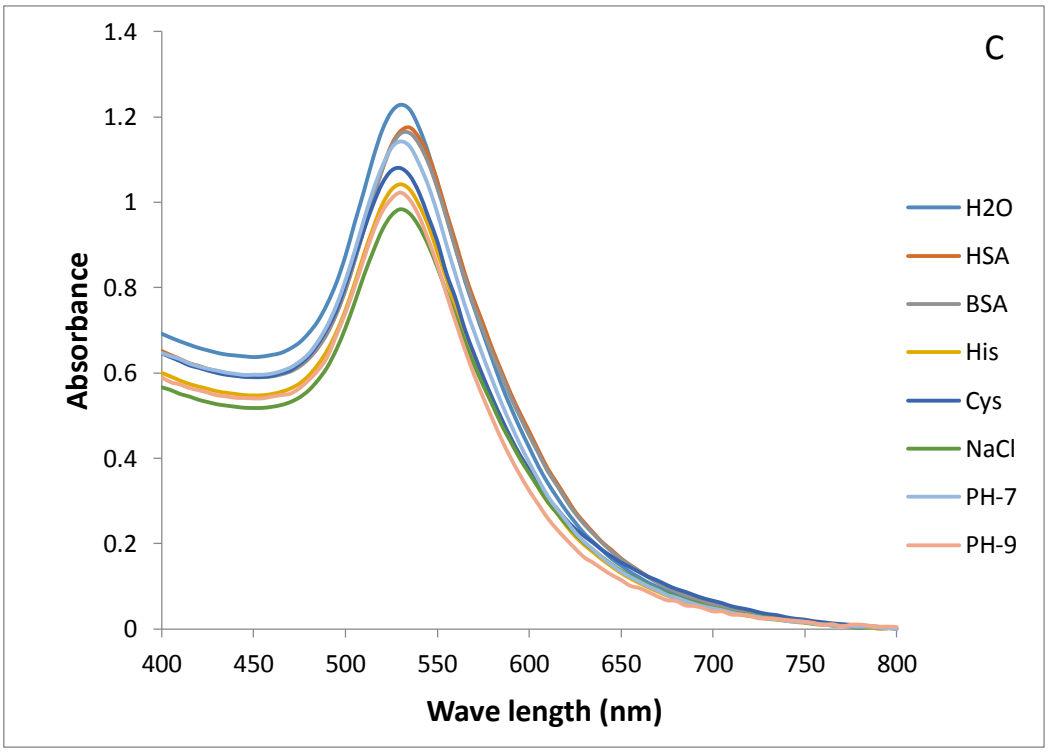

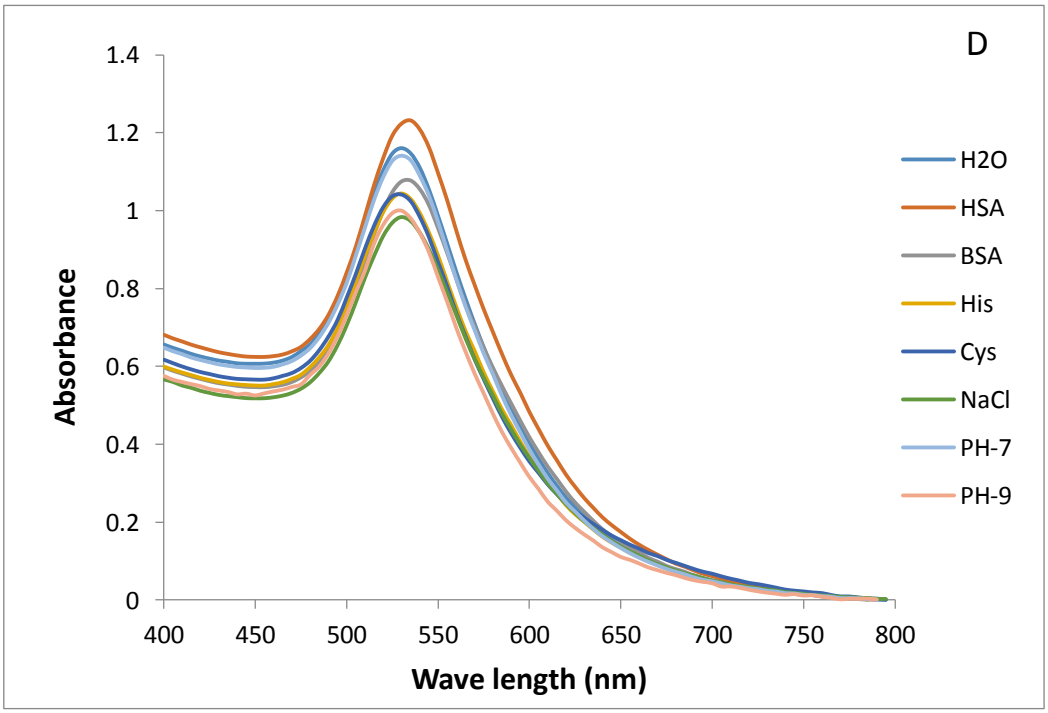

Figure 14: UV-Vis spectra showing the *in vitro* stability of MGF-AuNPs in biological solutions after 48 h (C) and 1 week (D) incubation.

3.1.4- Cellular internalization study

Cellular internalization study was undertaken to investigate the internalization ability of MGF-AuNPs. Cellular internalization studies provided important information on whether MGF-AuNPs can be used for therapeutic purposes.

In this current study, MGF-AuNPs with different concentrations were incubated with prostate cancer cells (PC-3) for four hours. At the end of the incubation time, the cells were washed vigorously with phosphate buffered saline (PBS; pH 7.4) to remove any unbound AuNPs. The cellular internalization of MGF-AuNPs within cancer cells were evaluated using dark field optical microscopy, TEM image analysis, and Neutron Activation Analysis. Cyto viva dark field microscopic images showed clearly the internalization of MGF- AuNPs within PC-3 cells (Figure 15). The images in Figure 15 show clearly that a significant amount of MGF-AuNPs were internalized in PC-3 cells contained in the cytoplasm and surrounding the nucleus without disrupting it. The internalized nanoparticles were found intact with clear boundaries, confirming high *in vitro* and *in vivo* stability of MGF-AuNPs. Also, it can be seen from dark field microscopic images that as the nanoparticles concentration increases, nanoparticle uptake by the cells increases.

The internalization of MGF- AuNPs was also evaluated independently by TEM image analysis of cancer cells. TEM images also confirmed that MGF-AuNPs were internalized within PC-3 cancer cells. Figure 16 shows how MGF-AuNPs accumulated in cytoplasm inside cells but did not enter the nucleus. It can

be observed that these nanoparticles have spherical shape and did not aggregate inside the cell

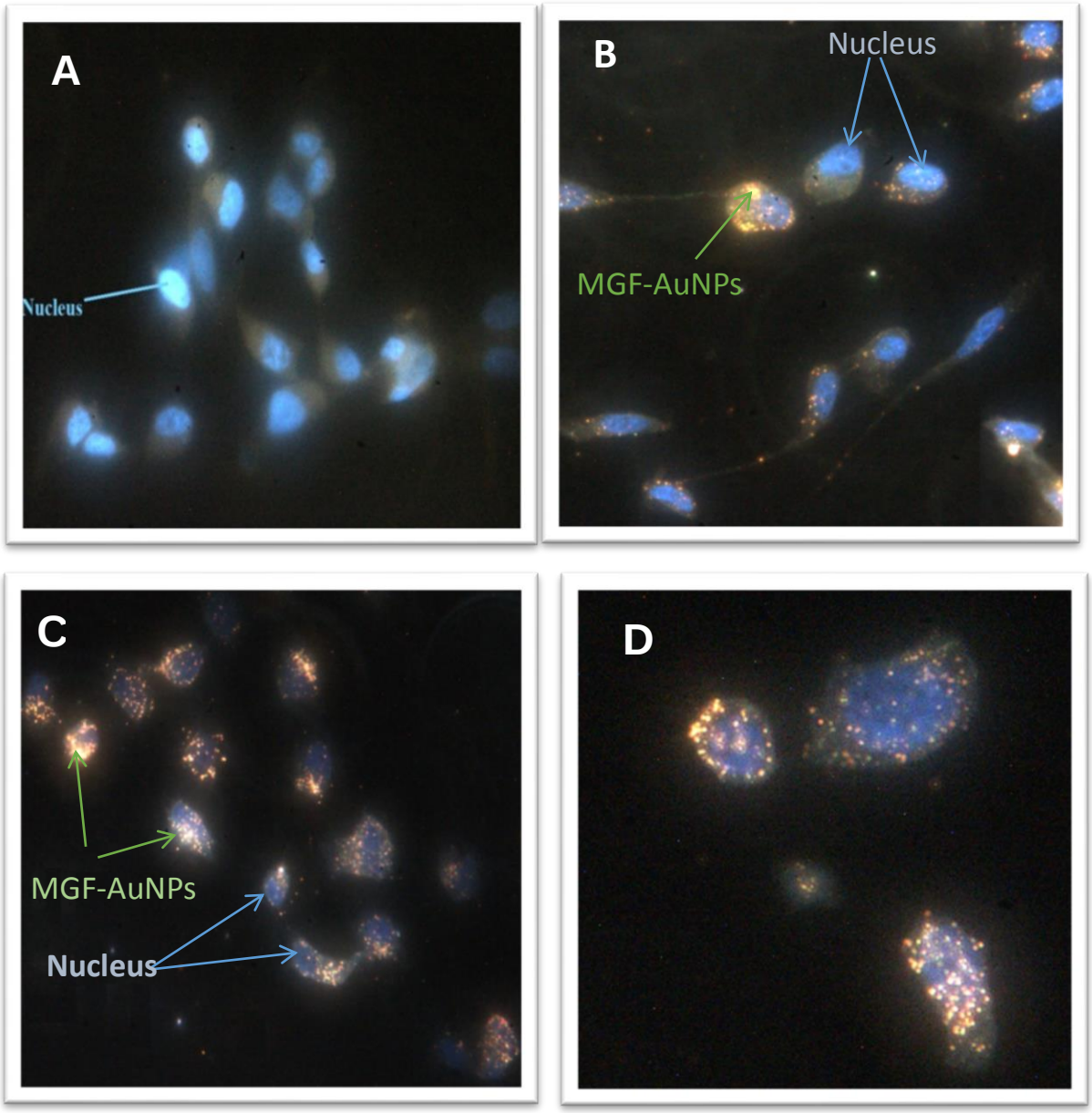

Figure 15: Dark field images showing nanoparticle uptake at 4h post treatment. (A) Control cells. (B) Cells were incubated with 25 µg/mL MGF-AuNPs. (C) Cells were incubated with 50 µg/ml MGF-AuNPs. (D) Magnified picture of the photo C.

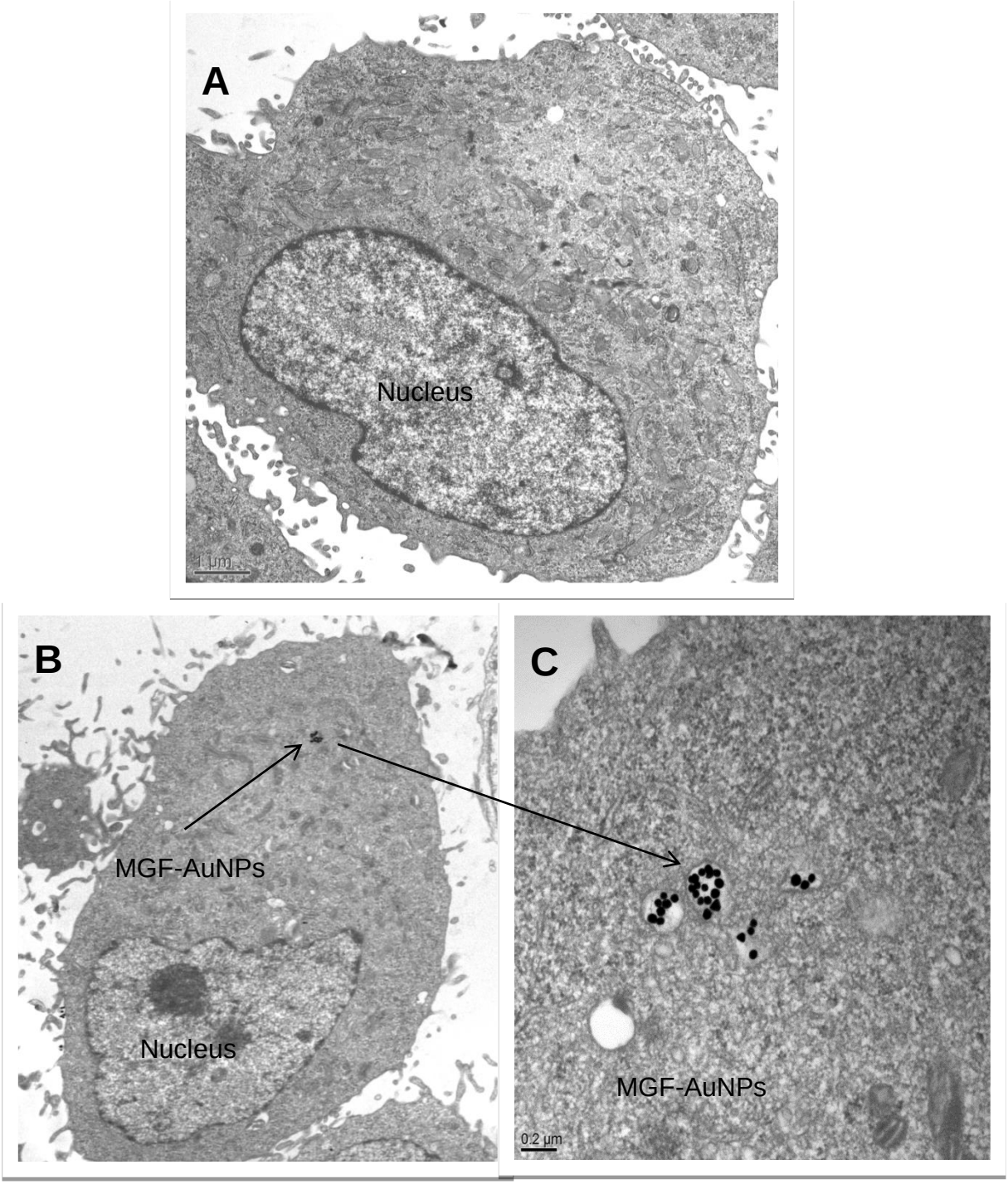

Figure 16: TEM images showing internalization of nanoparticles at 4h post treatment. (A) Control cells. (B) Cells incubated with 50 µg/ml MGF-AuNPs. (C) Magnified picture of photo B.

Dark field and TEM images clearly demonstrate that MGF- AuNPs are internalized into prostate cancer cells. Since the cellular internalization results showed that MGF-AuNPs were able to enter the cells, they can be used for therapeutic applications, particularly radio-therapeutic applications.

By comparing the dark field images of MGF-AuNPs with the image of EGCG-AuNP that was previously reported in the literature [7]. The internalization rate of both types of nanoparticles was comparable and did not show any differences in the amount of nanoparticles that were internalized inside the cells, although the concentration of EGCG -AuNPs was not written in that paper. In this literature [7], they performed blocking studies that shows the Laminin receptor was responsible for the internalization. In contrast, blocking studies have not been performed in the current study to see what is responsible for the internalization of MGF-AuNPs. MGF-AuNPs are assumed to be internalized to cells through endocytosis.

Neutron Activation Analysis (NAA) was performed to estimate the gold concentration in PC-3 cells that were incubated with MGF-gold nanoparticles. NAA allows for the detection and quantification of gold. NAA showed a significant amount of gold was internalized inside the cells, 6.83 µg of gold was inside the cell pellet sample that weighs 2960 µg.

Dark field microscopy, TEM, and NAA techniques all confirmed that MGF-AuNPs have the ability to be internalized in PC-3 cells, and this is a good result because it means radioactive -MGF nanoparticles have the same ability to be

internalized in PC-3 and deliver enough radioactivity to kill cancer cells without affecting normal tissues.

3.1.5- Cytotoxicity studies (MTT assay)

In order to investigate the biocompatibility of MGF-AuNPs, The cytotoxicity of MGF-AuNPs was studied on human aortic endothelial cells (HAEC) as well as in prostate cancer cells (PC-3) under *in vitro* conditions using a colorimetric cell-viability (MTT) assay. In this assay, only cells that are viable are capable of metabolizing a dye (3-(4,5-dimethylthiazol-2-yl)-2,5 diphenyltetrazolium bromide) efficiently producing purple colored crystals which are then dissolved in a detergent and analyzed spectrophotometrically. The cell viability was examined by the absorbance of formazan which is directly proportional to the number of live cells. The experiment was performed using a wide range of concentrations of MGF as free compound and within nanoparticle structure (0, 12.5, 25, 50, 100, and 200 µg /mL). The cells were incubated for 24 hours. Untreated and treated cells with 12.5, 25, 50, 100, and 200 µg /mL concentrations of MGF and MGF-AuNPs for 24 h were subjected to the MTT assay.

After 24 h of post incubation, HAEC cells showed excellent viability even up to 100 µg/mL concentrations of mangiferin or MGF-AuNPs. These results clearly show that the mangiferin as well as MGF-AuNPs is a nontoxic to the normal endothelial cells (Figure 17).

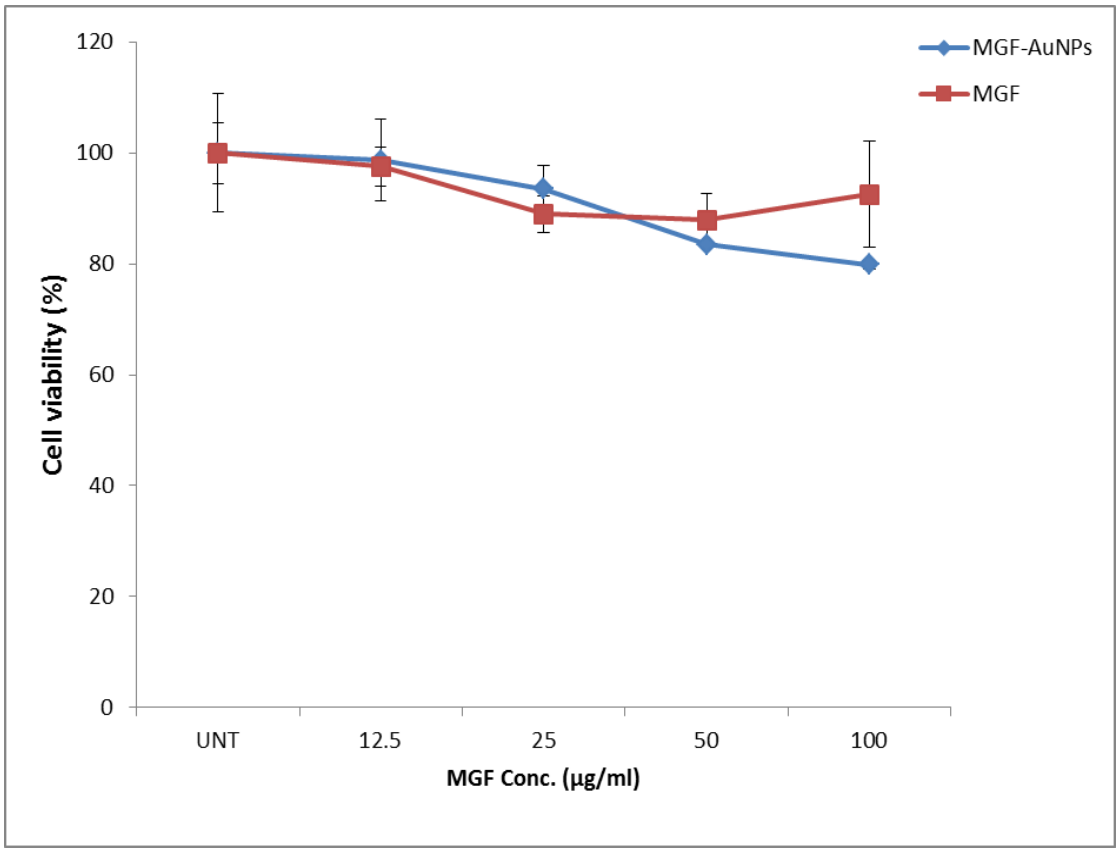

Figure 17: Cell viability of HAEC cells after 24 h post incubation with increasing amounts of MGF as free compound and within nanoparticles structure.

Additionally, After 24 h of post incubation of PC-3, the viability of the cells was less than the viability of normal cells, suggesting that mangiferin has anticancer properties (Figure 18).

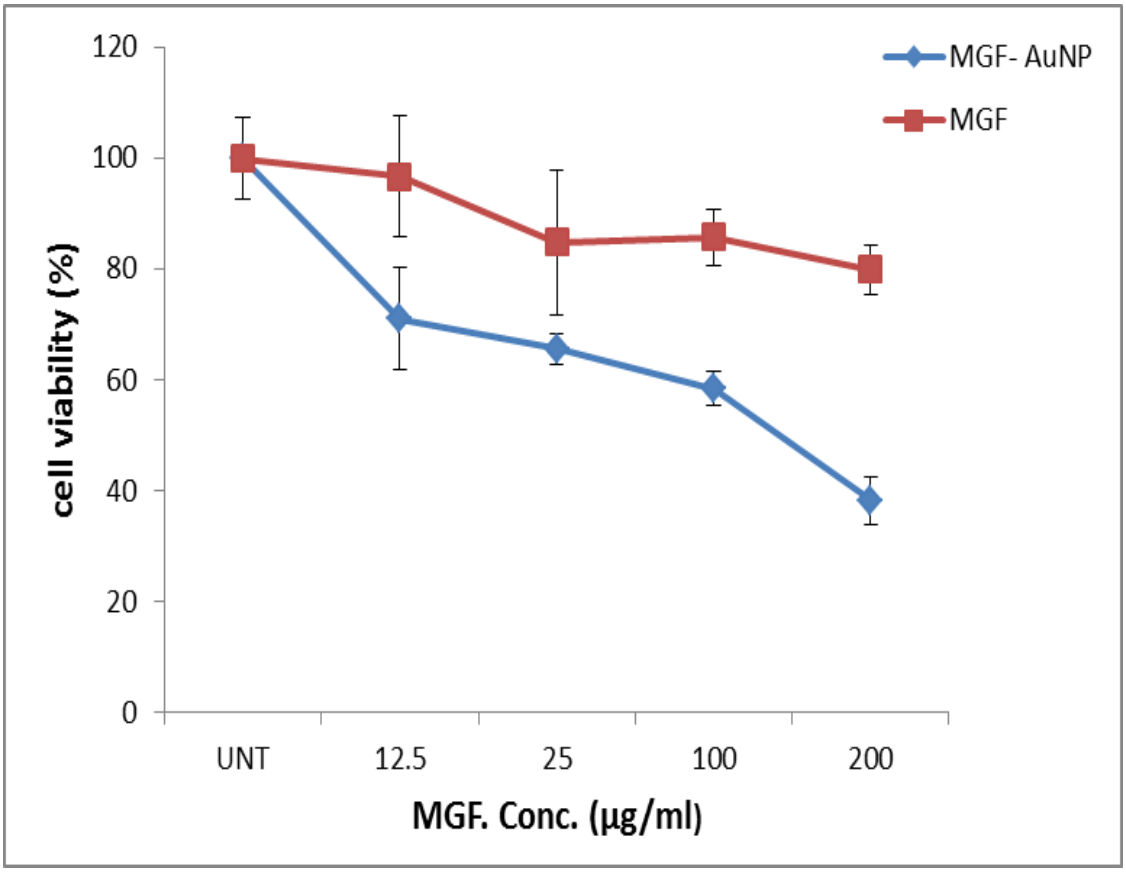

Figure 18: Cell viability of PC-3 cancer cells after 24 h post incubation with increasing amounts of MGF as free compound and within nanoparticles structure.

It is important to mention that gold (I) and gold (III) compounds are toxic due to the+1 and +3 oxidation state of gold [93, 94]. However, gold within nanoparticle structure is non-toxic because it is inert (it has 0 oxidation state). Previous studies [95] have shown that gold chloride has some toxicity; therefore it has not been evaluated in the current study.

In the present study, the concentrations of MGF as free compound or within nanoparticles structure were chosen based on the previous studies of nanoparticles [13, 93]. The cells were incubated with 12.5, 25, 50, 100, and 200 µg/mL of MGF as free compound or within nanoparticles structure. The corresponding volumes of these concentrations were 62.5,125, 250, 500, and 1000 µL respectively, which is approximately equal or larger than the volume of nanoparticles or mangiferin solution that would be injected for treatment into an animal.

3.1.6- Synthesis and characterization of radioactive MGF-^{198}AuNPs

MGF-^{198}AuNPs were synthesized according to the protocol that has been established in the current laboratories which was mentioned in materials and methods chapter. A radioactive gold precursor is prepared by mixing specific amounts of ^{198}Au with gold salt results in a radioactive gold precursor that has the desired activity. The mass of ^{198}Au that is mixed with Na_2AuCl_4 is determined according to the required activity and mass required for the final solution of nanoparticles.

After addition of radioactive gold salt to the MGF solution, a pale yellow solution immediately changed to red-purple. This color is a good indication of formation of radioactive MGF-^{198}Au nanoparticles as shown in Figure 19.

In order to confirm that the radioactive gold nanoparticles are stable, the resulting solution was characterized by measuring the surface plasmon resonance wave length (λ_{max}) and the yield of radioactive gold nanoparticles over time. The UV-Visible spectroscopy measurements showed that λ_{max} was in the range between 530-535 nm (Figure 19).

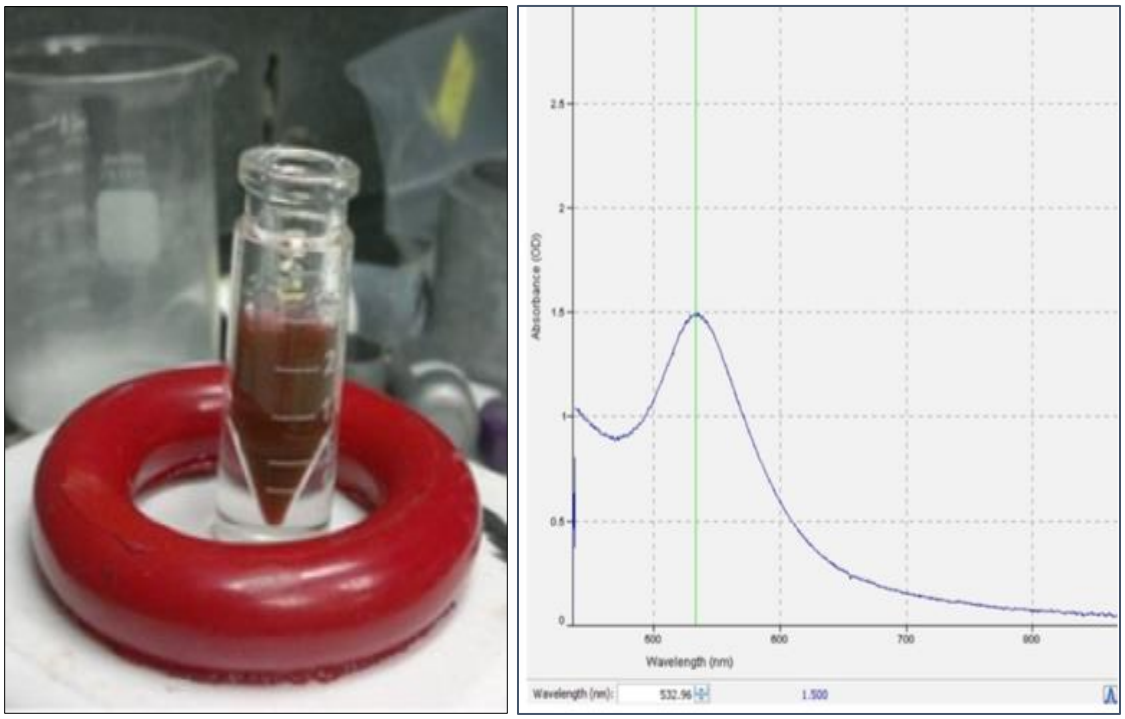

Figure 19: Radioactive MGF-^{198}AuNPs solution and UV-Visible spectrum of MGF-^{198}AuNPs, the peak appears at 532.96 nm.

Radio-TLC was conducted to estimate the yield of radioactive gold nanoparticles. It is desirable to have more than 95% of ^{198}Au as nanoparticles to prevent uptake in normal tissues. TLC plate has two regions, the origin at 50 mm (R_f = 0) and solvent front at 110 mm (R_f = 1). Gold nanoparticles remain at the origin (R_f = 0) because they do not move with mobile solvent (4 ml of methanol containing two drops of concentrated HCl) while free gold elutes with the mobile solvent (Rf = 1).

Two samples were analyzed by Radio-TLC. The first sample was mixture of ^{198}Au solution and gold salt solution in order to determine the peak's position of radioactive free gold and to ensure it is all in the $HAuCl_4$ form as that is what is needed to form the nanoparticles. If it is in the hydroxide or colloidal form it will not form nanoparticles. Therefore, Radio-TLC of $HAuCl_4$ should be performed first prior to nanoparticle formation. Whereas and a second sample was MGF-^{198}AuNPs solution to determine the percentage of ^{198}Au that existed as nanoparticles.

Radio-TLC results confirmed that over 97% of ^{198}Au was present as nanoparticulates. Figure 20 shows the spectrum of radioactive gold nanoparticles with its peak at the origin (R_f=0) with a yield of 97.5%, while 2.5% for a small peak that appears close to the peak of radioactive gold nanoparticles; it might be also nanoparticles. However, no peak of ^{198}Au appears in this figure since there is not any peak at solvent front (R_f=1) where the peak of free gold should appear.

Figure 21 shows the free gold migrates with the solvent front (R_f = 1). In comparison with Figure 20, there is no peak at solvent front region in Figure 20,

and that indicates clearly almost all ^{198}Au reacted to form radioactive gold nanoparticles.

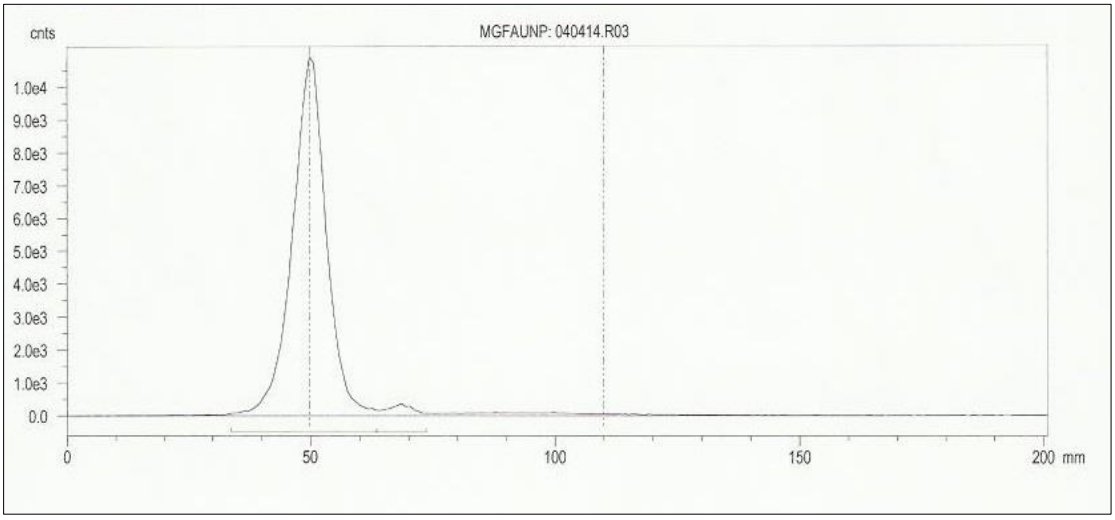

Figure 20: Radio-TLC of nanoparticles showing MGF-^{198}AuNPs peak at origin (R_f=0). Radio-TLC results confirmed that over 97% of ^{198}Au was present as nanoparticulates.

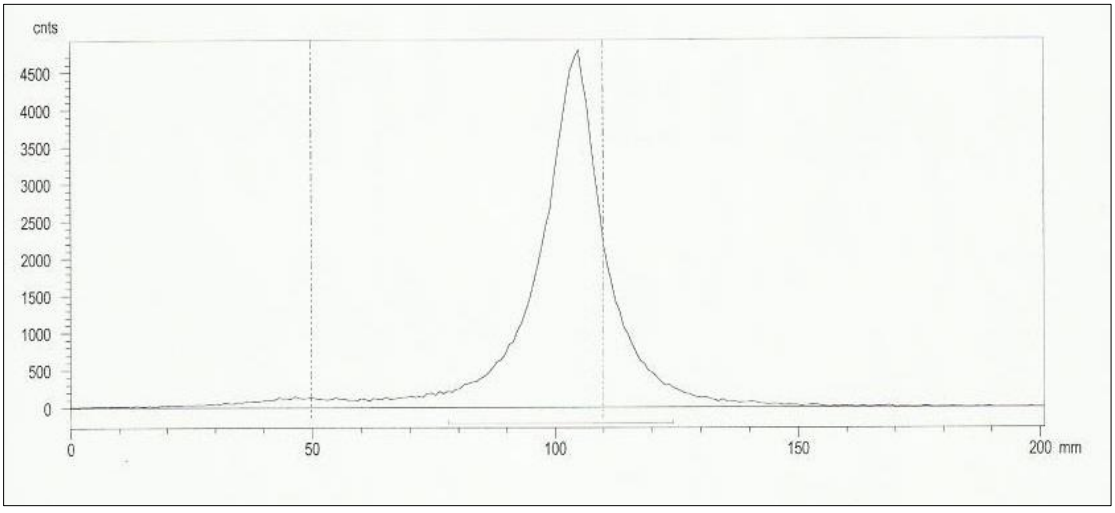

Figure 21: Radio-TLC of free (^{198}Au+$AuNaCl_4$) solution shows the ^{198}Au peak appears at solvent front region (R_f=1).

3.1.7- Stability study of radioactive MGF-^{198}AuNPs

In order to evaluate the mangiferin nanoparticles in animals, the pH of the solution needs to be 7 to match the pH of the animal's blood. This is critical as some types of nanoparticles precipitate and do not remain stable at pH of 7. Therefore a stability study was performed on these nanoparticles to insure they are still stable at pH 7.

Stability study involved formulating the nanoparticles at a pH of 2.4 and then raising the pH to nearly 7 using NaOH and DPBS, and then evaluating the pH, λ_{max}, absorbance, and Radio-TLC analysis every day for one week. If these measurements remain stable and do not vary this indicates the nanoparticles are stable. If we see that the wavelength is changing this indicates the particles are not stable.

Because the results of stability study are so crucial, five samples of radioactive MGF-^{198}AuNPs were prepared in order to evaluate their stability. These five samples were prepared with different activities, masses, and volumes of ^{198}Au in order to confirm that MGF-^{198}AuNPs are still stable even with changing of these three variables. The activities of the five samples were between (420 μCi – 4.2 mCi), the masses of ^{198}Au were between (0.0684 – 0.0126 mg), and the volumes of ^{198}Au were between (9 – 12 μl). After the preparation of these five samples of MGF-^{198}AuNPs, the pH was raised approximately to 7. Then, λ_{max}, Abs., TLC % and pH were measured over one week.

The measurements of λ_{max}, Abs., TLC % and pH of the five samples showed that MGF-^{198}AuNPs are stable because λ_{max}, Absorbance, TLC %, and pH did not vary much over one week. The standard deviation was very low indicating there is no significant change over one week. Table (3) shows the measurements of λ_{max}, Abs., TLC % and pH of one sample of nanoparticles over one week after raising the pH to 7.

Time points	λ_{max} nm	Abs.	TLC %	pH
After 1 hour	533	1.4	99.0	7.4
After 1 day	533	1.4	98.0	7.2
After 2 days	533	1.4	97.8	7.2
After 5 days	533	1.4	97.6	7.2
After 6 days	533	1.4	98.0	7.2
After 7 days	533	1.4	98.0	7.2
Mean	533	1.4	98.1	7.2
Standard deviation	--------	-------	0.40	0.05

Table 3: Measurements of λ_{max}, Abs., TLC% and pH over one week after raising the pH of nanoparticles solution to 7. Before raising the pH of nanoparticles solution to 7, the values of λ_{max}, Abs., TLC%, and PH were 533nm, 1.6, 99%, and 2.2 respectively.

3.1.8- *In vivo* stability study (bio-distribution) of MGF-^{198}AuNPs

In order to attain the maximum desired efficacy of MGF-^{198}AuNPs, they should remain stable and must not coagulate under *in vivo* conditions. Therefore, a bio-distribution study was performed to investigate the *in vivo* stability of MGF-^{198}AuNPs in normal mice.

Nanoparticles accumulation in specific organs after administration in animal models determines whether these nanoparticles are stable *in vivo* or not. Stable nanoparticles would be expected to show minimal uptake in blood and higher uptake in liver [96] whereas unstable nanoparticles would be expected to show higher uptake in blood because the free gold interacts with serum proteins in blood and/or the nanoparticles aggregate to form macro nanoparticles and thus, accumulate in blood and lungs. [12]. Therefore, the degree of aggregation *in vivo* can be measured by analyzing the concentration of nanoparticles in blood, the faster the clearance of nanoparticles from the blood, the more stable they are [12].

The uptake of nanoparticles in the liver and spleen is due to rapid removal of nanoparticles from circulation by the reticulo endothelial system (RES) [30]. The cells of reticuloendothelial system are distributed in the liver (nearly 85%), spleen (10%), and bone marrow (5%). These cells recognize small foreign substances in the blood and remove them by phagocytosis [97].

In the present study, bio-distribution studies of MGF-^{198}AuNPs in normal mice models was evaluated at various time periods (30 min, 1h, 2h, 4h, and 24h) after the administration of nanoparticles in mice. Mice (n=5) were euthanized at each time point and their organs were immediately harvested, weighed and counted along with standards in a NaI scintillation counter. Results are presented as the average% dose per organ and average %dose per gram per organ.

The results from this study showed higher up take of MGF-^{198}AuNPs in liver and spleen. However, the uptake of MGF-^{198}AuNPs in lung and blood was very low for all time periods studied.

As can be seen from figure 22 that represents the distribution profile of single dose of MGF-^{198}AuNPs in different organs of normal mice (percentage of injected dose (%ID) per organ), the majority of the nanoparticles accumulated in the liver post injection with values remaining steady from 30 min to 4 hours post injection. Quantitatively, (87.2±2.7% of the injected dose/organ in liver at 30 min, decreasing to 85.9±3.4% at 4h) followed by spleen (6.8±2.6% at 30 min, increasing to 8.6±3.0% at 4h). Low uptake of nanoparticles was found in the lungs and blood, 0.63±0.09% of injected dose in lungs at 30 min, decreasing to 0.30±0.07% at 4h, and 2.7±0.8% of injected dose in blood at 30 min decreasing to 1.4±0.2% at 4h. At 24h post injection, 95.0±1.1% of the injected dose was in the liver and 2.9±0.6% in spleen and only 0.14±0.03% in the lungs and 0.12± 0.03% in blood.

Figure 23 shows the percentage of injected dose per gram per organ, it can be easily seen that the major accumulation of nanoparticles was in the liver

and spleen whereas the lung accounted for minimum accumulation at all-time points. Quantitatively, a majority of the nanoparticles was accumulated in the liver after 24 hour post injection (from 57.0± 4.4% of the injected dose per gram of the organ, at the first 30 min after injection, 54.3±5.3% at 1h, 61.5± 5.7% at 2h, 62.5±3.6% at 4h, to 70.8±8.4% at 24 h), followed by spleen (49.5±14.9% at 30 min, 71.2±17.0% at 1h, 61.2±22.8% at 2h, 81.2±36.3% at 4h and 25.6±6.7% at 24 h post injection). Whereas very low percentage of nanoparticles was found in the lung and blood at 24h post injection, the percentage of injected dose per gram in lung was 3.3±0.7% at 30 min, 1.9±0.3% at 1h, 1.6±0.4% at 2h, 1.6±0.3% at 4h and 0.8±0.2% at 24 h post injection, and the percentage of injected dose per gram in blood was 1.7±0.5% at 30 min, 1.5±0.4% at 1h, 1.2±0.2% at 2h, 0.9±0.1% at 4h and only 0.07±0.02% at 24 h post injection. These results proved that MGF-^{198}Au nanoparticles are very stable *in vivo* and do not have tendency to aggregate.

By comparing the bio-distribution results of the present study with the results of bio-distribution study of gum arabic-^{198}AuNPs in mice that were reported previously by Katti et al (2006). Bio-distribution studies of gum arabic-^{198}AuNPs in mice showed > 80 % uptake in liver with minimal accumulation in blood and other non-target organs while the results from the present study showed higher up take of MGF-^{198}AuNPs in the liver (95.0+1.1% of the injected dose was in the liver at 24 h post injection) with very low uptake of MGF-^{198}AuNPs in lungs and blood (0.14±0.03% in the lungs and 0.12± 0.03% in blood

at 24 h post injection). Therefore, mangiferin-^{198}AuNPs are more stable *in vivo* than gum arabic-^{198}AuNPs.

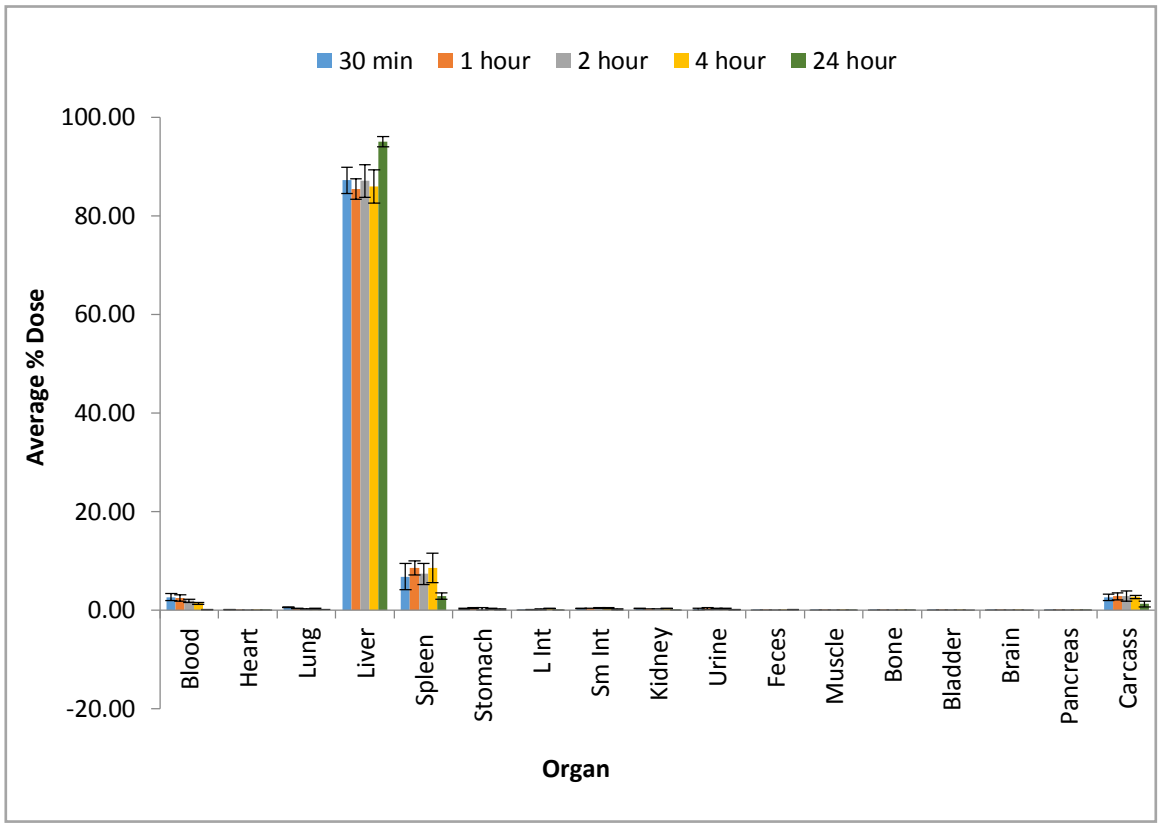

Figure 22: Bio-distribution profile shows the measurements of the radioactivity from different organs of the mice that were injected with single dose of MGF-^{198}AuNPs (8.0 µCi/100µL). The measurements were performed at 30 min, 1h, 2h, 4h, and 24h post injection. In this Figure, radioactivity obtained from different organs was calculated as the percentage of injected dose (%ID) per organ.

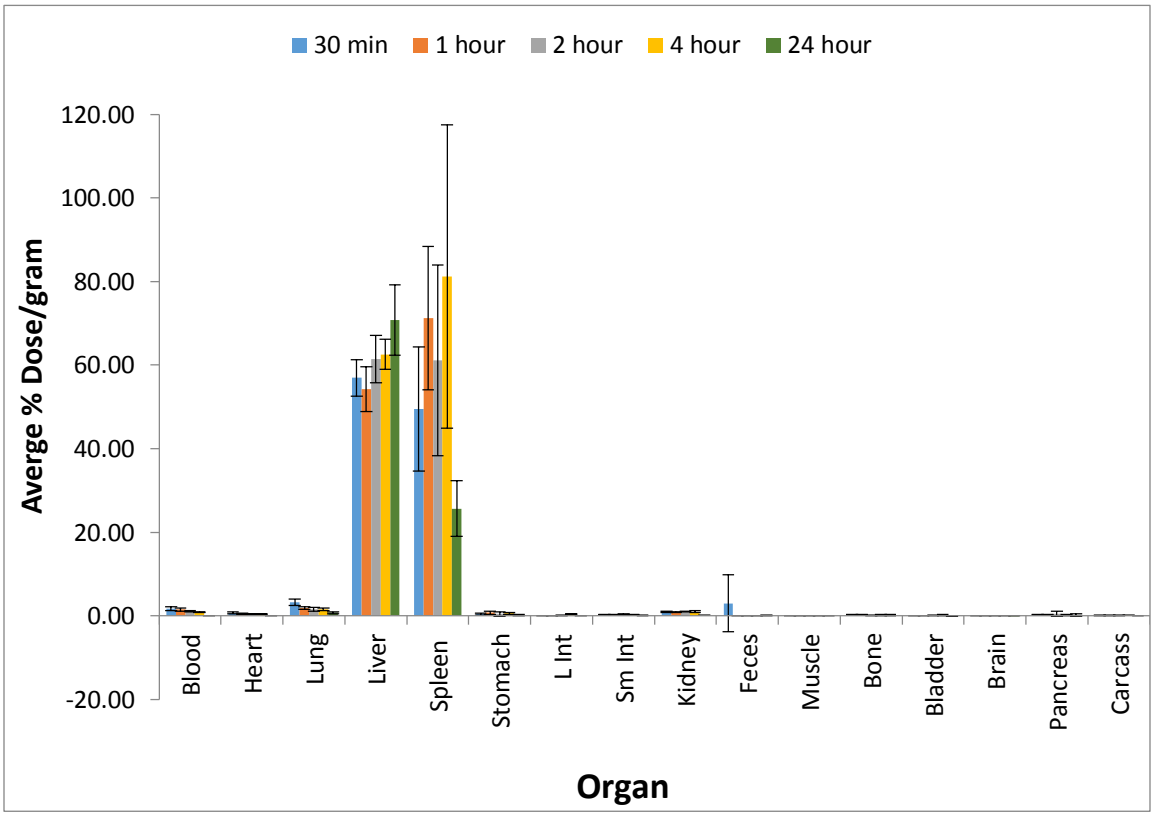

Figure 23: Bio-distribution profile shows the measurements of the radioactivity from different organs of the mice that were injected with single dose of MGF-^{198}AuNPs (8.0 µCi/100µL). The measurements were performed at 30 min, 1h, 2h, 4h, and 24h post injection. In this Figure, the radioactivity obtained from different organs was calculated as the percentage of injected dose per gram (% ID/g) of each organ.

3.1.9- *In vivo* tumor retention (intra-tumoral) study of MGF-^{198}AuNPs

Retention and clearance characteristics of MGF-^{198}AuNPs are very important properties because it determines the efficacy of therapeutic payloads within prostate tumors. High retention capability means delivery of maximum dose to the tumor with minimal side effects. Therefore, Intra-tumoral study must be performed first in order to evaluate the retention in the tumor and uptake in other organs to calculate what activity to administer to reach an effective dose.

In the present study, Intra-tumoral study in human prostate tumor bearing mice was performed In order to investigate the retention and clearance characteristics of radioactive MGF-^{198}AuNPs within prostate tumor. The Intra-tumor study included direct injection of radioactive MGF-^{198}AuNPs in prostate tumor and analysis of radioactivity in tumor as well as various organs post euthanasia of animals at 30 min, 1, 2, 4, and 24 h. Results are presented as the average% dose per organ and average %dose per gram per organ.

The results showed that nearly 80% of the injected dose (ID) of MGF-^{198}AuNP was retained in prostate tumors up to 24 h, and it was nearly constant from 30 min to 24 h. Figure 24 shows the uptake of MGF-^{198}AuNPs in various organs at different time points. As can be seen from this figure, most of the radioactive nanoparticles were retained in the prostate tumor with low leakage and subsequent uptake in the liver while there is no uptake observed in the blood. This result indicates the excellent retention of MGF-^{198}AuNPs.

To present the results numerically, the percentage of injected dose within tumor (%ID) was 80.98±13.39% at 30 min and 79.79±15.89% at 1 h, increasing to 86.68±3.58% at 2 h, decreasing to 77.80±18.45% at 4 h, and increasing to 79.82±10.55% at 24 h. There was a low leakage and subsequent uptake of MGF-^{198}AuNPs in the liver, the (%ID) in liver was 4.05±5.27% at 30 min increasing to 10.65±8.31% at 24 h, this result shows that a small amount of nanoparticles were cleared by the reticulo endothelial system to the liver. Also, there was very low leakage of injected dose into stomach and feces, 0.10±0.16% of injected dose in stomach at 30 min decreasing to 0.02±0.02% at 24 h, and 0.00±0.00% of injected dose in feces at 30 min increasing to 2.20±4.51% at 24 h. These results show that the main route of clearance is via the digestive system through the feces. In contrast, there was no noticeable leakage into blood and lung and other organs.

Figure 25 represents the percentage of injected dose divided by the mass of organs (% ID/g). In this figure it can be observed that the majority of the nanoparticles were retained within the tumor with minimum leakage to other organs. However, in comparison of this figure with the previous one, it can be seen that the (% ID/g) in tumor at 30 min is higher than the (% ID/g) at 4 and 24 h, and the reason behind this difference not because there is a leakage but because the average mass of tumors at 30 min is smaller than the average mass of tumors at 4 and 24 h. The average mass of tumors at 30 min was 0.26 mg while the average mass of tumors at 4 and 24 h were 0.39 mg and 0.47 mg

respectively. And this explains why the (% ID/g) is lower at 4 and 24 h when compared with the previous figure.

The results of intratumoral study showed that MGF-^{198}AuNPs have excellent ability to be retained within the tumor up to 24 hours with very minimum leakage to non-target organs.

In comparison of the retention characteristic of MGF-^{198}AuNPs in prostate tumor with retention characteristics of several types of radioactive gold nanoparticles in prostate tumor that have been previously reported in our laboratories [7, 58]. The results revealed that the MGF-^{198}AuNPs have a higher retention than other radioactive gold nanoparticles. The percentage of injected dose of MGF-^{198}AuNPs within tumor was higher than the percentage of injected dose of GA-^{198}AuNPs, EGCG-^{198}AuNPs, and Pomegranate-^{198}AuNPs in tumor. Therefore, it can be concluded from this comparison that MGF-^{198}AuNPs is excellent candidate to be used to treat prostate cancer and other cancers in future (Figure 26).

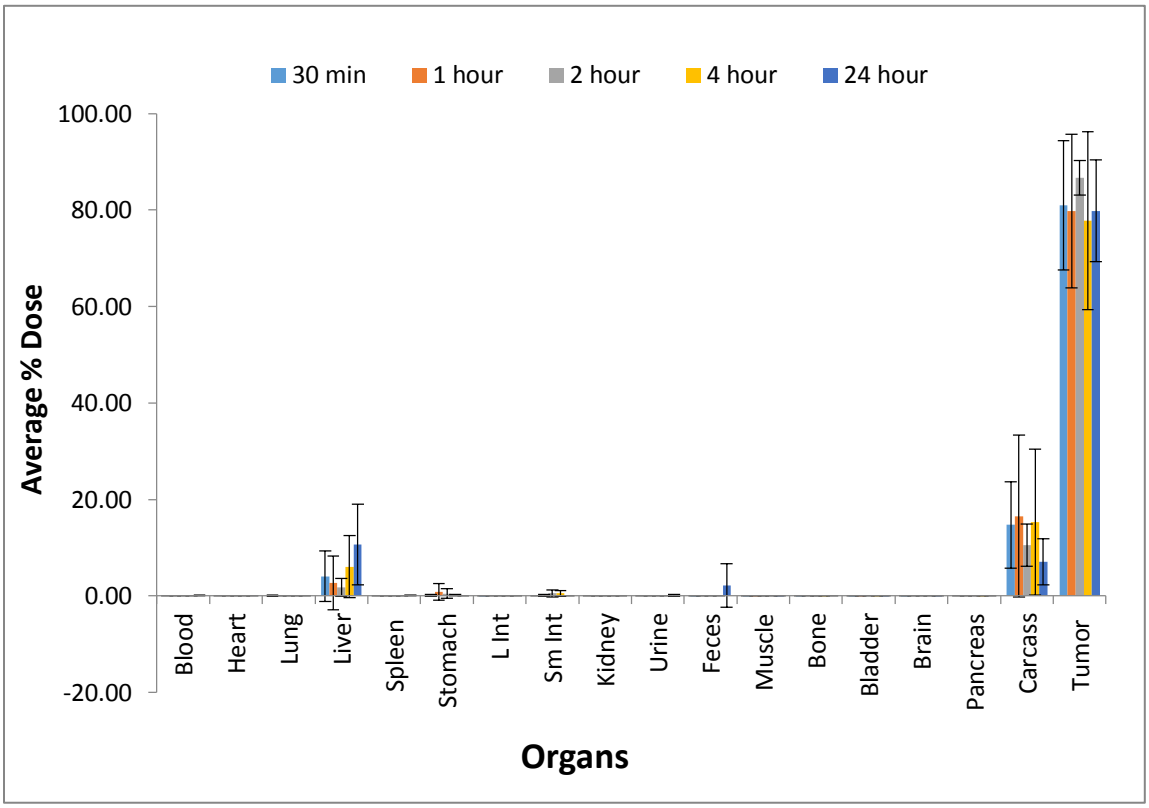

Figure 24: Shows the retention profile of radioactivity of MGF-^{198}AuNPs in tumor and the leakage to different non-target organs at 30 min, 1, 2, 4, and 24 hours after direct injection of single dose of MGF-^{198}AuNPs (4.0 µCi/30µL) in prostate tumor. In this figure, radioactivity obtained from different organs was calculated as the percentage of injected dose (%ID) of each organ.

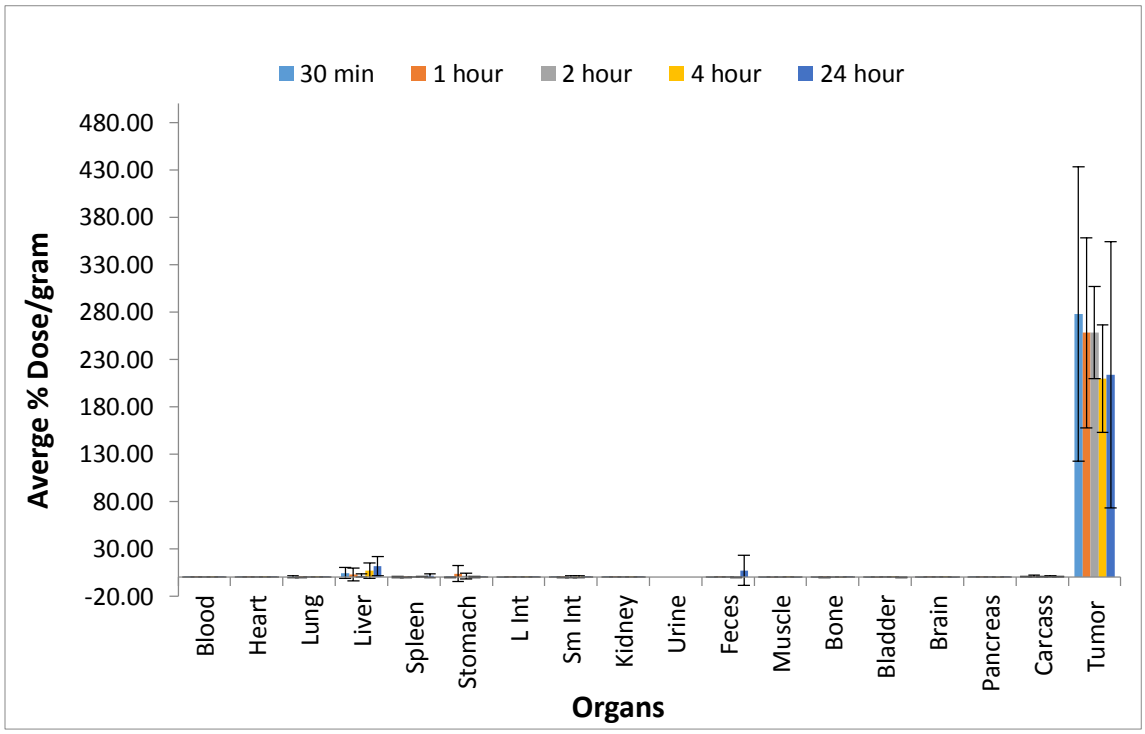

Figure 25: Shows the retention profile of radioactivity of MGF-^{198}AuNPs in tumor and the leakage to different non-target organs at 30 min, 1, 2, 4, and 24 hours after direct injection of single dose of MGF-^{198}AuNPs (4.0 µCi/30µL) in prostate tumor. In this figure, the radioactivity obtained from different organs was calculated as the percentage of injected dose per gram (% ID/g) of each organ.

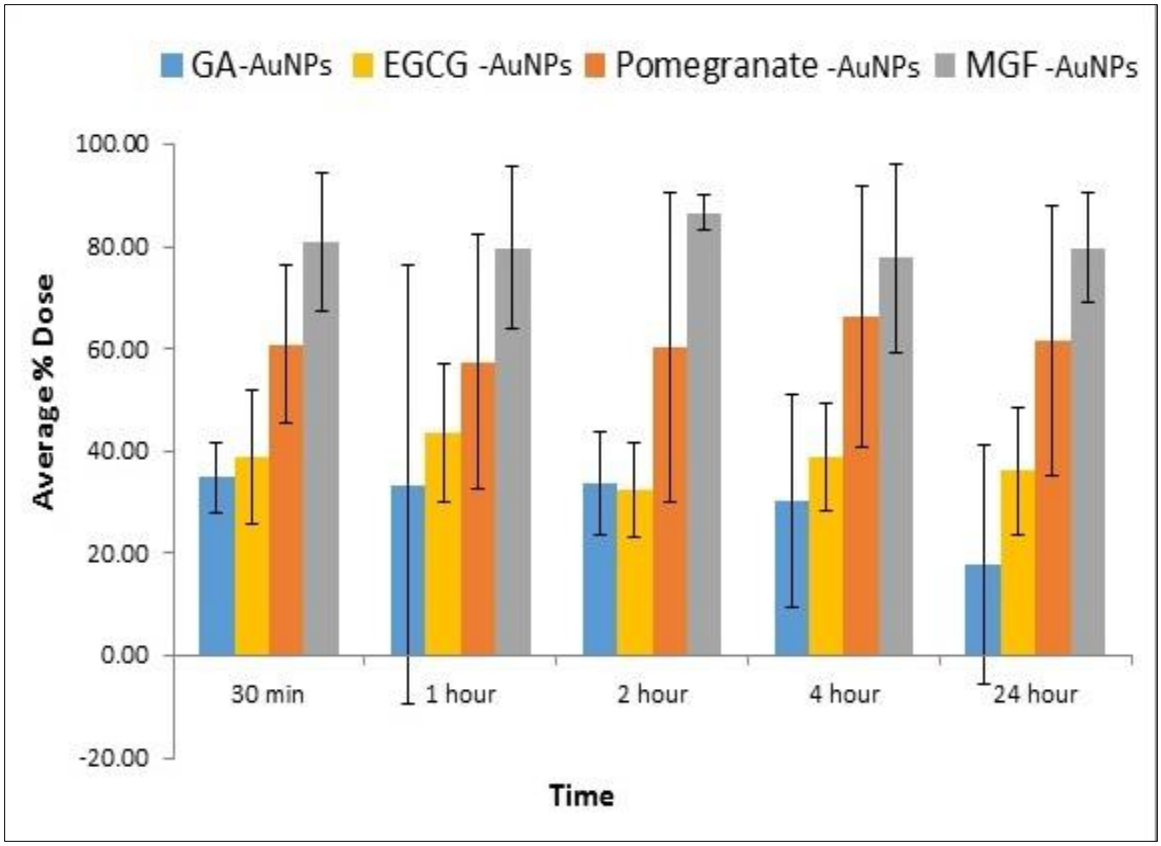

Figure 26: Comparison chart of the retention characteristics of several types of radioactive gold nanoparticles within prostate tumor. This figure shows the percentage of injected dose of MGF-^{198}AuNPs within prostate tumor is higher than that of GA-^{198}AuNPs, EGCG-^{198}AuNPs, and Pomegranate-^{198}AuNPs.

3.1.10- Therapeutic efficacy study of MGF-^{198}AuNPs

A study was performed in a human prostate tumor bearing model in order to investigate the therapeutic efficacy of radioactive MGF-^{198}AuNPs and non-radioactive MGF-AuNPs and their ability to control or reduce tumor size. The therapeutic efficacy of MGF-^{198}AuNPs was evaluated using human prostate PC-3 tumor-bearing SCID mice. As was mentioned in the materials and methods chapter, there were three groups of mice bearing prostate tumors with comparable size, the mean tumor volumes of the three groups ranged from 0.15–0.20 cm^3 and group mean body weights ranged from 16.4–24.6 g. A fourth group was evaluated also prostate tumor bearing but with larger volumes (0.43 cm^3). This fourth group had a mean body weight range of 17.2–21.8 g. The first and fourth groups were injected intratumorally with a single dose of radioactive MGF-^{198}AuNPs nanoparticles (160 µCi / 30 uL per tumor) whereas the second and third groups were injected intratumorally with 30uL of non-radioactive MGF-AuNPs and saline respectively. The group that was injected with saline served as the control group. There was an additional group of normal untreated mice that served as controls for the complete blood count (CBC) values. The study was conducted for 31 day post injection, the day of randomization was considered day 0 while the day of injection was day 2.

Results of the therapy study indicated radioactive MGF-^{198}AuNPs have the ability to reduce tumor volume in comparison to saline control group. Detailed *in vivo* therapeutic data are shown in Figure 27 which represents the effect of each solution on tumor size growth for 24 days.

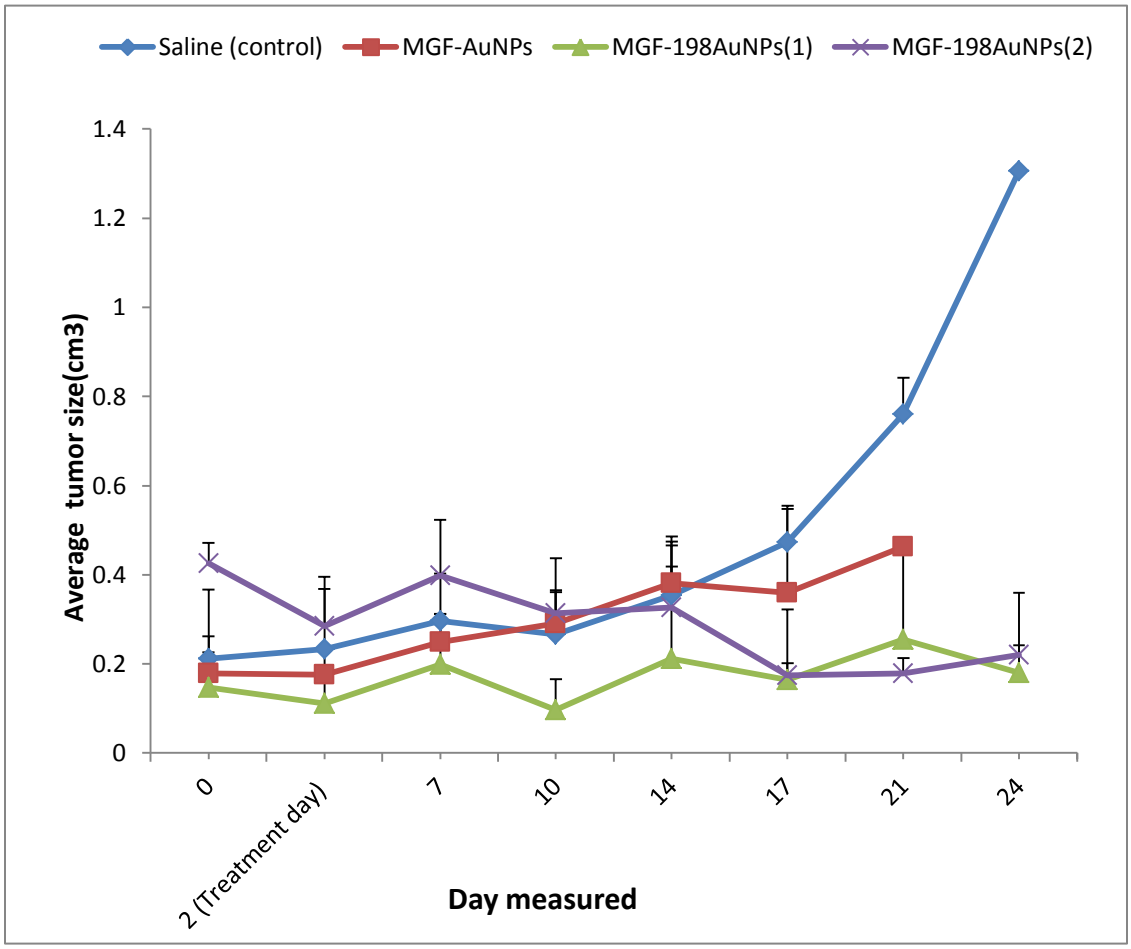

Figure 27: Therapeutic efficacy studies to control or reduce tumor size in human prostate tumor–bearing SCID mice after a single intra-tumoral administration of MGF-^{198}AuNPs, MGF-AuNPs, and saline. The graph represents mean tumor volume following 22 days of injection.

As can be seen from figure 27, after approximately one week of treatment (day 10), the tumor volume appeared to decrease in both groups that were injected with a single dose of MGF-^{198}AuNPs, in which the tumor volume of the first group was 0.11± 0.04 cm^3 on the day of treatment then showed a transient increase and then decrease to 0.10±0.06 cm^3 after the first week of treatment. The tumor volume of the second group was larger than the tumor volume of the first group on the day of injection; it was 0.29±0.11 cm^3 then increased to 0.40±0.12 cm^3 and then decreased to 0.31±0.12 cm^3 after the first week of the treatment. In contrast, the tumor volume appeared to increase in both groups that were injected with saline and MGF-AuNPs respectively, in which the tumor volume of the saline control group was 0.23±0.13 cm^3 on the day of injection and increased to 0.27±0.01 cm^3 one week post injection. The tumor volume of the non-radioactive MGF-AuNPs treated group was 0.17±0.08 cm^3 on the day of injection and then increased to 0.29±0.08 cm^3 one week post treatment.

Two weeks post injection (day 17), the tumor volume of the two groups that were injected with MGF-^{198}AuNPs was 0.16±0.15 cm^3 in the first group which was slightly greater than it was the previous week, and 0.17±0.03 cm^3 in the second group which was smaller than in the previous week. In contrast, the tumor volume of the group that was injected with non-radioactive MGF-AuNPs was 0.36±0.18 cm^3 which is much greater than one week ago, and the tumor volume of the control group was greater by two folds than the previous week (0.48±0.08 cm^3).

By three weeks post treatment (day 24), tumor volume of control group (saline) was much larger than the tumor volume of the groups injected with radioactive nanoparticles (1.31±0.00cm^3 for control versus 0.18± 0.17cm^3 for MGF-^{198}AuNPs1, and 0.22±0.02 cm^3 for MGF-^{198}AuNPs2). However, all the animals that were treated with non-radioactive MGF-AuNPs were terminated, so that there were no data to make comparison with respect to control.

It can be observed that the tumor volumes for the control animals were seven-fold larger with respect to those for the first group that was treated with MGF-^{198}AuNPs, six-fold greater with respect to those for the second group that was injected with MGF-^{198}AuNPs. Furthermore, it can be seen that the tumor volume of the second group was two-fold larger than that of control group on the day of injection but after three weeks the tumor volume was reduced while the tumor volume of the control group continued to increase and thus the tumor volume of this treated group was six-fold smaller than those of the control groups indicating the significant effect of MGF-^{198}AuNPs. These results indicate that radioactive MGF-^{198}AuNPs have significant therapeutic effect and they were able to control and reduce the tumor volume in comparison to control group as well as non-radioactive MGF-AuNPs during the three weeks. In addition, it can be concluded from the results that the surrogate non-radioactive MGF-gold nanoparticles, which were prepared by the same protocol that was used to produce radioactive MGF-^{198}AuNPs except non-radioactive gold was mixed with gold salt, did not reduce the tumor volume during the study period in comparison to radioactive nanoparticles. However, they prevented the tumor to grow fast in

comparison to control group. It can be seen from the graph at day 21 that the tumor volume of the group that were treated with MFG-AuNPs was smaller by approximately two fold than those of saline group. However, they were larger by two fold than those of the radioactive groups. Non-radioactive MGF-AuNPs slowed down the tumor growth but not as significantly as the radioactive version. The slowing down of tumor growth maybe due to the anti-cancer and anti-tumor properties of mangiferin as many studies showed that mangiferin has the ability to kill cancer cells.

The four weeks post treatment (day 31), data was not included in above graph because few animals remained alive while many animals were euthanized due to tumor burden during the study, At day 31, only 3 out of 6 animals from MGF-^{198}AuNPs first group, and 1 out of 3 animals from MGF-^{198}AuNPs second group remained alive. While all animals in MGF-AuNPs and saline group were euthanized. The tumor volume of the remaining animals increased slightly in both treated groups with radioactive nanoparticles. It can be assumed that after four weeks that the radioactivity was decayed. Thus, the cancer cells that still alive divided and the tumor began to regrow again.

By comparing the results of the present therapy study with the results obtained for EGCG -^{198}AuNPs that have been published, MGF-^{198}AuNPs and EGCG-^{198}AuNPs were able to reduce and control tumor volume. However, MGF-^{198}AuNPs has better ability to reduce the tumor volume than EGCG-^{198}AuNPs. After three weeks of injection, the mean tumor volume of the first group was treated with a single dose of MGF-^{198}AuNPs (160µCi/30µl) was seven-fold

smaller with respect to the control group that was treated with saline (30 µl). In contrast, the mean tumor volume of the group that was treated with a single dose of EGCG-^{198}AuNPs (136µCi/30µl) was five-fold smaller with respect to the control group that was treated with saline (30 µl). It is worth mentioning that the mean tumor volumes of the two groups (MGF-^{198}AuNPs1 and control) ranged from 0.15– 0.2 cm^3 at the start of the study whereas the mean tumor volumes of the EGCG-^{198}AuNPs study ranged from 0.03–0.04 cm^3, the mean tumor volumes of MGF-^{198}AuNPs study were approximately seven-fold larger than those of the EGCG-^{198}AuNPs study, and this may have some effects on how to control the tumor size as it is easy to reduce or eliminate tumors at the initial stages.

Intra tumoral study was performed to measure the radioactivity in residual tumor as well as organs of interest for each animal from the groups that were treated with MGF-^{198}AuNPs. This study was performed when animals were sacrificed at the end of study period or when tumors reached endpoint. The results from the first group showed that 69.70 ± 14.40 %ID remained in the tumor and 6.80 ± 5.90 %ID was observed in carcass whereas retention in other organs was negligible. Similarly, the results from the second group showed that 60.96 ± 25.56 %ID remained in the tumor and 13.00±10.97 %ID was observed in the carcass, 1.44 ± 2.97 %ID was observed in the liver while retention in other organs was negligible. These results clearly indicate the radioactive payload was retained in the tumor and there was minimal leakage to other organs. This suggests these radioactive nanoparticles may have potential to treat prostate

cancer as the majority of the radioactivity is retained in the tumor and does not leak to other organs.

Blood parameters within the tumor-bearing MGF-^{198}AuNPs, MGF-AuNPs, and saline treatment groups were compared with baseline levels from a fifth group of SCID mice that had not been experimentally manipulated and served as control for this analysis. Comparisons included mean counts for white cells, red cells as well as hemoglobin, lymphocytes, and platelets count. The analysis showed that the mean white blood cell (WBC) count for MGF-^{198}AuNPs-treated groups was $3.02\pm0.91\times10^3$ WBC/μL, for MGF-AuNPs treated group was $3.70\pm0.80\times10^3$ WBC/μL, and for saline treated group was $4.00\pm1.90\text{x}10^3$ WBC/μL. It can be observed from the data that (WBC) count in MGF-^{198}AuNPs-treated groups was slightly lower than (WBC) count in the other two groups. By contrast, (WBC) count for control group was $1.53\pm0.58\text{x}10^3$ WBC/μL which is lower than those of treated groups. Red blood cells count (RBC), lymphocytes, and Hemoglobin (g/dL) showed no significant differences among treated groups, and were slightly higher than those of the control group. Furthermore, the platelet counts for MGF-^{198}AuNPs-treated groups was $1098\pm327\times10^3$/μL, for MGF-AuNPs treated group was $982\pm134\times10^3$/μL, and for saline treated group was $981\pm260\times10^3$/μL whereas platelets count for control group was 741± 293 10^3/μL, It can be observed that the platelets count for all treated groups was higher than those for the control group.

3.1.11- Synthesis and characterization of radioactive MGF-^{199}AuNPs

MGF-^{199}AuNPs were produced according to the protocol described in the materials and methods chapter.

After addition of radioactive gold precursor to the MGF solution, a pale yellow solution immediately converted to a red-purple color. The red-purple color indicated the formation of radioactive MGF-^{199}Au nanoparticles.

The identity of MGF-^{199}AuNPs solution was confirmed and characterized via UV-Vis spectroscopy by measuring the surface plasmon resonance wave length (λ_{max}) and using Radio-TLC to determine the yield of radioactive gold nanoparticles. The UV-Vise spectroscopy measurements showed that λ_{max} was in the range of 534-537 nm which is slightly higher than the wave length of non-radioactive MGF-AuNPs.

Two samples were analyzed by Radio-TLC. The first was the free ^{199}Au solution and gold salt and the second was MGF-^{199}AuNPs solution. Radio-TLC results confirmed that over 98% of ^{199}Au was present as the nanoparticulate form.

Color of solution, UV-Vis spectroscopy, and Radio-TLC measurements confirmed the formation of MGF-^{199}AuNPs. Unfortunately, this protocol can be used only to produce MGF-^{199}AuNPs with low activity such as 2 mCi or less. Several experiments were preformed to increase the volume of ^{199}Au that leads to increase the activity of final solution of nanoparticles but all of them failed. The

reason behind this failure is perhaps that the increased acidity of solution might prevent the formation of nanoparticles at larger volumes of the ^{199}Au. Nevertheless, Production of MGF-^{199}AuNPs with low activity can be used in imaging procedures due to the low energy of ^{199}Au compared to ^{198}Au. An imaging agent for single photon emission computed tomography (SPECT) needs to emit gammas with energy high enough to penetrate from the patient to be detected by the camera and low enough to be collimated by the SPECT camera. Therefore, MGF-^{199}AuNPs with activity of 1-2 mCi is a good candidate to be used for this purpose. MGF-^{199}AuNPs needs to be evaluated *in vivo* in order to investigate their efficacy as imaging agent. However, *In vivo* evaluation was not performed in the present study.

3.2- Production and evaluation of radioactive citrate-^{199}AuNPs

The objective of this project was the production and evaluation of radioactive citrate-^{199}AuNPs as imaging probes for single photon emission computed tomography. In this study, radioactive citrate-^{199}AuNPs were produced and characterized. This is a joint collaboration with the University of Washington in St. Louis for developing nanoparticles that are comprised of dual SPECT imaging labels. Our part of this project was the production and purification of ^{199}Au and synthesis of the citrate-^{199}AuNPs which were then shipped to

Washington University to perform additional derivatization for targeted uptake and imaging.

3.2.1- Synthesis and characterization of radioactive citrate-^{199}AuNPs

Citrate-^{199}AuNPs were synthesized according to the protocol that was established and described in the materials and methods chapter. Briefly, 2 ml of 0.5 mM of $NaAuCl_4$ and 15 µl of ^{199}Au were mixed together, heated, and stirred until the solution boiled. Next, 206 µl of 38.8 mM of sodium citrate was added with continuous heating. After a few minutes the color of the solution turns gradually from pale yellow to wine red color indicating formation of citrate-^{199}AuNPs.

The resulting solution of nanoparticles was characterized by measuring the surface Plasmon resonance wave length (λ_{max}). The UV-visible spectroscopy measurements showed that λ_{max} was in the range of 523 -526 nm. This value of λ_{max} of radioactive-citrate gold nanoparticles was higher than λ_{max} of non-radioactive citrate gold nanoparticles by only 5 nm. The results of Grabar et al (1995) showed that the non-radioactive citrate-gold nanoparticles have λ_{max} of 520 nm and have core size of 13 nm. In the present work, radioactive-citrate^{199}AuNPs had a λ_{max} in the range of 523-526 nm indicating they are within the value reported in the literature.

Radio-(TLC) was conducted to estimate the yield of radioactive gold nanoparticles. It is desirable to have more than 95% of ^{199}Au as nanoparticles to

prevent uptake in normal tissues. As was mentioned previously, the origin was at 50 mm and the solvent front at 110 mm. Gold nanoparticles remain at the origin R_f = 0 because they do not move with mobile solvent (4 ml of methanol containing two drops of concentrated HCl) while free gold elutes with the mobile solvent with an R_f = 1.

Two samples were analyzed by Radio TLC. The first sample was a mixture of free ^{199}Au solution and gold salt solution to ensure it is all in the $HAuCl_4$ form as that is what is needed to form the nanoparticles. If it is in the hydroxide or colloidal form it will not form nanoparticles. Therefore, radio TLC of $HAuCl_4$ should be performed prior to nanoparticle formation. The second sample was citrate-^{199}AuNPs solution to determine the yield of ^{199}Au that existed in nanoparticles structure. Radio-TLC results confirmed that over 97% of ^{199}Au was present as the nanoparticulate form, and that means ^{199}Au reacted to form radioactive gold nanoparticles.

3.2.2- *In vivo* evaluation of radioactive citrate-^{199}AuNPs

Radioactive citrate-^{199}AuNPs have been successfully synthesized, and were shipped to Washington University to perform additional derivatization for targeted uptake and imaging. At Washington University, they designed a dual-radiolabeled metallic nanoparticles doped with ^{199}Au and surface functionalized with ^{111}In. And they evaluated this probe in a lung model targeting Matrix metallopeptidase 9 (MMP-9).

They did a comparison study between radioactive citrate-^{199}AuNPs (370 µCi) that were produced at MURR laboratories and non-radioactive citrate-AuNPs that were labeled with radioactive ^{125}I (500 µCi) in order to investigate the *in vivo* stability of these nanoparticles. These two gold nanoparticle constructs were injected intratracheally into the lungs of mice and imaged immediately, at 3 h, and 24 h post injection. They observed clear differences in clearance between the two probes. Whereas there was no significant decrease in uptake values of radioactive citrate-^{199}AuNPs from the lung even 24 hours after injection, a 76% decrease was observed with the ^{125}I-labeled nanoparticles as shown in figure 28. These preliminary experiments provide evidence that radioactive citrate-^{199}AuNPs are a viable alternative to the unstable ^{125}I-labeled gold nanoparticles. Therefore, they proceeded to design an activatable SPECT imaging probe by using a dual-radiolabeled metallic gold nanoparticle doped with ^{199}Au and surface functionalized with ^{111}In. And they evaluated this probe in a lung model targeting MMP9.

The ability to synthesize radioactive citrate-^{199}AuNPs with high activity (10-16 mCi) allowed researchers enough time to do further labeling with peptides or antibodies to target specific types of cancer or perform dual radiolabeling with other radioactive isotopes such as ^{111}In in order to get two-channel SPECT imaging.

In comparison with radioactive citrate-^{199}AuNPs, MGF-^{199}AuNPs were synthesized with low activity (2 mCi) which can be used for SPECT imaging as they are, without labeling to target specific cancers.

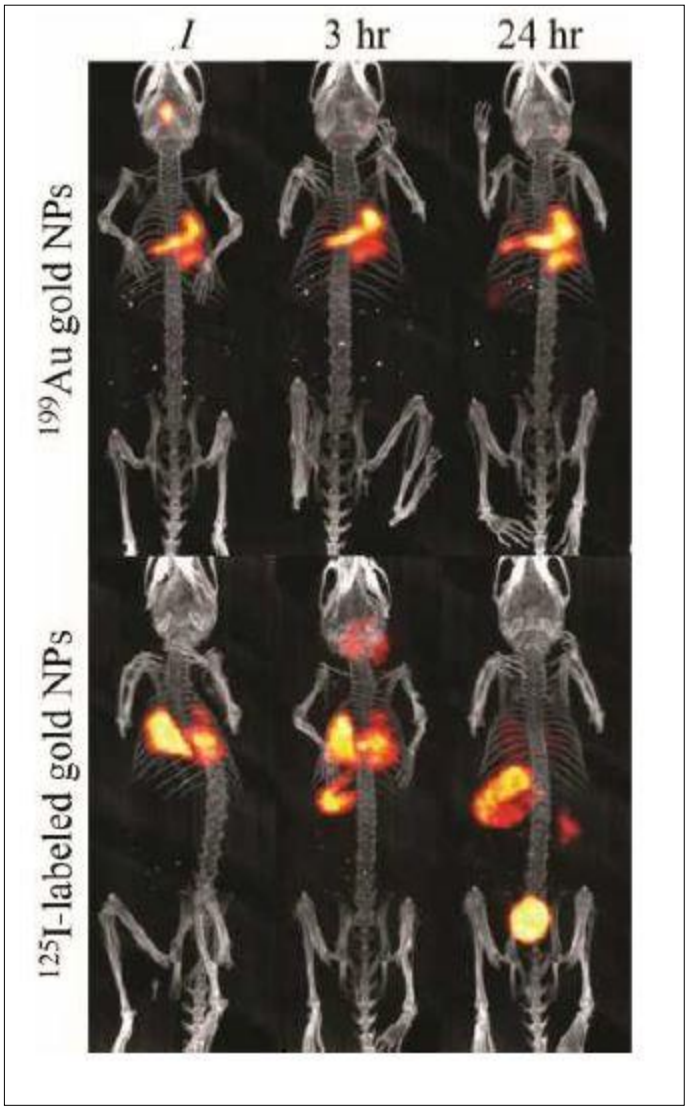

Figure 28: *In vivo* evaluation of ^{125}I-labeled citrate-AuNPs and radioactive citrate-^{199}AuNPs that were injected intratracheally into the lungs of mice and imaged immediately, 3h, and 4h post injection.

3.3- MCNP simulations

The objective of the third project was to calculate, by means of MCNP simulations, the dose distribution delivered by radioactive gold nanoparticles (^{198}AuNPs or^{199}AuNPs) to tumor inside the human prostate as well as to the normal tissues surrounding the tumor using water and A-150 tissue equivalent plastic phantoms.

Water and A-150 tissue equivalent plastic phantoms have been used to simulate the normal tissues as well as tumor tissues in order to investigate the dose distribution profile of betas and gammas in each medium. Both ^{198}Au and ^{199}Au emit photons and electrons,the most recent version of MCNP allows for the simulation of coherent nuclear decay processes. Hence, we were able to simultaneously compute dose from photons and electrons with a coherent gold source emitting betas and gammas in proper ratios based on the amount of gold used.

3.3.1- MCNP simulations of ^{198}AuNPs

As mentioned previously, ^{198}Au emits both photons and electrons. Therefore, MCNP simulations were performed for both photon and electron transport to calculate the dose that is deposited by betas and gammas that are emitted from ^{198}Au. MCNP code calculated the dose distribution for each decay as a function of distance.

Simulation results showed that the maximum dose was delivered at the center of the tumor (r=0) and then decreases with distance moving from the center to the outer edges. Figure 29 shows the dose profile as function of distance.

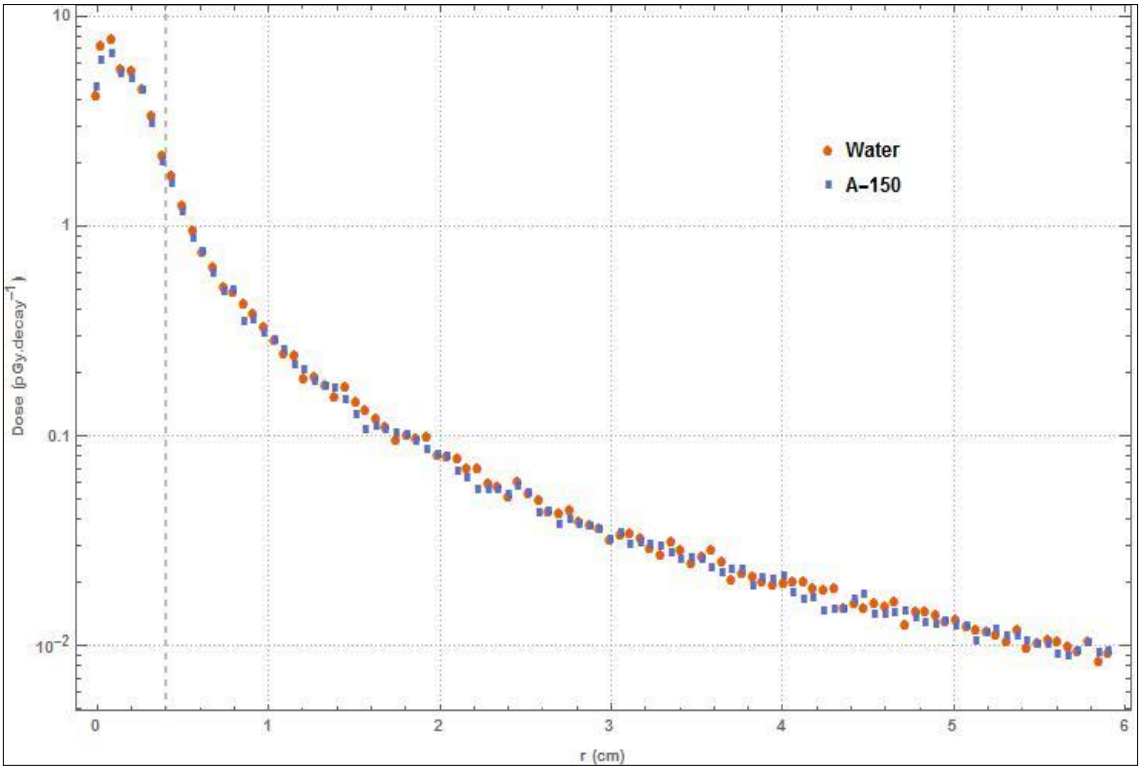

Figure 29: Distribution of deposited dose as a function of distance r from the tumor center for ^{198}AuNPs. r=0 refers to center of tumor, r=0.4 cm refers to periphery of tumor, r=2 periphery of prostate, and r=2.5 cm refers to periphery of bladder or rectum that is close to prostate. Water and A-150 phantoms were used.

Figure 29 represents dose delivered by each decay of ^{198}Au to tissues. In this figure, it can be observed that the dose distribution curves of both water and A-150 phantoms are nearly similar and have nearly the same values. As can be seen, the dose at the center of the tumor is approximately **9 PGy/decay** and decreases exponentially to reach **1.1 PGy/decay** at the periphery of the tumor, whereas the dose at the periphery of the prostate is only **0.08 PGy/decay**. The center of the tumor is assumed to be at 0, the periphery of the tumor at 0.4 cm, and the the periphery of the prostate at 2 cm on the plot (see section 2.4.1). Furthermore, the dose decreases to **0.04 PGy/decay** at the periphery of the bladder or rectum that is close to the prostate whereas the dose at the center of the bladder is only **0.01 PGy/decay**.

The ratio of deposited dose in the center of the tumor to deposited dose in the periphery of the tumor is (9/1.1) = 8.18 which means the dose in the center of the tumor is 8.18 fold higher than the dose at the periphery of the tumor. Likewise, the ratio of deposited dose in the center of the tumor to deposited dose in the periphery of the prostate is (9/0.08) = 112.5 which means the dose in the center of the tumor is 112.5 fold higher than the dose in the periphery of the prostate. In addition, the ratio of deposited dose in the center of the tumor to deposited dose in the center of the bladder is (9/0.01) = 900 showing the dose in the center of the tumor is higher than the dose in the center of the bladder by 900 fold.

If we suppose that a patient was injected in the tumor with radioactive ^{198}AuNPs that have an activity of 10 mCi which is equal to 3.7×10^{8} Bq. One Bq is

defined as the activity of a quantity of radioactive material in which one nucleus decays per second. Therefore, the deposited dose rate in the center of the tumor would be equal to the dose deposited by each decay in the the center of the tumor that was calculated by MCNP multiplied by the activity in (dis/sec) that was given to the patient.

Dose rate= 9×10^{-12} Gy/dis× 3.7×10^{8} dis/sec= 33.3×10^{-4} Gy/sec

Dose rate = 12 Gy/h dose delivered to the center of tumor.

Since the dose in the center of tumor is higher than the dose in the periphery of the tumor by 8.18 fold as it was calculated before, then the deposited dose in the periphery of the tumor would be equal to 12 Gy/h / 8.18 = 1.46 Gy/h

Or we can calculate it by using the previous method, in which deposited dose in the periphery of tumor would be equal to dose deposited by each decay in periphery of tumor that was calculated by MCNP multiplied by the activity in (dis/sec) that was given to the patient.

Dose rate= 1.1×10^{-12} Gy/dis× 3.7×10^{8} dis/sec= 4.07×10^{-4} Gy/sec

Dose rate = 1.46 Gy/h dose delivered to the periphery of the tumor.

Since the dose in the tumor is higher than the dose at the periphery of the prostate by 112.5 fold, then the deposited dose in the periphery of prostate would be equal to 12Gy/h / 112.5 = 0.1Gy/h

Or we can calculate by using previous method, in which deposited dose in the periphery of prostate would be equal to dose deposited by each decay that was calculated by MCNP multiplied by the activity in (dis/sec) that was given to the patient.

Dose rate= 0.08×10^{-12} Gy/dis× 3.7×10^{8} dis/sec= 0.296×10^{-4} Gy/sec

Dose rate = 0.1 Gy/h dose delivered to the periphery of the prostate.

The results of the computations clearly shows that the dose delivered by ^{198}AuNPs is highest in the tumor and then decreases significantly toward the periphery and surrounding normal tissues.

3.3.2- MCNP simulations of ^{199}AuNPs

As mentioned previously, ^{199}Au isotope emits both photons and electrons. Therefore, MCNP simulations were performed for both photon and electron transport to calculate the dose that is deposited by betas and gammas emitted from ^{199}Au isotope. MCNP code calculated the dose distribution for each decay as a function of distance.

Simulation results showed that the dose is highest at the center of tumor and decreases significantly toward the periphery of tumor and normal tissues. Dose distribution of ^{199}Au is similar to that of ^{198}Au. However the deposited dose by ^{199}Au is significantly lower than the dose deposited by ^{198}Au. It is known that the energies of betas and gammas that are emitted by ^{199}Au are lower than those

that are emitted by ^{198}Au. Hence, the dose deposited by ^{199}Au must be lower than the dose deposited by ^{198}Au even though they have the same activity, and MCNP results are in good agreement with this.

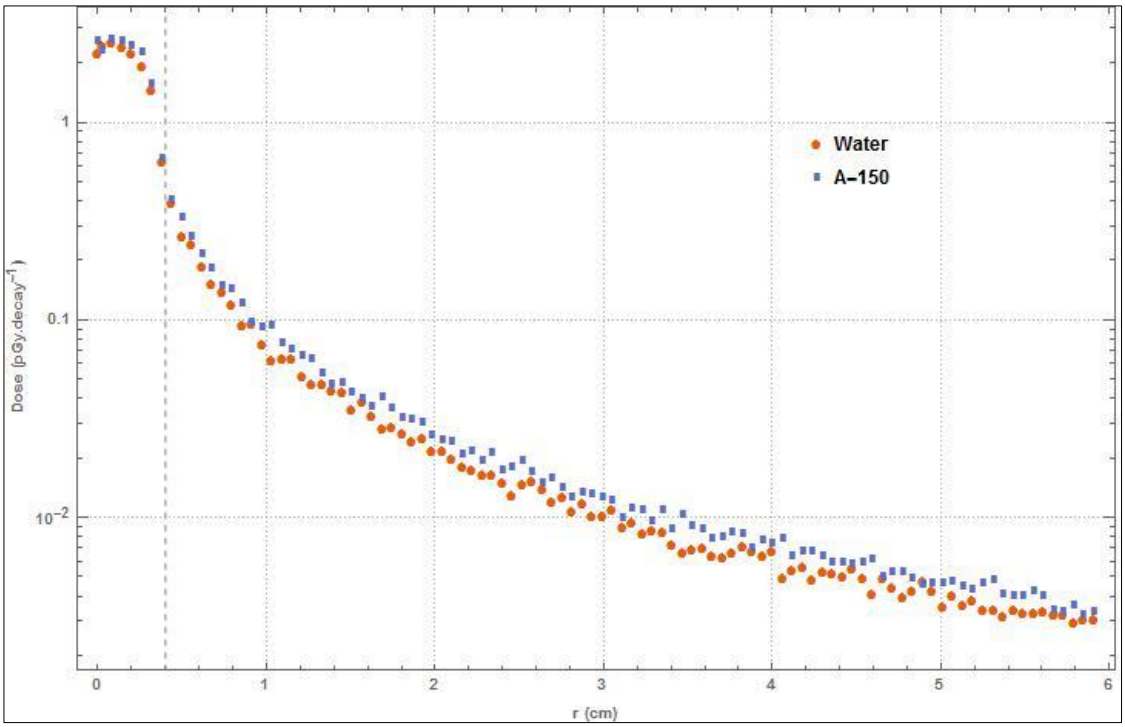

Figure 30: Distribution of deposited dose as a function of distance r from the tumor center for ^{199}AuNPs. r=0 refers to center of tumor, r=0.4 cm refers to periphery of tumor, r=2 cm refers to the periphery of prostate, and r=2.5 cm refers to the periphery of bladder or rectum that is close to prostate. Water and A-150 phantoms were used.

Figure 30 represents dose delivered by each decay of ^{199}Au to tissues. It can be seen from this figure that the dose distribution curves of both water and A-150 phantoms are similar and have nearly the same values at the tumor region

but beyond that, the dose in A-150 phantom is slightly higher than the dose in water phantom. Dose distribution curve in water phantom is explained below.

In Figure 30, it is observed that the dose at the center of the tumor is approximately **1.2 PGy/decay** and decreases exponentially to reach **0.4 PGy/decay** at the periphery of the tumor, whereas the dose at the periphery of the prostate is only **0.02 PGy/decay**. (See section 2.4.1regarding the radii of tumor and other organs). Furthermore, the dose decreases to reach only **0.01 PGy/decay** at the periphery of the bladder or rectum that is close to prostate whereas the dose at the center of bladder is only **0.001 PGy/decay**.

The ratio of deposited dose in the center of tumor to deposited dose in the periphery of tumor is (1.2/0.4) = 3 which means the dose in the center of the tumor is 3 fold higher than the dose in the periphery of the tumor. Also, the ratio of deposited dose in the center of the tumor to deposited dose in the periphery of the prostate is (1.2/0.02) = 60 fold. In addition, the ratio of deposited dose in the center of the tumor to deposited dose in the center of bladder is (1.2/0.001) = 1200 fold

If we take the same example that was mentioned previously in which a patient is injected in the tumor with radioactive ^{199}AuNPs that have activity of 10 mCi which is equal to 3.7×10^{8} Bq. Then the deposited dose rate in the center of tumor would be equal to dose deposited by each decay in the center of tumor that was calculated by MCNP multiplied by the activity in (dis/sec) that was given to the patient.

Dose rate= 1.2×10^{-12} Gy/dis× 3.7×10^{8} dis/sec= 4.44×10^{-4} Gy/sec

Dose rate = 1.6 Gy/h dose delivered to the center of tumor

Since the dose in the center of the tumor is higher than the dose at the periphery by 3 fold then the deposited dose in the periphery of tumor would be equal to 1.6 Gy/h / 3 = 0.53 Gy/h

Since the dose in the tumor is higher than the dose at the periphery of the prostate by 60 fold then the deposited dose in the periphery of prostate would be equal to 1.6 Gy/h / 60 = 0.026 Gy/h

The results of the computations clearly show that the dose that is delivered by ^{199}AuNPs to the tissues is highest in the tumor region and decreases significantly toward the periphery and normal tissues.

MCNP simulations results indicate radioactive gold nanoparticles (^{198}Au NPs/ ^{199}AuNPs), which are distributed homogenously in the tumor, deposit most of their energy in the tumor region. The dose deposited by ^{198}Au is significantly higher than the dose deposited by ^{199}Au at the tumor region as well as normal tissues. Therefore, ^{198}Au is a preferred probe for use in therapeutic applications while ^{199}Au is well-suited for applications in imaging. Table 4 summarizes the deposited dose by ^{198}Au/^{199}Au nanoparticles in tumor, prostate, and normal organs in human model.

Tissue	Dose rate (Gy/h)	
	^{198}AuNPs(10 mCi)	^{199}AuNPs (10 mCi)
Center of tumor	12	1.6
Periphery of tumor	1.46	0.53
Periphery of prostate	0.1	0.026
Periphery of bladder and rectum that is close to the prostate	0.053	0.013
Center of bladder	0.013	0.0013
Center of rectum	0.026	0.004

Table 4: Lists the deposited dose of ^{198}Au/^{199}Au nanoparticles to the tumor, prostate, and normal organs in human model.

3.4- Conclusions

This work resulted in the development of three types of radioactive gold nanoparticles: MGF-^{198}AuNPs, MGF-^{199}AuNPs, and citrate-^{199}AuNPs. Our results infer that MGF-^{198}AuNPs are excellent therapeutic probes for treating prostate cancer whereas the corresponding MGF-^{199}AuNPs and citrate-^{199}AuNPs are well-suited for use in imaging applications. Detailed MCNP calculations, performed as part of this investigation have shown that these nanoparticles deposit most of their energy at the tumor sites.

In the first project of this study, phytochemical mangiferin acted as reducing and stabilizing agent to reduce gold within gold salt to corresponding stable gold nanoparticles. The protocols that were established to synthesize radioactive MGF-^{198}AuNPs and MGF-^{199}AuNPs by using mangiferin as reducing and stabilizing agent were successful. Based on the results radioactive MGF-^{198}AuNPs are stable *in vitro* as well as *in vivo,* and can be produced with high activity. It can be concluded from Intra-tumoral and therapeutics studies that MGF-^{198}AuNPs is good candidate to be used to treat prostate cancer. MGF-^{199}AuNPs are also stable *in vitro*. However, *in vivo* evaluation was not performed. MGF-^{199}AuNPs were produced only with low activity (2 mCi). Nevertheless, they can be used for imaging applications that need low activity.

In second project of this study, the protocol that was developed to synthesize radioactive citrate-^{199}AuNPs by using sodium citrate as reducing and stabilizing agent was successful in producing this type of radioactive gold nanoparticles. Results of testing the *in vivo* stability of citrate-^{199}AuNPs as

imaging probe in lungs showed that they were retained in the lung and there was no clearance up to 24 hours after injection. These results indicated that citrate-^{199}AuNPs can be used as imaging probe for SPECT. Furthermore, the ability to synthesize radioactive citrate-^{199}AuNPs with high activity (10-16 mCi) by using this protocol allowed researchers enough time to do further conjugation to peptides or antibodies to target specific types of cancer or perform dual radiolabeling with other radioactive isotopes.

In the third project of this study, MCNP simulation results showed that the deposited dose by ^{198}AuNPs or ^{199}AuNPs, which are distributed homogenously in the tumor, is highest in the tumor and decreases as you move towards the tumor periphery and surrounding organs. The dose deposited by ^{198}Au is significantly higher than the dose deposited by ^{199}Au in all regions. It can be concluded from these results that radioactive gold nanoparticles deposit most of their energy at the tumor while depositing negligible amount of energy at organs at risk such as the bladder and rectum. Since ^{198}Au energy is high and its radiation energy would be delivered to tumor site without harming normal tissues or organs at risk, it can be concluded that ^{198}AuNPs are a promising modality to treat prostate cancer and other cancers. The combined effect of the anti-oxidative and anti-cancer activities of mangiferin with the energy of beta and gamma that are emitted from ^{198}Au would kill cancer cells efficiently. As expected due to the low beta and gamma energy for ^{199}Au MCNP calculations showed doses to the normal organs, such as bladder and rectum, are acceptable and less than the

reported value of maximum tolerated dose [98]. Therefore, ^{199}AuNPs could be used for imaging purposes.

3.5- Future work

The promising results of the present work suggest several directions for future research.

In vivo evaluation results of radioactive MGF-^{198}AuNPs in mice showed that these nanoparticles are stable *in vivo* and are able to control and reduce the tumor size efficiently. Studies in larger animals such as dogs or monkeys should be performed as these animals and their diseases are known to more closely mimic the diseases in humans and thus more accurately reflect how these agents will behave in humans. Since radioactive MGF-^{198}AuNPs were able to control and reduce induced prostate tumors within mice, MGF-^{198}AuNPs should be evaluated for possible treatment of other cancers such as breast cancer. Also in future one should investigate the ability of MGF-^{198}AuNPs to be labeled with peptides or antibodies to target specific types of cancer using active targeting mechanism.

In the present study, MGF-^{199}AuNPs with low activity were produced and their *in vitro* stability evaluated. However, *in vivo* evaluation was not performed. Therefore, *in vivo* evaluation of MGF-^{199}AuNPs to investigate their efficacy as imaging agents for SPECT needs to be performed in future. Also, more

experiments need to be performed to modify the protocol of synthesis of MGF-^{199}AuNPs in order to synthesize MGF-^{199}AuNPs with higher activities

In the present study, radioactive citrate-^{199}AuNPs were produced and evaluated. A group from Washington University designed a dual-radiolabeled metallic nanoparticles doped with ^{199}Au and surface functionalized with ^{111}In. They evaluated this probe in a lung model targeting matrix metallopeptidase 9 (MMP-9) and the results of these experiments are promising to use them as multispectral agent for SPECT. Citrate-^{199}AuNPs may have promise as imaging agents in more than lung administration applications and therefore more studies need to be performed to evaluate them.

Regarding dose distribution MCNP computations, we used simple models for prostate and the surrounding tissues and organs. The nanoparticle distribution was assumed uniform in the tumor. It will be of interest to use more realistic models and a range of particle distributions.

REFERENCES

1. Wang, Z., *Plasmon—resonant gold nanoparticles for cancer optical imaging.* Science China Physics, Mechanics and Astronomy, 2013. **56**(3): p. 506-513.
2. Brawley, O.W., *Prostate cancer epidemiology in the United States.* World journal of urology, 2012. **30**(2): p. 195-200.
3. http://www.cancer.org/research/cancerfactsfigures/cancerfactsfigures/cancer-facts-figures-2013.
4. http://www.cancerresearchuk.org/about-cancer/type/prostate-cancer/treatment/chemotherapy/about-chemotherapy-for-prostate-cancer.
5. Abu-Ghanem, Y., et al., *Treatment modalities for localised prostate cancer.* Trends in Urology & Men's Health, 2012. **3**(2): p. 21-25.
6. Pugh, T.J., et al., *Radiation therapy modalities in prostate cancer.* Journal of the National Comprehensive Cancer Network, 2013. **11**(4): p. 414-421.
7. Shukla, R., et al., *Laminin receptor specific therapeutic gold nanoparticles (198AuNP-EGCg) show efficacy in treating prostate cancer.* Proceedings of the National Academy of Sciences, 2012. **109**(31): p. 12426-12431.
8. Mesbahi, A., *A review on gold nanoparticles radiosensitization effect in radiation therapy of cancer.* Reports of Practical Oncology & Radiotherapy, 2010. **15**(6): p. 176-180.
9. Dueitt, B., *Comparisons of External Beam Radiation Therapy, Brachytherapy, and Combination Therapy in the Treatment of Prostate Cancer.*
10. Chanda, N., et al., *Radioactive gold nanoparticles in cancer therapy: therapeutic efficacy studies of GA-198 AuNP nanoconstruct in prostate tumor–bearing mice.* Nanomedicine: Nanotechnology, Biology and Medicine, 2010. **6**(2): p. 201-209.
11. Khan, F.M., *The Physics of Radiation Therapy*. fourth ed.
12. Katti, K., et al., *Hybrid gold nanoparticles in molecular imaging and radiotherapy.* Czechoslovak Journal of Physics, 2006. **56**(1): p. D23-D34.
13. Nune, S.K., et al., *Green nanotechnology from tea: phytochemicals in tea as building blocks for production of biocompatible gold nanoparticles.* Journal of materials chemistry, 2009. **19**(19): p. 2912-2920.
14. Jeremic, B., A.R. Aguerri, and N. Filipovic, *Radiosensitization by gold nanoparticles.* Clinical and Translational Oncology, 2013. **15**(8): p. 593-601.
15. Jain, S., D. Hirst, and J. O'sullivan, *Gold nanoparticles as novel agents for cancer therapy.* 2014.
16. Abdelhalim, M.A.K., M.M. Mady, and M.M. Ghannam, *Physical properties of different gold nanoparticles: ultraviolet-visible and fluorescence measurements.* J Nanomed Nanotechol, 2012. **3**(133): p. 2.
17. Kulkarni, R., *Quantification of absorbed doses from radioactive gold nanoparticles and chromium 51 seed implants*. 2012.

18. Singh, R. and J.W. Lillard, *Nanoparticle-based targeted drug delivery.* Experimental and molecular pathology, 2009. **86**(3): p. 215-223.

19. http://www.udel.edu/udaily/2014/nov/cancer-nanotherapeutic-112213.html.

20. Patra, C.R., et al., *Fabrication of gold nanoparticles for targeted therapy in pancreatic cancer.* Advanced drug delivery reviews, 2010. **62**(3): p. 346-361.

21. Voliani, V., *Update on gold nanoparticles from cathedral windows to nanomedicine*. 2013.

22. Jain, P.K., I.H. El-Sayed, and M.A. El-Sayed, *Au nanoparticles target cancer.* nano today, 2007. **2**(1): p. 18-29.

23. Wang, Z. and L. Ma, *Gold nanoparticle probes.* Coordination Chemistry Reviews, 2009. **253**(11): p. 1607-1618.

24. Hampp, E.B., R.; Odusanya, O.S.; Anuku, N.; Malatesta, K.A.; Soboyejo, W.O.,, *Biosynthesis and adhesion of gold nanoparticles for breast cancer detection and treatment.* Materials Research Society, 2012. **27(22)**.

25. Ghosh, P., et al., *Gold nanoparticles in delivery applications.* Advanced drug delivery reviews, 2008. **60**(11): p. 1307-1315.

26. Gu, F.X., et al., *Targeted nanoparticles for cancer therapy.* Nano today, 2007. **2**(3): p. 14-21.

27. Mitra, A., Lee, C., Cheng, K., *Advanced drug delivery*. 2013.

28. http://www.medixselect.com/page/averageprostatesize.

29. Jhaveri, A.M. and V.P. Torchilin, *Multifunctional polymeric micelles for delivery of drugs and siRNA.* Frontiers in pharmacology, 2014. **5**.

30. Webster, T., *Safety of Nanoparticles: From Manufacturing to Medical Applications*. 2008.

31. http://www.malvern.com/en/products/measurement-type/zeta-potential/default.aspx.

32. Olson, E., *Zeta Potential and Colloid Chemistry.* Journal of GXP Compliance, 2012. **16**(1).

33. Nano Composix, Z.p.a.o.n., http://nanocomposix.com.

34. http://en.wikipedia.org/wiki/File:Diagram_of_zeta_potential.

35. http://www4.ncsu.edu/~hubbe/Defnitns/ShearPln.htm.

36. Mady, M.M., et al., *Biophysical characterization of gold nanoparticles-loaded liposomes.* Physica Medica, 2012. **28**(4): p. 288-295.

37. Tabrizi, N., *Generation of Nanoparticles by Spark Discharge*. 2009.

38. Boddu, S.R., et al., *Gold, silver, and palladium nanoparticle/nano-agglomerate generation, collection, and characterization.* Journal of Nanoparticle Research, 2011. **13**(12): p. 6591-6601.

39. Möller, W., et al., *Gold nanoparticle aerosols for rodent inhalation and translocation studies.* Journal of nanoparticle research, 2013. **15**(4): p. 1-13.

40. Backman, F., *Gd2O3 nanoparticles fabricated by aerosol technique:"A promising approach for future applications".* 2010.

41. Boddu, S., et al., *Carbon nanoparticle generation, collection, and characterization using a spark generator and a thermophoretic deposition cell.* Nuclear Technology, 2011. **173**(3): p. 318-326.

42. Akbarzadeh, A., et al., *Synthesis and characterization of gold nanoparticles by tryptophane.* American Journal of Applied Sciences, 2009. **6**(4): p. 691.

43. Masala, O. and R. Seshadri, *Synthesis routes for large volumes of nanoparticles.* Annu. Rev. Mater. Res., 2004. **34**: p. 41-81.

44. Wong, S. and B. Karn, *Ensuring sustainability with green nanotechnology.* Nanotechnology, 2012. **23**(29): p. 290201.

45. Philip, D., *Rapid green synthesis of spherical gold nanoparticles using Mangifera indica leaf.* Spectrochimica Acta Part A: Molecular and Biomolecular Spectroscopy, 2010. **77**(4): p. 807-810.

46. Chanda, N., et al., *An effective strategy for the synthesis of biocompatible gold nanoparticles using cinnamon phytochemicals for phantom CT imaging and photoacoustic detection of cancerous cells.* Pharmaceutical research, 2011. **28**(2): p. 279-291.

47. Pandey, S., et al., *Green synthesis of highly stable gold nanoparticles using Momordica charantia as nano fabricator.* Arch Appl Sci Res, 2012. **4**: p. 1135-41.

48. Shukla, R., et al., *Soybeans as a phytochemical reservoir for the production and stabilization of biocompatible gold nanoparticles.* Small, 2008. **4**(9): p. 1425-1436.

49. Li, H., et al., *Mangiferin exerts antitumor activity in breast cancer cells by regulating matrix metalloproteinases, epithelial to mesenchymal transition, and β-catenin signaling pathway.* Toxicology and applied pharmacology, 2013. **272**(1): p. 180-190.

50. Zhi-quan, W.J.-g., D.; and Li, Y.; , *Pharmacological Effects of Mangiferin. .* Chinese Herbal Medicines, 2011. **3(4):** : p. 266-271. .

51. Li, H.-W., et al., *Protective effects of mangiferin in subchronic developmental lead-exposed rats.* Biological trace element research, 2013. **152**(2): p. 233-242.

52. http://www.inrfood.com/ingredients/419.

53. http://pubchem.ncbi.nlm.nih.gov/summary/summary.cgi?cid=6224#x94.

54. http://www.medicinenet.com/sodium_citrate_alk_citric_acid-oral_liquid/article.htm.

55. http://www.webmd.com/drugs/drug-3023-sodium+citrate-citric+acid+Oral.aspx?drugid=3023&drugname=sodium+citrate-citric+acid+Oral.

56. http://www.modernistpantry.com/sodium-citrate.html.

57. http://en.wikipedia.org/wiki/Sodium_citrate#/media/File:Trisodium_citrate.png.

58. Kannan, R., et al., *Functionalized radioactive gold nanoparticles in tumor therapy.* Wiley Interdisciplinary Reviews: Nanomedicine and Nanobiotechnology, 2012. **4**(1): p. 42-51.

59. JA Campbell, J. and J. Durlacher, *Clinical usefulness of radioactive gold 198.* The Journal of the Indiana State Medical Association, 1955. **48**(4): p. 374-383.

60. http://en.wikipedia.org/wiki/Neutron_capture#mediaviewer.

61. Neves, M., A. Kling, and R. Lambrecht, *Radionuclide production for therapeutic radiopharmaceuticals.* Applied radiation and isotopes, 2002. **57**(5): p. 657-664.

62. radioisotopes, I.a.e.a.M.f.r.p., 2003.

63. Wiles, A., *Quantitative planar imaging with Au-198*. 2012.

64. Jones, B., *Monte Carlo Calculations of Microscopic Dose Enhancement for Gold Nanoparticles-aided Radiation Therapy*. 2009.

65. Briesmeister, J.F., *MCNPTM-A general Monte Carlo N-particle transport code.* Version 4C, LA-13709-M, Los Alamos National Laboratory, 2000.

66. Speiser, M.P., *Development and Validation of a Virtual Monte Carlo Radiotherapy Source: Model and Characterization of the Influence of Heterogeneities on Dose Calculation Accuracy*. 2008: ProQuest.

67. Hendricks, J.S., *MCNPX Model/Table Comparison*. 2003, Los Alamos Nat. Lab.

68. Shultis, J.K. and R.E. Faw, *An MCNP primer.* Dept. of Mechanical and Nuclear, 2011.

69. http://www.webmd.com/urinary-incontinence-oab/picture-of-the-prostate.

70. Lee, C.H., O. Akin-Olugbade, and A. Kirschenbaum, *Overview of prostate anatomy, histology, and pathology.* Endocrinology and metabolism clinics of North America, 2011. **40**(3): p. 565-575.

71. http://en.wikipedia.org/wiki/Prostate.

72. Shrivastava, A. and V.B. Gupta, *Various treatment options for benign prostatic hyperplasia: A current update.* Journal of mid-life health, 2012. **3**(1): p. 10.

73. Nam, J., et al., *pH-induced aggregation of gold nanoparticles for photothermal cancer therapy.* Journal of the American Chemical Society, 2009. **131**(38): p. 13639-13645.

74. http://academyofinventors.org/conference/docs/fellows-program-2014.pdf.

75. http://issuu.com/academyofinventors/docs/final_fellows_program_for_web/1.

76. Cutler, C., et al. *In vivo evaluation of gum arabic stabilized gold-199 nanoparticles in normal dogs*. in *Society of Nuclear Medicine Annual Meeting Abstracts*. 2012. Soc Nuclear Med.

77. Lal, S.S. and P. Nayak, *Green synthesis of gold nanoparticles using various extract of plants and spices.* International journal of science innovations and discoveries, 2012(2): p. 325.

78. Turkevich, J.a.S., C.; and Hillier, J.; A . , *study of the nucleation and growth processes in the synthesis of colloidal gold.* Discussions of the Faraday Society, 1951. **11**: p. 55–75.

79. Frens, G., *Controlled Nucleation for Regulation of Particle-Size in Monodisperse Gold Suspensions. .* Nature-Physical Science, 1973. **241**: p. 20-22.

80. Grabar, K.C., et al., *Preparation and characterization of Au colloid monolayers.* Analytical chemistry, 1995. **67**(4): p. 735-743.

81. Ojea-Jiménez, I., et al., *Small gold nanoparticles synthesized with sodium citrate and heavy water: insights into the reaction mechanism.* The Journal of Physical Chemistry C, 2010. **114**(4): p. 1800-1804.

82. Li, C., et al., *Facile synthesis of concentrated gold nanoparticles with low size-distribution in water: temperature and pH controls.* Nanoscale research letters, 2011. **6**(1): p. 1-10.

83. Verma, H., P. Singh, and R. Chavan, *Gold nanoparticle: synthesis and characterization.* Veterinary World, 2014. **7**(2): p. 72-77.

84. Kimling, J., et al., *Turkevich method for gold nanoparticle synthesis revisited.* The Journal of Physical Chemistry B, 2006. **110**(32): p. 15700-15707.

85. Vijayakumar, S., *In vitro stability studies on gold nanoparticles with different stabilizing agents.* INT J CURR SCI, 2014. **11**.

86. Connor, E.E., et al., *Gold nanoparticles are taken up by human cells but do not cause acute cytotoxicity.* Small, 2005. **1**(3): p. 325-327.

87. Freese, C., et al., *Uptake and cytotoxicity of citrate-coated gold nanospheres: Comparative studies on human endothelial and epithelial cells.* Part Fibre Toxicol, 2012. **9**(1): p. 23.

88. Vetten, M.A., et al., *Label-free in vitro toxicity and uptake assessment of citrate stabilised gold nanoparticles in three cell lines.* Part Fibre Toxicol, 2013. **10**(1): p. 50.

89. Vijayakumar, S. and S. Ganesan, *In vitro cytotoxicity assay on gold nanoparticles with different stabilizing agents.* Journal of Nanomaterials, 2012. **2012**: p. 14.

90. Bouchat, V., et al., *Radioimmunotherapy with radioactive nanoparticles: first results of dosimetry for vascularized and necrosed solid tumors.* Medical physics, 2007. **34**(11): p. 4504-4513.

91. Nuttens, V., et al., *Determination of biological vector characteristics and nanoparticle dimensions for radioimmunotherapy with radioactive nanoparticles.* Applied Radiation and Isotopes, 2008. **66**(2): p. 168-172.

92. Hanaichi, T., et al., *A stable lead by modification of Sato's method.* Journal of electron microscopy, 1986. **35**(3): p. 304-306.

93. Khoobchandani, M., et al., *Green Nanotechnology from Brassicaceae Development of Broccoli Phytochemicals–Encapsulated Gold Nanoparticles and Their Applications in Nanomedicine.* International Journal of Green Nanotechnology, 2013. **1**: p. 1943089213509474.

94. Katti, K., et al., *Green nanotechnology from cumin phytochemicals: generation of biocompatible gold nanoparticles.* International Journal of Green Nanotechnology: Biomedicine, 2009. **1**(1): p. B39-B52.

95. Behra, R., et al., *Colloidal Stability and Toxicity of Gold Nanoparticles and Gold Chloride on Chlamydomonas reinhardtii.* Aquatic Geochemistry, 2015: p. 1-12.

96. Poon, Z., et al., *Controlling in vivo stability and biodistribution in electrostatically assembled nanoparticles for systemic delivery.* Nano letters, 2011. **11**(5): p. 2096-2103.

97. Bushberg, J.T. and J.M. Boone, *The essential physics of medical imaging*. 2011: Lippincott Williams & Wilkins.

98. Welch, M.J. and C.S. Redvanly, *Handbook of radiopharmaceuticals.* Radiochemistry and Applications. Wiley, 2003. **3**.

VITA

Amal Yousif Al-Yasiri was born in Baghdad- Iraq. She received her Bachelor's degree in Physics from the College of Science/ University of Baghdad in Iraq. Immediately, after her graduation, she worked as a Physical Assistant in the department of Basic Science, College of Dentistry, University of Baghdad, in Baghdad-Iraq. After two years, she went on to earn an MS in Medical Physics from the College of Medicine/ Al- Mustansirya University in Iraq. After she earned the Master degree, she returned to her work at the University of Baghdad as Assistant Lecturer. Then she received a scholarship from her government to pursue a Ph.D degree in Medical Physics. Therefore, she came to the USA and enrolled in a Ph.D program in Nuclear Science and Engineering Institute/ University of Missouri–Columbia. Her Ph.D research is directed toward developing new protocols to produce radioactive gold nanoparticles to be used to image and treat cancer. Amal is planning to graduate from the University of Missouri in May of 2015.Then, she will go back home to continue her work at the University of Baghdad as faculty member.